ir. Liesbeth Bouckaert

Dependency of organic matter decomposition on soil pore network structure as revealed by X-ray micro-CT

Thesis submitted in fulfillment of the requirements for the degree of
Doctor (PhD) in Applied Biological Sciences:
Land and Forest Management

Dutch translation of the title:

De rol van de bodemporiën netwerk structuur in organische stof afbraak
bepaald met X-stralen micro-CT

Cover illustration: Soil volume with segmented air-filled (in yellow) and water-filled (in orange) pore space visualized with Avizo Fire 6.2.

To refer to this thesis:

Bouckaert, L. (2012) Dependency of organic matter decomposition on soil pore network structure as revealed by X-ray micro-CT. Ph.D. thesis, Faculty of Bioscience Engineering, Ghent University, Ghent, Belgium, 177 pp.

Dankwoord

In dit stukje tekst krijg ik de kans om de fantastische crew van mijn leven te bedanken. Hier komt niet de wetenschapster aan het woord, maar wel de persoonlijkheid die erachter zit (als beide kunnen ontkoppeld worden tijdens de 15 minuten dat ik dit schrijf).

Wat een fantastische vier jaren heb ik achter de rug. Een rollercoaster in Bellewaerde is er niets bij vergeleken! Zowel mijn werkomgeving als mijn vrienden en familie hebben hun uiterste best gedaan om mij te stimuleren, te amuseren, te ambeteren,.. naargelang hun eigen unieke talenten. Niettemin, elke bijdrage tot de ontplooiing van mezelf en dit onderzoek werd met dank aanvaard!

Eerst en vooral wil ik mijn promotor Stefaan De Neve bedanken voor het volste vertrouwen in mij om dit project tot een goed einde te brengen. Ook dank aan mijn co-promotor Steven Sleutel voor de onvoorwaardelijke steun en advies tijdens het onderzoek. Jullie bijdrage is van onschatbare waarde geweest de voorbije vier jaar. Bedankt aan alle projectleden voor jullie inspiratie tijdens onze bijeenkomsten. Luc Van Hoorebeke en Patric Jacobs, bedankt voor jullie initiatief om dit boeiende project mede te ontwikkelen. Veerle Cnudde en Manu Diericks, bedankt voor jullie praktische kijk op de zaak. Een oprechte bedanking gaat ook uit naar Denis Van Loo voor het onvermoeibare uitvoeren van alle X-stralen scans en het verstaanbaar maken van de theorie rond X-stralen CT. Bedankt Loes Brabant voor alle hulp bij de beeldverwerking en de ontwikkeling van algoritmen 'at request'.

Een dikke merci aan alle collega's van de vakgroep bodembeheer! Nele en Steven, het was een plezier om met jullie een bureau en kinderweetjes te delen. Nele, ik wens je alle geluk toe met 'de baby'. Steven, zeer veel plezier met je gezin en succes met je nieuwe functie! Sara, veel plezier met de nieuwe veulentjes en bedankt voor onze congres avonturen. Funny, dé persoon voor een leuke babbel, ik heb je gemist de laatste maanden. Dave en Bram, jullie visie op ecologisch leven was een inspiratie voor me! Jeroen, Azita and Mesfin, Yeevan, Shamim, Kader, thanks for the funny conversations during resto time! Rudy en Peter voor de aangename lunch momenten in 'de kerk' en het delen van dessertjes indien ik weer eens geen keuze kon maken. Alle laboranten en medeonderzoekers, bedankt voor jullie humor tijdens de koffiepauze, voor de eindeloze discussies waar enkel Google ons kon redden (kriek vs. kers) en voor het bijspringen in mijn ambitieuze labexperimenten. Bedankt aan Loes, Veerle, Denis, Matthieu, Jan en Pieter voor de plezierige tijd in New Orleans. What happens in New Orleans,

probably stays on the hard disk of UGCT forever ☺. Ook bedankt aan alle thesisstudenten (Bram, Hilda, Wim, Brecht) voor jullie inzet!

Tot zover de crew tijdens de week… hier komt de weekendploeg: Beste vrienden en familie, al probeer ik hier nog zo origineel uit de hoek te komen, het blijft onmogelijk jullie vriendschap en liefde tegemoet te komen met een paar woordjes. Sophie, onze telemomenten resulteerden vaak in urenlange parlé over koetjes en kalfjes, en ik hoop dat het zo zal blijven! Sarah en Kris, ik kijk al uit naar meer van die weekendjes aan zee! Peter, ik koester onze ijzersterke band en je onvermoeibare steun doorheen al mijn avonturen. Ilse, gelukkig kon ik je ieder moment van de dag bellen met mijn zorgen, in de toekomst draaien we de rollen wel eens een keertje om! Frieda en Bart, mijn bedje stond altijd klaar bij jullie indien het pendelen me teveel werd de laatste maand. Een welgemeende merci voor jullie gastvrijheid. Ruben, bedankt om me te doen sprankelen de laatste maanden. Mijn buitenverblijf in West-Vlaanderen met zijn inwoners waren de hoofdverantwoordelijken voor het plezier in mijn leven en worden vriendelijk verzocht vooral zichzelf te blijven! Mijn ganse familie, ouders, Gudrun, broers Sam en Jonas en zussen Sarah en Josefien, schone broers Lander en Abou en zus Ilse, Stitch en Hercules; jullie losse vijzen waren en blijven onmisbaar voor me! Bij jullie kan ik altijd thuiskomen welk avontuur ik ook tegemoet ga!

Liesbeth

TABLE OF CONTENTS

LIST OF ABBREVIATIONS

C, N, P, S	Carbon, Nitrogen, Phosphorus, Sulfur
CO_2	Carbon dioxide
PSD	Pore Size Distribution
WRC	Water Retention Curve
WP	Wilting Point
FC	Field Capacity
SOM	Soil Organic Matter
OM	Organic Matter
WFPS	Water-Filled Pore Space
2D, 3D	Two-Dimensional, Three-dimensional
X-ray CT	X-ray Computed Tomography
2,4 D	2,4-dichlorophenoxyacetic acid
POM	Particulate Organic Matter
PND	Pore Neck size Distribution
VP	Visible Porosity
T	Threshold value
REV	Representative Elementary Volume
$Ø_{eq}$	Equivalent Sphere Diameter
TPV	Total Pore Volume
θ_s	water content at saturation
PLFA	Phospholipid Fatty Acid
$C_{cum,38}$	38-days cumulative C mineralization
MBC	Microbial Biomass Carbon
TOC	Total Organic Carbon

PNP	p-nitrophenol
CS:FS:C+S	Coarse Sand, Fine Sand and Clay + Silt fraction
SOC	Soil Organic Carbon
BD	Bulk Density (g cm^{-3})
$C_{cum,35}$	35-days cumulative C mineralization
TP	Total Porosity
VOI	Volume of Interest

LIST OF TABLES

LIST OF FIGURES

Chapter 1:

Introduction

Soil is the primary resource for life on our planet. It provides us vital ecosystem services, such as the production of food, the storage of clean water, and the habitat for species rich natural ecosystems. Soil is a vital component in all global environmental processes. Because soil Carbon (C) represents the largest C pool of terrestrial globally C, approximately 1580 Pg C (estimated to 1 m depth), compared to 610 Pg of C in vegetation and 750 Pg in the atmosphere (Figure 1-1), it has a huge potential for either sequestering of releasing C into the atmosphere (Kutsch *et al.*, 2009).
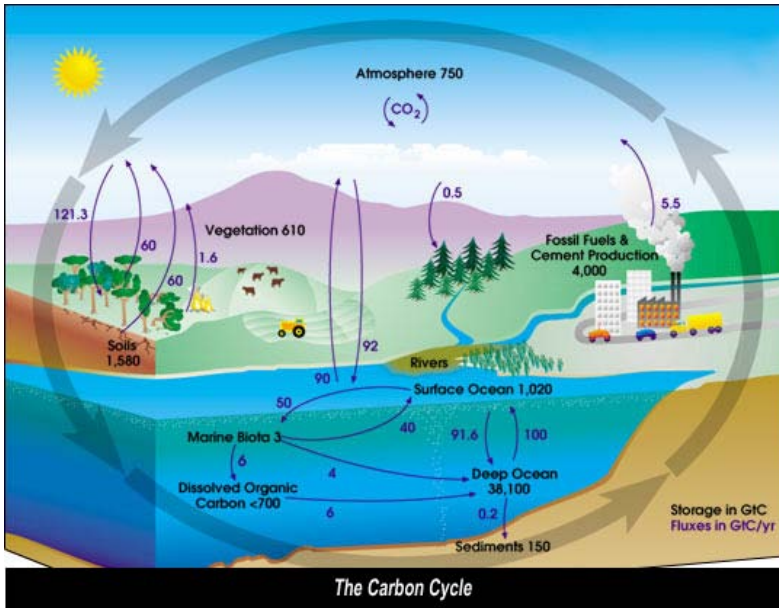
Figure 1-1: The global C cycle with C pools in the atmosphere (750 Pg), vegetation (610 Pg), soil (1580 Pg) and oceans ($38*10^3$ Pg) and yearly fluxes between these pools (Source: http://www.global-greenhouse-warming.com/global-carbon-cycle.html).

By controlling the CO_2 concentration in the atmosphere, the C cycle regulates the Earth's climate. CO_2 is important for its contribution to the greenhouse effect; a natural phenomenon in which heat generated from sunlight at the Earth's surface is trapped by certain gasses and prevented from escaping through the atmosphere. The CO_2 concentration in the Earth's atmosphere has increased with 30% compared to the natural background level during the last 150 years, which has caused a rise in the global temperature. Because this temperature increase is the primary cause for the changing climate, interest in the C cycle is increasing globally.

Soil C sequestration is viewed as a realistic option to contribute to mitigating climate change (Lal, 2004). For example Freibauer *et al.* (2004) estimated the potential for soil C sequestration through changes in the management of agricultural soils in Europe to be 16-19 Mt C year^{-1}. However, others such as Powlson *et al.* (2011) emphasized that C sequestrations has its limitations; (i) the quantity of C that can be stored in soil is finite, (ii) the process is reversible and (iii) an increase in SOC may induce changes in the fluxes of other greenhouse gasses such as methane and nitrous oxide (N_2O). Overall, science faces the enormous challenge of understanding the C cycle in order to provide policy makers with rational information on the contribution of C sequestration to climate change mitigation strategies.

1.1 The building stones of soil

1.1.1 Influence of soil structure and texture on the soil water distribution

Soil formation starts when mineral material from rocks and organic matter from plants and animals combine. Rock fragments without organic matter are unable to support plant growth and although organic matter inputs can support plant growth, organic matter lacks many of the physical characteristics that are commonly associated with soil. It is the combination of mineral and organic matter that gives soil its unique properties.

Soil is built up of three phases; a solid, liquid and gaseous phase. The solid phase is the combination of mineral components and organic matter. The proportion of the three soil mineral components (sand, silt and clay) determines **soil texture**, which influences the soil's capacity to store and supply plant nutrients. The way in which sand, silt and clay particles are bound together in larger units called aggregates, defines **soil structure**. Soil structure in its widest sense refers to the size, the shape and stability of **soil aggregates**. Soil aggregation includes aggregate formation and stabilization. Aggregates are formed when the soil is subjected to swelling-shrinking, plant-root penetration or freezing and thawing. Aggregates are said to be stable when they can resist pressures caused by processes such as compaction and sudden wetting. Aggregates can be divided into two size groups (Tisdall & Oades, 1982): micro aggregates (<250 µm) and macro aggregates (>250 µm). According to the hierarchy model of Tisdall & Oades (1982), macro aggregates are collections of micro aggregates which are bound together with organic matter. The lower the clay content in soil, the more important organic matter is for aggregate stabilization.

The soil space that is not occupied with solid matter is the pore space. **Soil porosity** is the proportion of pore space in the soil volume. Pore space can be water-filled or air-filled depending on the **soil water** content and the **pore size distribution** (PSD). Based on the capillarity law, pores will be water-filled depending on the dimension of their necks or throats, i.e. smallest pore openings connecting adjacent pores. Among many different pore size definitions, Lal & Shukla (2004) classify pores in relation to their function; the macro pores or transmission pores (>50 µm) allow the rapid movement of water and gas through the soil; meso pores or storage pores (0.5-50 µm) hold water against the force of gravity and micro pores or residual pores (<0.5 µm) hold water very tightly, even too tight for plant uptake. A relationship between the water content and water tension (expressed as pF-value, the negative logarithm of pressure head *h*) is used in soil science. It is referred to as the **water retention curve** (WRC) (Figure 1-2). Soil texture and soil structure largely influence the tension at which water is held in soil.
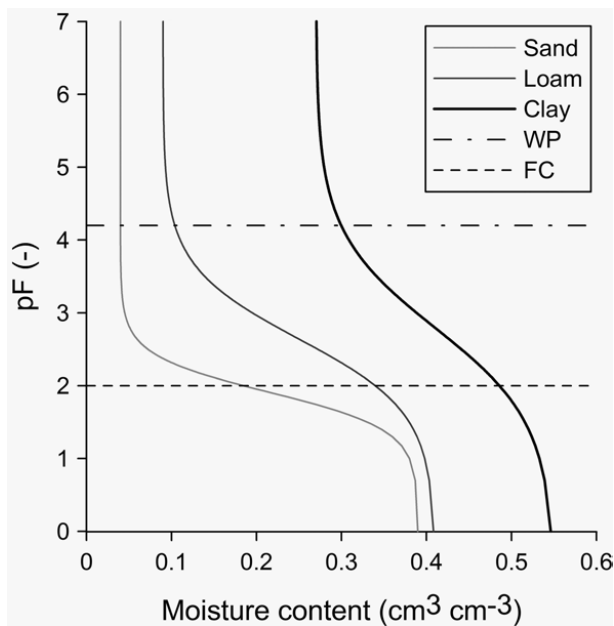
Figure 1-2: Water retention curve of a sand, loam and heavy clay soil according to Vereecken *et al*. (1989). The wilting point (WP) at pF 4.2 and field capacity (FC) at pF 2 are the lower and upper limits of the amount of available water for plant growth, respectively.

1.1.2   Soil organic matter (SOM) fractions and their contributions to soil functioning

Physical SOM fractionation techniques are based on the concept that SOM can be divided into fractions that are associated with particles of various sizes (Six *et al*., 2001; Hayes, 2006) or density fractions (light-medium-heavy). Density fractionation is based on the theory that more humified SOM becomes particularly associated with the soil mineral matrix which has a higher density (Beldini *et al*., 2010). Chemical fractionation distinguishes SOM fractions based on their respective solubility's in various extractants and their reactivity with acid and oxidants (Hayes, 2006). The following SOM classification is based on differences in chemical composition of SOM fractions. The term 'SOM' covers all the living and dead organic matter in the soil. The main component of SOM is C, typically accounting for around 50% of total SOM weight (Sleutel *et al*., 2005). SOM consists of fresh residue (<10%), living soil fauna and micro flora (<5%), partially decomposed plant and animal residues (33-50%) and humic substances (33-50%) (Figure 1-3). Humic substances are the end product of decaying SOM. It is better known as "humus", a very stable material (possibly >1000 years old) that gives the dark brown colour to soil. Its stability relates to its intimate interactions with soil mineral phases and its chemical complexity.
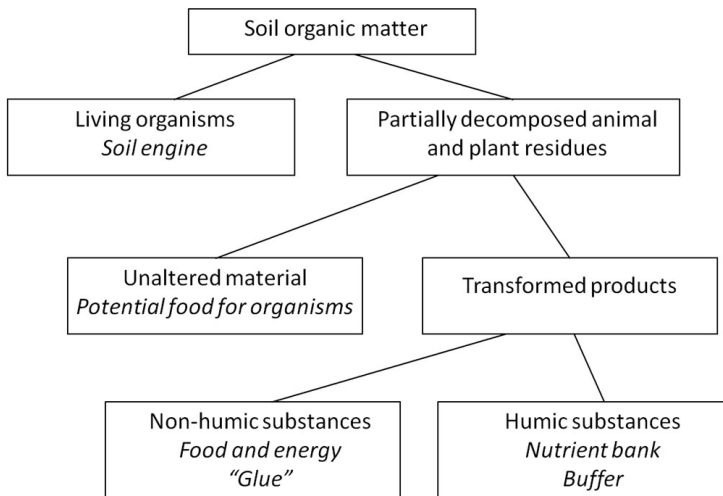
Figure 1-3: Components of Soil Organic Matter (SOM) and their contribution to soil functioning (Source: Bot & Benites, 2005).

During the last decades, the general view on organic matter dynamics has evolved. Organic matter does not persist because of the intrinsic properties of the organic matter itself, but because of physicochemical and biological influences from the surrounding environment that reduce the probability (and therefore rate) of decomposition, thereby allowing organic matter to persist (Schmidt *et al*., 2011). The persistence of soil organic carbon is thus primarily not a molecular property, but an ecosystem property.

The total organic matter (OM) content of a soil is the sum of several different pools of SOM which are related to modelling approaches. Three fractions or portions of SOM can be analytically determined (Brady & Weil, 2002; von Lützow *et al.*, 2006).

The **active fraction** of SOM comprises 10-20% of total SOM and consists of materials with an approximate C/N ratio of 15-30 that are easily decomposable. This fraction includes the living biomass, the partially decomposed animal and plant residues and some of the more labile fulvic acids. This fraction provides most of the readily accessible organic substrate for soil organisms. It is responsible for structural stability that leads to enhanced water infiltration, resistance to erosion and ease of tillage. The active fraction can be easily increased by addition of fresh plant and animal residue, but it can also be lost rapidly when such additions are reduced or when tillage is intensified. This fraction has a turnover time of about 1-2 years in a temperate climate and is also called **the labile OM pool** (Jenkinson & Ladd, 1981; von Lützow *et al.*, 2006).

The **passive fraction** of SOM accounts for 60-90% of SOM in most soils and consists of very stable materials remaining in the soil for hundreds or even thousands of years. This fraction includes most of the humus physically protected in clay-humus complexes, most of the humin and much of the humic acids. This fraction only increases or decreases very slowly and is closely associated with the colloidal properties of soil humus. It is responsible for most of the cation-exchange-capacity of soil and part of the soils water-holding capacity. Humus functions as an important buffer, reducing soil acidity and nutrient availability fluctuations (Bot & Benites, 2005). This slowly decomposing SOM fraction is also called the **refractory C pool**.

The **third fraction** of SOM comprises SOM with intermediate properties between the active and passive fraction. The turnover rate of this intermediate pool is about 10-100 years (von Lützow *et al.*, 2006).

Although SOM comprises only a small fraction of the total mass of most soils, this dynamic soil component exerts a dominant influence on many soil physical, chemical and biological properties (Brady & Weil, 2002). In terms of improving soil structure, the active and some of the resistant soil organic components, together with micro-organisms (especially fungi), bind soil particles together into discrete units called aggregates. Secondly, during SOM decomposition (see 1.2.1), nutrients are released in a plant-available form, functioning as a storehouse of plant nutrients.

1.2 SOM dynamics

1.2.1 SOM decomposition

CO_2–C from the atmosphere is incorporated into organic compounds through the process of photosynthesis (Figure 1-4). Plant roots, soil microbes and fauna release CO_2 belowground through their metabolism, contributing to '**soil respiration'**. About half of the soil respiration derives from metabolic activity to support and grow roots and associated mycorrhizae (**autotrophic respiration**). Most of the remaining part of soil respiration (10 to 95%) is associated with **heterotrophic respiration** from microbial communities consuming plant structural compounds or other organic matter (Hanson *et al.*, 2000), called SOM decomposition.
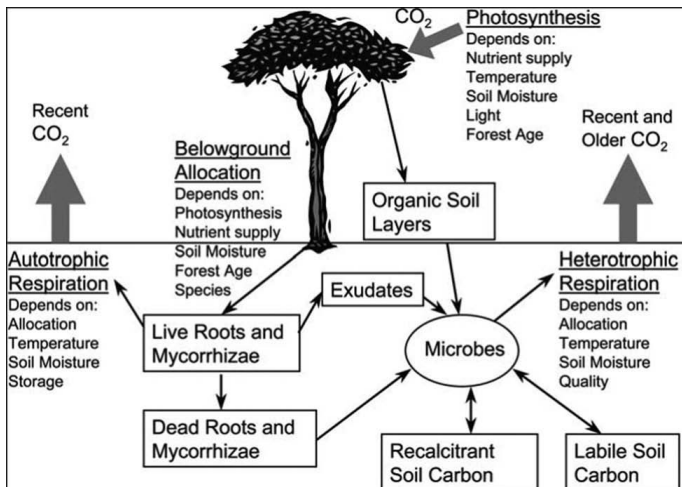
Figure 1-4: Conceptual model of the components and responses of soil respiration (Source: Ryan & Law, 2005).

SOM decomposition is a biological process that includes the physical breakdown and biochemical transformation of complex molecules of dead organic material into simple organic and inorganic molecules (Juma, 1998). The term '**mineralization'** refers to the release of nutrients (C, N, P and S) to the soil when SOM is decomposed. Approximately 85-90% of SOM decomposition is microbially mediated and about another 10-15% is utilized by soil animals (Wolters, 2000). Abiotic chemical oxidation, in contrast, is likely to account for less than 5% of SOM decomposition (Lavelle *et al.*, 1993).

Soil organisms mediate SOM decomposition and play thus an important role in nutrient cycling. As plant and animal residues enter the soil, they are colonized by a whole range of micro-organisms. As the residues are broken down, nutrients are released and recycled through the soil. Initially, the easiest compounds to break down are attacked first, leaving the more resistant compounds to accumulate in the soil. Eventually, microbial waste products and resistant plant residues combine after transformations to form soil humus in a process called '**humification'**. Although the combined weight of all C contained in soil microorganisms accounts only for 2-5% of the total mass of soil C, all the residues entering the soil must be broken up and recycled by micro-organisms before they can be used by plants again. 80-90% of all soil processes are known to be microbially mediated (Nannipieri *et al.*, 2002) and therefore result from the interaction of soil organisms and SOM. Microorganisms therefore perform a crucial function.

1.2.2   Environmental influences on SOM dynamics

Transformation of SOM is a dynamic process influenced by climate, soil type, vegetation and soil organisms.

Climate can influence SOM decomposition rates through changes in temperature and rainfall patterns. The higher SOM levels in cooler climates are the consequence of the temperature sensitivity of SOM decomposition rate. **Temperature** sensitivity of soil respiration is commonly described using Q_{10} values; a temperature increase of 10°C is estimated to increase soil respiration rate by a factor 1.56-2.7 (Chen *et al.*, 2010). Soil organic matter levels commonly increase as mean annual **precipitation** increases. Conditions of elevated levels of soil moisture result in greater biomass production, which provides more residues, and thus more potential food for soil biota (Bot & Benites, 2005). Because SOM decomposition is microbially regulated, a good soil aeration and water availability are necessary for optimal microbial activity. According to Linn & Doran (1984), optimal

microbial activity occurs at a moisture content of 60% water-filled-pore-space (WFPS). On the other hand, anaerobic conditions due to water saturation reduce decomposition rates because fungi and Actinomycetes will be suppressed and only bacteria that survive these conditions can decompose SOM. Long term saturated soil conditions can lead to very large organic matter contents in soil (e.g. peat soils).

SOM decomposition rates are higher in coarse textured soils compared to fine textured soils (Six *et al.*, 1999). Ladd *et al.* (1985) compared retention of labeled SOM with clay contents ranging from 5-42% with similar climatic conditions and found that soil clay content and SOM retention were nearly proportional. It is unclear whether it is **clay content** per se that causes this relationship between **soil texture** and SOM decomposition, or that other factors like varying PSD with different texture are involved. Firstly, adsorption of SOM onto surfaces of clays or organic complexes might retard SOM decomposition (von Lützow *et al.*, 2006). Secondly, soils with higher clay content have generally better aggregate formation and macro aggregates are known to protect SOM physically from mineralization (Elliot & Coleman, 1988). Thirdly, the effect of soil texture on SOM decomposition also shows through the influence of PSDs on the grazing intensity of microbes. A large proportion of bacteria may occupy pores <3 μm (Kilbertus, 1980), while protozoa and nematodes are restricted to larger pores. Consequently, a large part of the bacterial population will be protected from their predators (Postma & Van Veen, 1990) and this protection differs among different PSDs. Indeed, Hassink *et al.* (1993) found that sandy soils have higher grazing intensities on bacteria by bacterivorous nematodes than loam and clay soils leading to higher N mineralization rates in these sandy soils. In contrast, Scott *et al.* (1996) examined the effects of soil texture on litter decomposition and SOM mineralization and found that soil texture had no effect on litter decomposition. Still, according to Van Veen & Kuikman (1990), **soil architecture** is the most dominant control over microbial mediated decomposition processes in terrestrial ecosystems.

The rate of soil organic matter accumulation depends largely on the **quantity and quality of organic matter input** (i.e. vegetation). Readily degradable materials with low C/N ratios favor decomposition while plant materials with both large C/N ratios and lignin contents such as cereal straw and grasses generally favor nutrient immobilization, organic matter accumulation and humus formation, with increased potential for improved soil structure development. The fundamental differences between fungi and bacteria, such as the filamentous growth and the higher C/N ratio of the fungal biomass (Six *et al.*, 2006; de Ruiter *et al.*, 2011), suggest that their contributions to decomposition will vary with both physical

and chemical aspects of the substrate. Organic matter (OM) with a high C/N ratio is believed to stimulate the fungal contribution to decomposition (Henriksen & Breland, 1999; Thiet *et al.*, 2006).

1.3 SOM stabilization

1.3.1 *Mechanisms of SOM stabilization*

SOM is protected from decomposition by micro-organisms through a number of stabilization mechanisms (Sollins *et al.*, 1996; Six *et al.*, 2002; Mikutta *et al.*, 2006; von Lützow *et al.*, 2006):

(i)   **physical stabilization** through micro aggregation

Occluded OM is spatially protected against decomposition (=physical stabilization) due to (i) reduced access for the micro organisms and their enzymes, which control further food web interactions, (ii) reduced diffusion of enzymes into the intra-aggregate space and (iii) restricted aerobic decomposition due to reduced diffusion of oxygen. It is primarily the PSD that controls the above-mentioned processes as it influences the proportions of pores that are water-filled as well as those pores functioning as a possible habitat for micro organisms.

(ii)   intimate **association with silt and clay particles**

Evidence for stabilization of OM due to binding to mineral surfaces comes from the fact that OM in fine silt and clay fractions is older (Eusterhues *et al.*, 2003) or has a longer turnover time (Balesdent, 1996) than OM in other soil fractions.

(iii)   biochemical stabilization through the formation of **recalcitrant SOM compounds**

The selective degradation of less recalcitrant compounds by microbes gradually increases the average recalcitrance of the non-respired-C, a process that is called selective preservation (Sollins *et al.*, 1996). However, more recent studies have found that the soil biotic community is able to break down any OM of natural origin (Marschner *et al.*, 2008), so that molecular recalcitrance of OM should be interpreted as relative, rather than absolute recalcitrance (von Lützow *et al*., 2006). Ekschmitt *et al.* (2008) agrees on the fact that the decomposer community is provided with the chemical and physical tools to degrade virtually all kinds of SOM compounds in the long term,

but attributes preferential substrate utilization by soil organisms to produce a large and stochastically stable C pool with a broad range of components, without relying on an inert status of the C.

The three above mentioned mechanisms of SOM stabilization may be operating simultaneously (Sollins *et al.*, 1996), but to different degrees. According to von Lützow *et al.* (2006) and Kögel-Knabner *et al.* (2008), recalcitrance is only important during early stages of decomposition and in active surface soils, while during late decomposition stages and in the subsoil, the relevance of spatial inaccessibility and organo-mineral interactions for SOM stabilization increases. The larger turnover time for C in micro aggregates (412 years) compared to macro aggregates (140 years), indicates that old C associated with micro aggregates may be both biochemically recalcitrant and physically protected (Jastrow *et al.*, 1996). Overall, the term 'stabilization' means a decrease in the potential for SOM loss by respiration, erosion or leaching (Sollins *et al.*, 1996) and the present study focuses only on the first process.

1.3.2   *Relationship between soil pore structure and soil biological processes*

The interactions between SOM, soil structure and availability of water are very complex. The physical structure of soil is likely to have a major impact on the diversity of biophysical microenvironments for soil microbes (Young & Crawford, 2004). The **pore system** represents an important functional **bridge between the physics and biology of soil**. It is characterized by physical and temporal heterogeneities across all measuring scales from nm to km (Young & Ritz, 2000; O'Donnell *et al.*, 2007).

The structure of solid and pore space results in a complex distribution of oxygen, water films and gradients of solutes spanning distances as small as a few micrometers and therefore result in radically different local conditions at very fine scales (Ruamps *et al.*, 2011). As a consequence, the micro-structure of soil also affects the spatial location of the soil biota (Nunan *et al.*, 2003), thus controlling the degree of contact between organisms (Nunan *et al.*, 2006). Several studies have demonstrated that **bacterial communities are not randomly distributed in soil**. Spatial patterns have been identified in the distribution of bacteria and their function at scales from several meters to millimeters (Robertson *et al.*, 1997; Grundmann & Debouzie, 2000; Nunan *et al.*, 2002) and even below the mm scale, bacterial patchiness has been found (Grundmann *et al.*, 2001; Nunan *et al.*, 2002). Data of Nunan *et al.* (2003) suggested that bacterial patches may be associated with local deposits of substrate, but they

could not confirm this. The first evidence for a significant microbial geography at the pore scale in undisturbed soil cores was found by Ruamps *et al*. (2011) who demonstrated that microbial community structure differed significantly among pore size classes. If microbial community structure is non-random at the micro habitat scale, then one can expect interactions at this scale to affect the relationship between microbial diversity and function.

The fact that soil organisms are not randomly distributed in soil may indicate that the **location of OM within the soil matrix might affect its availability to decomposition**. Adu & Oades (1978) first demonstrated the importance of both available pore space and trophic interactions of soil organisms of different size classes in interpreting decomposition and mineralization patterns in soil. Killham *et al*. (1993) found a greater turnover of added substrates to soil when they were located in larger pores (6-30 µm neck diameter) compared to smaller ones (<6 µm neck diameter) and particularly when these larger pores were water-filled. Strong *et al*. (2004) have found different decomposition rates of native SOM and added substrate among pore size classes. They concluded that OM in large air-filled pores (>300 µm pore neck diameter) decomposes more slowly than in intermediate-sized pores (15-60 µm pore neck diameter) due to organisms mobility, decreased diffusion of solutes and decreasing intimacy of contact between OM and soil minerals. C that was located in smaller pores (<4 µm pore neck diameter) was protected against decomposition. The concept of habitable pore space suggests that there is a relation between the size of an organism and the zone of soils they are physically able to inhabit (Young & Ritz, 2000). A minimum pore neck-diameter of 4 µm for protozoa and of 30 µm for nematodes has been suggested (Jones & Thomasson, 1976). Indeed, Hassink *et al*. (1993) found a close positive relationship between the bacterial biomass and the pore volume with diameters 0.2-1.2 µm and between nematode biomass and the pore volume with diameters 30-90 µm. In addition, they have found evidence for enhanced N mineralization by grazing of bacterivorous nematodes and flagellates on bacteria. Wright *et al*. (1995) also demonstrated the important role of pore size and the location of bacterial cells within pores in both protecting bacterial prey from predation and in determining the influence of released nutrients on bacterial activity. Other studies investigating the effect of soil compaction (1.0 to 1.5 g cm^{-3}) on nutrient turnover of organic materials found that the decreased turnover was caused by a decreased habitable pore space of nematodes. Consequently, the lower grazing level of nematodes on microbes retarded total C and N turnover in soil (van der Linden *et al*., 1989; Breland & Hansen, 1996). Moreover, the grazing effect on nutrient turnover seems to be relatively more important in coarse textured

soils compared to fine textured ones, because more pores were accessible for nematode feeding on amoebae in coarse textured soil (Elliot *et al.*, 1980). But Griffiths & Young (1994) demonstrated that reduction in spore space alone could not account for the large decrease in protozoan biomass measured when they compacted soil, and any difference they observed in soils of different structure was primarily related to differences in water regimes rather than the structure per se. As a consequence, it is not merely the basic spatial architecture of pore networks that modulates biological activity in soils, but the interaction between pores and water (Young & Ritz, 2000). Despite the growing body of evidence showing the importance of micro-habitat structure for many microbial processes, little detail is known about the topology of soil pore networks at the micro-habitat scale (Nunan *et al.*, 2006).

Apart from the significant influence of soil structure on microbially regulated soil processes like SOM decomposition, evidence also shows that this relationship is mutual. The **hierarchical aggregation model** developed by Tisdall & Oades (1982) emphasizes the importance of bacteria, fungi, and roots in binding and stabilizing the soil from sub micrometer to centimetre scale. At the smaller scale, the importance of bacteria and roots in rearranging and stabilizing soil properties was showed by using thin sections (Foster, 1988; Bruand *et al.*, 1996). Several studies have shown evidence that microbes micro engineer their own habitat, by changing the morphology of the pore structure (De Gryze *et al.*, 2006) and by altering the pore geometry and stability through physical movement of particles and/or microbial action (Feeney *et al.*, 2006). These results support the hypothesis that the **soil-plant-microbe complex is self-organized** (Young & Crawford, 2004; Feeney *et al.*, 2006).

1.4 Techniques for characterizing the soil pore structure

Quantifying the physical habitat of soil systems has been an area of intense research with relatively little reward. Most of the techniques at large (m) and small (μm to nm) scales have revealed a staggering variability in pore structures but have failed to relate such variability to function in a meaningful way (Young *et al.*, 2001).

Many studies have attempted to tackle this complexity by using measurements of **soil aggregates as surrogates for the soil structure** (Adu & Oades, 1978; Six *et al.*, 1999; Six *et al.*, 2000). Letey (1991) was the first to state his concerns over the utility of the concept of aggregates as structural surrogates. Later on, Young *et al.* (2001) remarked that aggregation does not necessarily imply the development of distinct soil aggregates within the soil profile.

Indeed, the undisturbed profile in reality exists as a continuous convoluted pore, bounded by solid, and not as a bed of aggregates. Functional traits of soil structure, at all scales, rely on the connectivity, tortuosity and the heterogeneity of pore space in 3D. Soil microstructure has a significant impact on soil processes by protecting micro-organisms from predation, by regulating the diffusion of substrates to and metabolites from microbial cells, and in summary by causing a variety of micro-environments to develop that are more or less suitable for microbial growth, survival and activity (Nunan *et al.*, 2005). Therefore, a way to consider the soil organization, other than as a collection of aggregate sizes is within the framework of the soil pore system. Since the soil pore system constitutes the actual habitat of micro-organisms, which in turn mediate SOM decomposition, it is more evident to establish a link between SOM dynamics and soil pore structure, rather than between SOM dynamics and aggregate stability.

The main reason why few studies have examined the role of the soil pore structure in SOM dynamics is the inability to non-destructively quantify its characteristics. It is difficult to visually inspect and measure pores, so often tests were used that relate pore characteristics to other more easily measured properties. A technique that includes information about the connectivity and tortuosity of the soil pore space is the assessment of a WRC based on the water desorption method (Klute, 1986). Starting with a saturated sample, the gradual removal of the soil water combined with measurements of the water volume removed between consecutive steps, allows one to equate the water volume removed to the soil pore-volume drained. Based on capillarity, the pores with largest pore openings, called 'necks', should drain first, followed by successively smaller pores. Based on the Young-Laplace equation relating the capillary suction to pore dimensions by means of the effective pore radius, a PSD is calculated from the WRC (Rose, 1966). However, because of soil hysteresis, the relationship between soil matric potential and volumetric moisture content is not a unique function but depends on the prior soil wetting/drying history (Lal & Shukla, 2004). Moreover, WRCs based on the pressure cell method could be significantly affected by the applied gas pressure (Dane & Topp, 2002), changing soil structure itself even for gas pressures of about 10 kPa (Eching & Hopmans, 1993). Besides, the water desorption method only includes measurements of open porosity, i.e. porosity that is connected with the border of the sample. A similar relationship where the measured value of the hydrostatic pressure is in equilibrium with the liquid in the pore space can be determined by sorption of a liquid other than water, e.g. mercury (Dullien, 1981). Comparing micro-computed tomography results for porosity

measurements of a limestone and a sandstone with Hg-porosimetry results demonstrated a slightly lower porosity for the latter (Van Geet *et al.*, 2003). Ideally, pore testing methods should be non-destructive, so that pores can be viewed and measured without altering their structure.

An alternative technique that allows quantification of the pore space is **thin section microscopy** (Dalrymple, 1957; Murphy *et al.*, 1977). Thin sections are cut from polished soil that has been impregnated with resin and pore characteristics are analysed microscopically using transmitted polarized light. The application of this method has had various applications in soil science. With the use of thin sections, the spatial distribution of bacteria in undisturbed soil has been quantified (Nunan *et al.*, 2001), root-soil contact was found to increase with bulk density (Kooistra *et al.*, 1992), compaction was found to negatively influence root growth and water and nitrate uptake efficiency was found to decrease from compacted to loose soil (Veen *et al.*, 1992). Zhang *et al.* (2005) used 2-dimensional (2D) thin sections to measure soil pore geometry, and attempted to reconstruct 3-dimensional (3D) soil structure. Using a lattice Boltzman simulation of water flow, the hydraulic conductivity of the soil could be calculated and did not significantly differ from the measured hydraulic conductivity using the constant head method. The advantage of thin sections is that they can provide high resolution images (2 µm) of 2D soil structures. The main problems of this technique, however, are the relatively long lead times between sampling and the final product (the resin-impregnated soil should dry several months before polishing), the usage of chemicals in the production of thin sections and possible alteration of the microstructure of the soil (Young *et al.*, 2001). Any technique based on thin sectioning is furthermore eventually limited by the difficulty in inferring the properties of the original 3D structure (Young & Crawford, 2004).

In conclusion, there has been a lack of available technology to study pore geometry resulting in failure to provide insight into soil microbial processes (Young & Crawford, 2004). Besides the above mentioned techniques, non-destructive X-ray computed tomography may be an alternative technique to characterize the soil pore structure, which has already been applied by many researchers to reveal pore size distributions (see 1.5.3).

1.5   <u>X-ray computed tomography (X-ray CT)</u>

1.5.1   *Principle of the technique*

CT scanning set-up

Computed tomography (CT) provides us information on the internal structure of an object, and most importantly, in a non-destructive manner. During data acquisition, an X-ray source produces a polychromatic X-ray beam that penetrates the object of interest. Behind the object, a pixellated detector records the transmitted X-ray beam, which yields per pixel an intensity which relates to the total amount of energy deposited by the X-rays hitting the detector pixel (Figure 1-5). Because the object rotates during the scan, radiographic images are obtained at different angles covering a 360° range. Following CT scanning, a 3D image is then constructed using reconstruction algorithms. The reconstruction procedure is based on an algorithm that finds the attenuation values in each voxel (=pixel in 3D) based on all the measured data in the projection profiles (Sandborg, 1995).
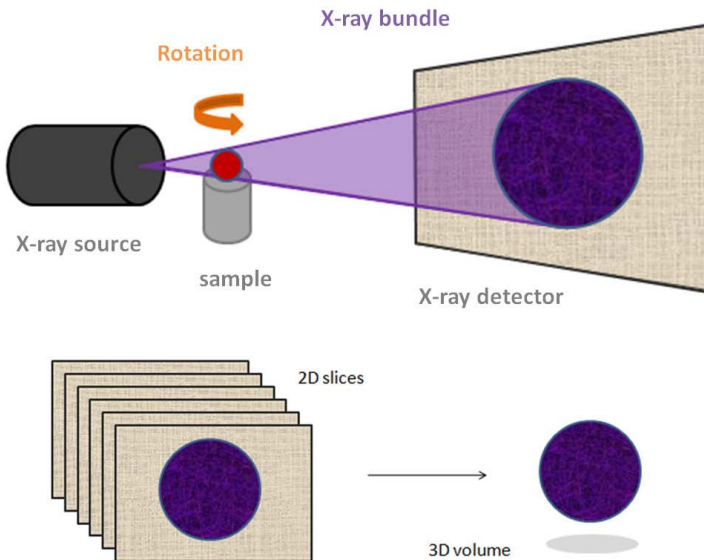
Figure 1-5: Schematic set-up of micro-CT and the principle of 3D volume rendering out of a stack of 2D slices with computer software.

X-ray characteristics

X-rays are a type of short wavelength electromagnetic radiation (12-0.002 nm) with a very high energy (Cnudde, 2005). They occur in finite bundles of energy, called photons. X-rays are produced when electrons with high speed ejected from a heated cathode filament strike a metal object. The acceleration of the electrons is created by electrical forces in a vacuum tube, which contains a cathode and anode. When electrons collide with the anode, their kinetic energy is transferred to the anode and converted into thermal energy (typically 99%) and electromagnetic energy in the form of X-rays (typically 1%). Therefore, targets should have a high melting point and the ability to conduct the produced heat. Often tungsten, a high atomic weight material with a high melting point, is used as a target. The higher the voltage difference between cathode and anode, the higher the velocity of the electrons and the more X-rays with higher energy will be created.

The production of X-rays is caused by two different processes, creating two types of X-rays. The first kind, "**Bremsstrahlung**" is created when the high speed electrons themselves are slowed down when interacting in the anode. The second type of X-rays are emitted when excited electrons of the anode material fall back to a lower energy shell position from a higher energy state, and are called **characteristic X-rays**. The combination of both processes results in a broad continuous spectrum of X-rays on which peaks are superimposed (Wildenschild *et al.*, 2002). However, the produced low energetic photons are partially or fully absorbed by the target and exit window of the X-ray tube (Figure 1-6).
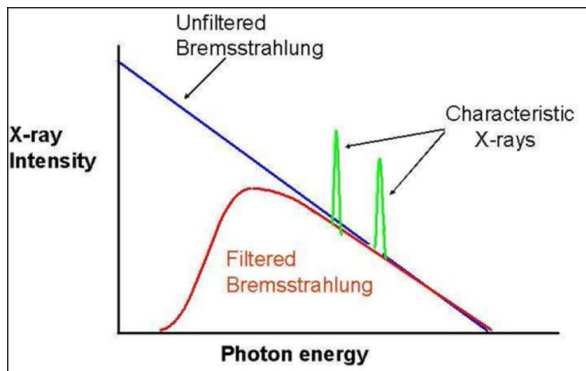
Figure 1-6: Typical broad continuous spectrum of X-rays which is the combination of two types of X-rays: Bremssthralung and characteristic X-rays (from Cnudde, 2005).

Interactions of X-rays with matter

An X-ray beam passing through an object undergoes progressive attenuation due to interactions with the material (Figure 1-7). This progressive attenuation depends on the composition and density of the material and on the energy of the used X-rays. Beer's law describes the attenuation of a beam of monochromatic X-radiation through a homogeneous object:

$$I/I_0 = e^{(-\mu h)} \quad \text{(Eq. 1)}$$

where I_0 and I are the incident and attenuated beam intensities in J m^{-2} s^{-1}, μ is the linear attenuation coefficient (length^{-1}) and h is the thickness of the (scanned) object. For an inhomogeneous object, like soil, the product μh is a sum over all the different phases, i, $\Sigma \mu_i h_i$ encountered by the beam (Taina *et al.*, 2008).
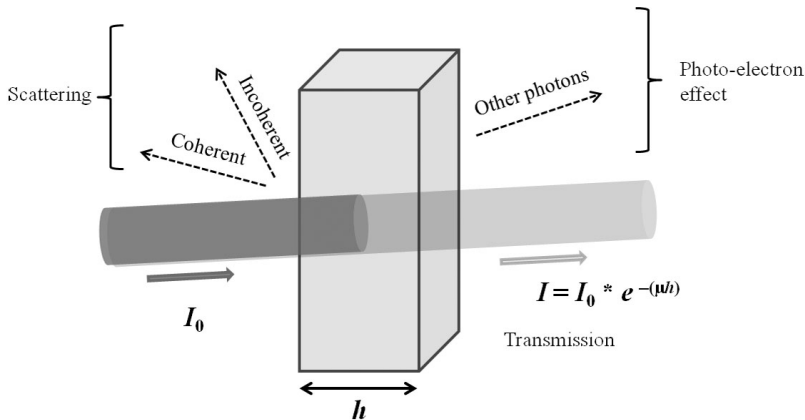
Figure 1-7: Interactions of X-ray photons with matter can cause scattering, absorption or transmission of photons which is described by Beer's law $I=I_0*e^{-(\mu h)}$.

This attenuation of X-rays is mainly caused by absorption and scattering of X-ray photons by the material of interest (Figure 1-7). **Photoelectric absorption** is the complete removal of an X-ray photon from the beam because its photon energy is completely transferred to an atomic electron so that the electron (named photoelectron) is ejected. This effect will dominate X-ray attenuation at low X-ray energies up to 50-100 keV and is strongly dependent on effective atomic number (Mees *et al.*, 2003). **Scattering** leads to a deflection of X-ray photons after interaction with atoms of the material. Incoherent or Compton scattering is the partial transfer of photon energy to an electron (ejecting it), producing a scattered lower energetic photon and a recoil electron. Compton scattering is more dependent on the scanned

material's density than on the effective atomic number (Mees *et al.*, 2003) and its relative importance increases with increasing X-ray energy in the energy range of interest. Coherent scattering is the redirection of the X-ray photon without a loss of energy by coherently interacting with all the electrons of an atom. This process is significant only for low photon energies. For most practical purposes only photoelectric absorption and Compton scattering need to be considered (Wildenschild *et al.*, 2002).

Two materials with different mass density and atomic composition can still have the similar linear attenuation values, because the effects of both characteristics on X-ray attenuation can compensate each other. In this case, the difference between the effects of Compton scattering (mainly influenced by bulk density) and photoelectric absorption (mainly based on the effective atomic number of the material) can provide contrast when the material is scanned twice with different energies of the X-rays. This approach to enhance image contrast is called '**dual-energy**' imaging. Enhanced contrast can also be achieved by adding a relatively heavy element to the phase of interest and adjusting the X-ray energy to levels immediately below and above the photoelectric absorption edge for the element (Wildenschild *et al.*, 2002; Van Loo *et al.*, 2012).

Quality of CT images

The quality of an image and thus the accuracy of the information that is extracted from it, depends on spatial resolution and contrast.

Contrast is a measure of how well a feature can be distinguished from the surrounding background (Wildenschild *et al.*, 2002) and is often defined as the difference in attenuation between feature and background, divided by the background attenuation. Given the strong contrast in X-ray attenuation of soil pores and associated solids, their discrimination in CT imagery is relatively easy (Taina *et al.*, 2008). Because water content has a significant influence on X-ray image contrast in samples that contain also organic components (Taina *et al.*, 2008), samples should be air-dried before scanning occurs. Contrast can be enhanced by assigning just a narrow interval of grey values to the entire grey scale (0 to 255 for an 8 bit image), called window technique (Sandborg, 1995).

Spatial resolution describes the level by which details in an image can be resolved (Wildenschild *et al.*, 2002). Two objects will not be separable in an image if the spatial resolution of the image is larger than the distance between them (Al-Raoush & Willson, 2005). Spatial resolution is mostly quantified as the minimum separation distance for which

attenuation values at two known points can be observed as separate entities and thereby accurately measured. It depends on magnification (ratio of the distance between source and detector over the distance between source and sample), focal spot size of the X-ray tube, pixel size of the detector and physical phenomena such as X-ray scattering and interaction between detector pixels (Cnudde, 2005; Sleutel *et al.*, 2008). Micro-CT scanners have a smaller focal spot size than medial scanners, and allow a closer placement of sample to the X-ray source, generating a primary magnification and enhanced resolution (Van Geet *et al.*, 2000). Moreover, a trade-off exists between sample size and spatial resolution (factor ±1000-1500, related to the number of detector pixels in the direction perpendicular to the rotation axis, provided that the focal spot size is sufficiently small). Furthermore, the capability of CT to resolve micro scale features is one thing, but interpretation of these features is only possible when the features of interest are an order of magnitude greater than the scan resolution (Grevers *et al.*, 1989). Overall, as image quality increases, so does the accuracy of measurements of the objects of interest (Nielsen, 2004). A description of different image artefacts is given in appendix I.

Grey scale histogram

Soils are composed of three main components: pores (air-or water-filled), organic matter, and mineral components (including very dense components) (see 1.1.1), with different mass densities and atomic composition causing different attenuation of X-rays. The attenuation during a CT-scan increases in the order: air-filled pores < water-filled pores or organic matter < soil mineral components < very dense mineral components. X-rays transmitted through the sample accumulate onto the detector and cause an intensity related to the number of photons. Thus X-rays passing through mineral soil will yield a lower intensity on the detector compared to those passing through air-filled pores. Eventually, accumulated intensities on the detector are inversed so that air-filled pore space is represented by black voxels, organic matter of water-filled pore space are dark grey and the mineral matrix is light grey and very dense mineral occlusions are represented by white voxels (Figure 1-8). Grey values range from 0 to 255 for an 8 bit image (Figure 1-8), with 0 and 255 representing black and white voxels, respectively. A grey scale histogram visualizes the amount of voxels of a certain grey value. Figure 1-9 visualizes the histogram of all voxels ('All') in a sub image containing only voxels that represent pores ('Air'), organic matter ('OM') and mineral components ('Min') (Figure 1-9). The peak at gray value 255 corresponds to voxels with gray values which are

larger than the maximum value shown in the histogram. Those voxels contain strongly attenuating material.
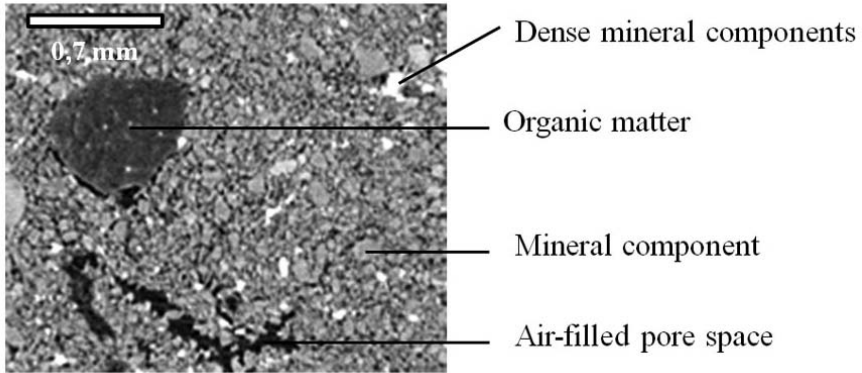
Figure 1-8: Reconstructed two-dimensional grey scale image from CT-scanning. Different grey values of voxels represent differences in X-ray attenuation resulting from differences in the material's density and elemental composition.
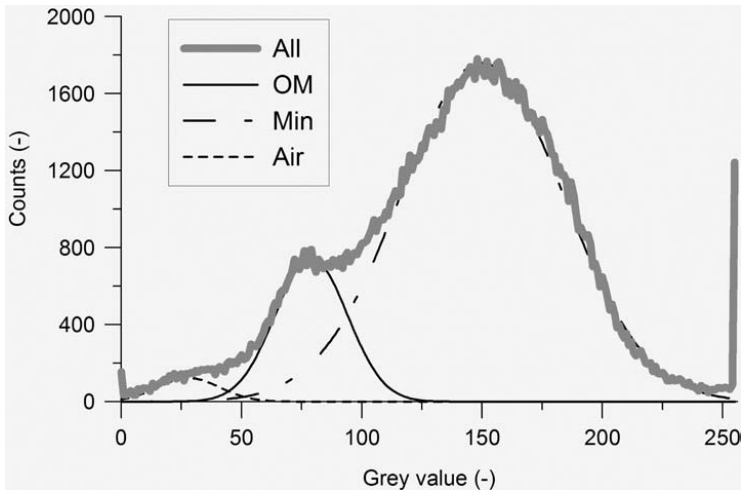
Figure 1-9: Grey scale histogram of voxels in the grey scale image (8 bit) shown in Figure 1-8 for the entire image ('All') and for sub regions of voxels representing only mineral components ('Min'), organic matter ('OM') or pores ('Air'). The peak at grey value 255 represents very dense mineral components that strongly attenuate the X-ray bundle.

1.5.2   Image analysis

Computerized image analysis was introduced in Yanuka *et al.* (1984). Software to identify pores and pore necks using stacks of successive 2D slices was described in Kwiecien *et al.* (1990).

In general, image processing follows a number of consecutive steps, which are shown in Figure 1-10. First, grey scale images are **filtered** to reduce noise, which simplifies the second step, segmentation. **Segmentation** refers to the process of partitioning a digital image into multiple segments (sets of voxels) which receive the same visual characteristics. It assigns a label to every voxel in the image, separating the background features from the ones that are interesting to analyze. This second step of image processing results in a binary image, where background voxels turn black (value 0) and foreground voxels of interest turn white (value 1). All further image processing steps are applied to these white foreground voxels. The third step is **labeling**, which assigns a label (=number) to every discrete object. Because a large part of the pore volume in soil is interconnected, this step results in one object with a large volume, and a number of small objects. In reality, the pore matrix does consist of interconnected pores, but they are connected through narrow pore necks. By determining the location of these pore necks, this large object is divided into a number of objects. This division is done in steps 4 and 5. Step 4 calculates a **distance map** which labels each voxels of an image with the distance to the nearest edge of its object. This distance map is used as input for step 5, a **watershed-based separation**. This step results in a labeled image, where each soil pore is represented by a different label number which allows analysis of these objects, step 6. A detailed description of commonly used image analysis techniques for image filtering, image segmentation and pore neck based separation of the pore space, including the ones used in this PhD thesis, are given in appendix II.
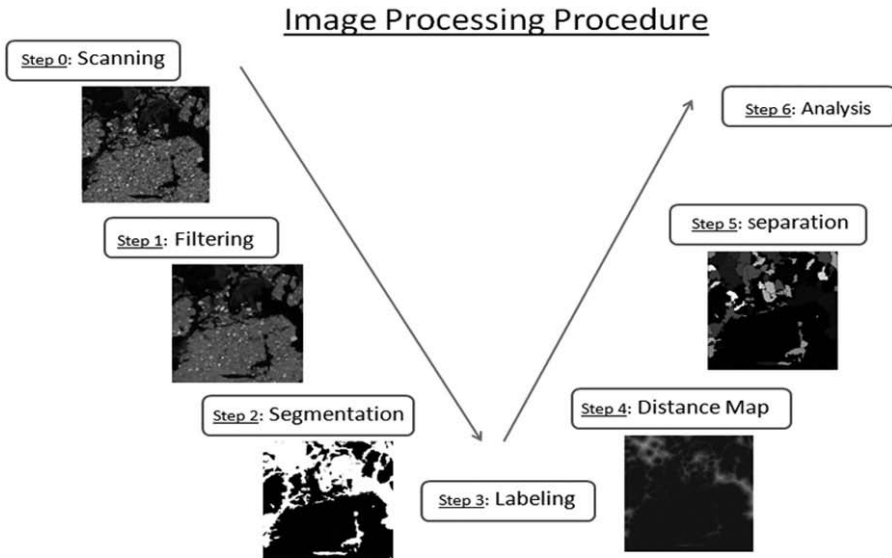
Figure 1-10: Consecutive steps of the image processing procedure.

1.5.3 X-ray CT vs. other techniques

Although traditional techniques like electron microscopy and thin sections offer higher resolutions than X-ray CT, these techniques are limited to 2D (Anderson & Hopmans, 1994). Elliot & Heck (2007) compared optical and X-ray CT technique for void analysis in soil thin sections and found that CT identified a category of pores that was often overlooked by optical imagery classification and concluded that X-ray CT could be an excellent complementary technique to optical thin section analysis. However, in a second study, they found that results from 2D and 3D thresholding of the same X-ray CT imagery yielded different pore space results, showing that the X-ray CT's ability to assess object characteristics in 3D is more promising than 2D techniques. Gregory *et al.* (2010) assessed a model that describes the effects of soil deformation and shrinkage on the WRC with the use of X-ray CT. Grevers *et al.* (1989) also compared macro pore characteristics derived from both CT image analysis and air-dried and resin-impregnated soil samples. Although shrinkage of macro pores had occurred during the hardening of the resin in impregnated soil samples, macro porosity derived from thin sections was comparable with X-ray CT calculated macro porosity. Although resinous pores resulting from impregnating porosity during the thin section creation process cannot be differentiated from SOM due to their similar density in CT images (Stoops,

2003), X-ray CT contains plenty of advantages for the study of soil structure over thin sections. Eventually, the findings of Dal Ferro *et al.* (2012) showed that both techniques reveal different pore characteristics compared to the other. They therefore emphasized that X-ray CT and traditional techniques should be combined together. After all, a single technique cannot detect the compositional heterogeneity and the architecture of biogeochemical interfaces but a combination of methods capable of determining biological, organic, and inorganic constituents of biogeochemical interfaces and of noninvasive techniques to visualize the 3D structure of these domains is promising (Rennert *et al.*, 2012). Whereas X-ray CT has been known to contribute to the latter domain, noninvasive visualization of the 3D soil structure, we believe that it also has potential for localizing organic constituents in soil.

1.5.4   X-ray CT set-up at the Ghent Centre for X-ray tomography (UGCT)

The "Centre for X-ray Tomography" of the Ghent University (UGCT) is a research facility which performs research on the X-ray micro/nanotomography technique and its applications in a scientific context (www.UGCT.ugent.be). The facility has developed and built several modular micro- and nano-CT scanners and developed the reconstruction software package Octopus and the 3D analysis software package Morpho+ which were used in this PhD thesis.

Nanowood (Figure 1-11) is the latest multi-resolution X-ray tomography setup developed at UGCT. All the X-ray CT scans in this study were performed with Nanowood. It consists of an 8-axis motorized stage combined with two X-ray tubes and two X-ray detectors, specifically designed to permit very high resolution scans as well as scans of larger objects. The two X-ray detectors are a Varian Paxscal 2520 (1820x1460 pixels of 127 μm pixel pitch) with CsI scintillator and a Photonic Science VHR (3600x3200 pixels of 7.74 μm pixel pitch) with thin gadox scintillator. Both detectors are placed on a translation and magnification stage in order to be used in combination with one of both X-ray tubes to scan small samples with low or high attenuation as well as large samples (up to 37 cm in diameter). Reconstructed voxel size can be chosen arbitrarily ranging from 200 μm to 5 0 nm with maximal scan-efficiency. The two X-ray tubes are a Hamamatsu L9181 (130 kV, 35 W source with down to 5 μm spot size) and a Hamamatsu L1711 (100/160 KV, LaB6/W filament, 3W, down to 400 nm spot size). Larger samples are scanned using the L9181 tube due to its high power while smaller samples (resolution <3 μm) are scanned with the L1711 tube due to its very small spot size. The combination of both tubes covers all resolutions in an optimal way.

The system offers a large range of operation freedom with an 8-axis motorized stage for sample rotation/magnification/positioning, tube and detector selection and tiling; all combined in versatile acquisition routines (standard or fast scanning, tilling, helix,...).
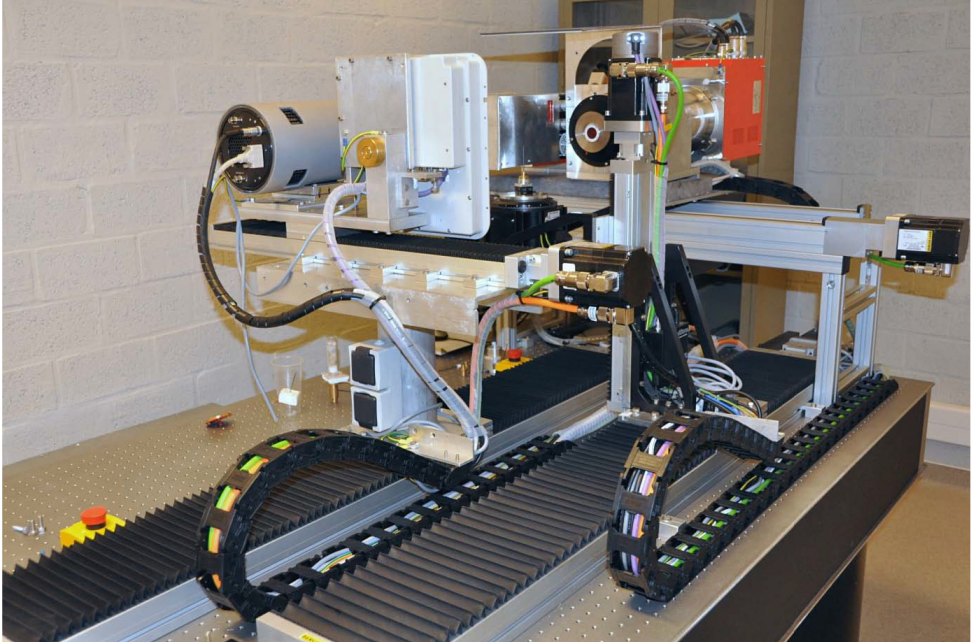
Figure 1-11: Set-up of Nanowood, a multi-resolution X-ray tomography scanner located at the laboratory of Wood Technology, a member of UGCT.

1.6 <u>Objectives</u>

This thesis aims at contributing to the fundamental study of the role which soil pore network structure plays in SOM decomposition and stabilization.

Despite the growing body of evidence showing the importance of pore structure for microbial processes such as decomposition of SOM, data is lacking for quantification of the relative importance of these stabilization mechanisms in the overall process of SOM decomposition. This lack of knowledge is largely due to the limitations of current techniques to explore the spatial organization of the soil, and particularly of the spatial location of OM and microorganisms in the soil matrix. For example, functional traits of soil structure rely on the connectivity, the tortuosity and the heterogeneity of the pore space in 3D. Aggregates or data relating to soil particles do not provide such information (Young *et al.*, 2001). By studying undisturbed soil cores instead of aggregates, soil organization is considered as a collection of aggregates sizes within the framework of the soil pore system, and this will lead to a better understanding of the complex interaction between SOM and the soil matrix. Accordingly, the general aim behind the present PhD was to investigate if the application of non-destructive X-ray CT would open up valuable new opportunities to study soil structural aspects of the biologically mediated SOM decomposition process through its ability to directly quantify the internal architecture of soil, and this in 3D.

A first objective (**objective O1**) was to develop a methodology for X-ray CT scanning and related image processing to quantify the soil pore space.

The range of particle sizes considered in individual studies that focus on the interaction between SOM dynamics and the soil matrix were often limited to a particular soil pores size: e.g. mesopores (Mayer *et al.*, 2004), fine to medium pores (Strong *et al.*, 2004) and medium to coarse pores (De Gryze *et al.*, 2006). Along with these studies only part of the whole pore size range that is relevant to the SOM decomposition process may be covered by the CT scans of soil samples. A second objective (**objective O2**) was to investigate which soil pore network characteristics can be reliably quantified from X-ray CT scans for a range of scales going from the micro aggregate level to the undisturbed soil core level.

Because a trade-off exists between X-ray CT resolution and object dimension (see 1.5.1), sufficiently small soil cores are required to achieve adequate resolution for soil biological studies. A third objective (**objective O3**) was to investigate the usage of small sample sizes in soil incubation experiments and to adapt biological assays to an X-ray CT compatible scale. The achievement of objective 3 would allow the integrated use of X-ray CT in biological experiments, providing us with valuable information on the direct influence of the soil pore network structure on SOM decomposition.

In order to fully test the relationship between soil microbial community and the soil pore network, its habitat, a combination of non-destructive 3D visualization with assays of the microbial activity would be a great step forward. A fourth objective (**objective O4**) was to investigate the impact of X-ray CT scanning itself on soil microbial functioning. We wanted to test the hypothesis that X-ray CT induces only a very limited disturbance of the microbial biomass and its activity and could therefore be applied in running soil biological studies.

The location of SOM within the soil matrix affects its availability to decomposition. Six *et al.* (2000) developed a conceptual model linking the turnover of particulate organic matter (POM) to turnover of aggregates. According to this model micro aggregates are formed within macro aggregates (which are formed around fresh residue, POM), because the intra-aggregate OM that derives from the decomposition and subsequent fragmentation of coarse POM becomes encrusted with clay. Carbon that is located within these stable micro aggregates becomes stabilized in the long term. In addition to the direct influence of soil structure on SOM dynamics, constraints in the dynamic nature of soil water and air distribution cause a spatial differentiation between soil organisms and their substrates. For example, considerable microbial activity has been related to medium sized pore space class 15-60 µm (Strong *et al.*, 2004). A fifth objective (**objective O5**) was to use X-ray CT in lab scale incubation experiments to study the relationship between pore network structure and SOM decomposition. In objective 5a, variation in pore network structure was created by artificially manipulating the soil structure in repacked soil cores, while in objective 5b variation in the soil pore structure was achieved by sampling undisturbed soil cores along a textural gradient. We hypothesized that intermediate pores are important for SOM decomposition, that SOM decomposition is retarded in fine pores and that very fine pores are responsible for SOM protection.

1.7 <u>Thesis outline</u>

The general aim of this study was to validate X-ray CT as a usable tool in biological experiments in order to reveal the relationships between soil pore architecture and soil biological functioning (<u>chapter 1</u>).

In a first study (<u>chapter 2</u>), we developed a methodology to retrieve a pore neck size distribution from the unprocessed raw CT volumes (**O1**). Different sample sizes (undisturbed soil core and three aggregate sizes) were scanned with X-ray CT to compare the spatial information which may be retrieved through CT scanning and image analysis at these sizes. An attempt was made to compare X-ray CT derived data with the pore neck size distribution calculated from the moisture retention characteristic. The scale dependent retrieval of pore characteristics was then also related to soil processes active at theses scales in chapter 2 (**O2**).

Practical constraints for the use of X-ray CT in combination with soil biological experiments were investigated in <u>chapter 3</u>. Firstly, we tested how the usage of smaller soil volumes needed for high resolution CT scanning affected measurement of soil microbial functioning (**O3**). Secondly, the effect of X-radiation on soil microbial functioning was evaluated by incubating X-radiated undisturbed soil cores (**O4**).

The importance of the pore network structure on SOM decomposition was evaluated in two separate incubation studies with disturbed and repacked soil cores on the one hand and undisturbed soil cores on the other. In the repacked soil cores, treatments of artificially altered pore network structure were combined with addition of substrate (<u>chapter 4</u>). The influence of both on C mineralization was investigated by relating the amount of C mineralization to pore neck size volumes from repacked soil cores (**O5a**). In <u>chapter 5</u>, soil pore size classes relevant to SOM decomposition were identified by measurements of the soil pore size distribution with X-ray CT and quantification of SOM decomposition during an incubation study. Undisturbed soil cores were taken in the field from a single field plot with a clear gradient in soil texture. This provided the opportunity to investigate how natural variation in the pore size distribution regulates SOM (**O5b**).

In <u>chapter 6</u>, we compared the results of all chapters in a general discussion and conclusion.

Chapter 2:

Scale-dependence of soil architecture

Abstract

Drastic improvements in resolution in the last decade allowed characterization of pore size ranges that are relevant to microbial processes in soil, including soil organic matter decomposition. However, visualization of objects in images depends on the spatial resolution. When working with digitized data, two questions should be addressed. How do the results depend on voxel size resolution and how do the results depend on the total image volume? Our objectives were to address both these questions by comparing visible pore space at different scales (core, macro, sub-macro and micro aggregate) from the same soil.

Scanning soil samples at four different scales with micro focus X-ray CT resulted in 16 datasets with voxels sizes of 27.7, 10.0, 0.6 and 0.3 µm at the soil core, macro, sub-macro and micro aggregate level, respectively (four replicates per sample level). The results for porosity, open porosity and pore connectivity all correlated significantly with voxel size, indicating that quantification of these sample properties was different between sample levels. Also all pore properties (number of necks and pores, pore density, number of neighbours and sphericity) correlated significantly with voxel size. Based on a representative elementary volume (REV) analysis we suggest minimal REV sizes for porosity measurements of approximately 21, 37, 6 and 12 (expressed as ratio between cube side length and average object diameter) for soil samples with approximate diameter of 5 cm, 2 mm, 500 and 250 µm. Although the REV analysis revealed that the original cube side length of the analyzed volume was too small at the macro and micro aggregate level for adequate porosity measurements, the use of five replicate cubes per sample for image analysis must have decreased the REV size. X-ray CT derived pore neck size distributions generally overestimated porosity compared to the water retention curve data. The dimensions of pore network characteristics in this study showed that X-ray CT data acquired at the soil core level would be useful in the study of soil processes like water flow and the alteration of the soil structure by earthworms and other soil fauna. The application of X-ray CT at the aggregate level (macro, sub-macro or micro) is more useful for the visualization of the physical environment in which microbes and grazers operate and shows potential for investigating the mutual interaction between soil structure and SOM decomposition through visualizing the habitat of soil organisms. In conclusion, X-ray CT can support scientists in interpreting the significance of soil physical organization with respect to biological functioning.

2.1 <u>Introduction</u>

Soils contain numerous interconnected micro sites that result from the spatial arrangement of solids and associated voids. Several studies have shown that soil structure is a key determinant of the intensity and rates of transport processes in soil (De Wever *et al.*, 2004; Horn & Smucker, 2005). Our understanding of the mechanisms that control soil functions including soil organic matter decomposition, remains limited as long as the spatial arrangement of the soil phases is not taken into account in future soil biological experiments.

Since the 1990'ies, X-ray CT has been applied as a tool to describe soil architecture and its 3D features. The earliest studies could only characterize macro porosity due to limited image resolutions of the X-ray CT equipment. Perret *et al.* (1999) presented in detail the geometry and topology of macro pore networks in undisturbed soil cores, showing that 4/5th of the networks were composed of only one independent pore path. Drastic improvements in resolution in the last decade allowed characterization of pore size ranges that are relevant to microbial processes in soil, including soil organic matter decomposition. De Gryze *et al.* (2006) demonstrated that microbial activity during decomposition of added plant residues shaped the morphology of pore space with a pore diameter above 27 µm, a phenomenon described earlier by Young & Crawford (2004) as 'the self-organization of the soil-microbe complex'. Similarly, Feeney *et al.* (2006) found soil biota to significantly alter their habitat towards a more porous, ordered and aggregated structure, observations that support the hypothesis that the soil-plant-microbe complex is self-organized. These studies prove that the interaction between soil structure and SOM dynamics is mutual. Nunan *et al.* (2006) investigated the habitat of microbes at even lower spatial scales (between 4.4 µm and 2 mm) and discovered a high level of heterogeneity in pore morphology. They mentioned that the importance of such structural variability for soil function has not been demonstrated yet, but that heterogeneous distributions of O_2 (Sexstone *et al.*, 1985), bacteria (Nunan *et al.*, 2003) and 2,4 D degradation (Dechesne *et al.*, 2003) at the micro scale suggest that soil function might depend on structural variability. These studies at different scales all demonstrate how our understanding of the interaction between soil structure and SOM dynamics could be improved from experiments which employ high resolution X-ray CT. Visualization of objects in images depends on the spatial resolution; e.g. Adderley *et al.* (2001) compared porosity values of undisturbed soil and sediment samples that were measured with X-ray CT and thin sections and found that the resolution mismatch between the methods (100 µm in CT vs. 30

μm in thin sections) resulted in greater porosity values for the latter. O'Donnell *et al.* (2007) mentioned that quantifying the complexity of soil-micro-organisms interactions can be difficult as system dynamics are often scale-dependent; processes that shape microbial diversity and activity at one scale may be less important at another. The selection of a technique for visualizing soil architecture directly determines at which scale information will be derived. Al-Raoush & Willson (2005) used synchrotron CT images to extract pore network features of porous media systems other than soil and they concluded that a resolution sensitivity analysis should be executed in every X-ray CT study. Lindquist *et al.* (2000) also mentioned that when working with digitized data, two questions should be addressed. How do the results depend on voxel size resolution and how do the results depend on the total image volume?

Our objectives were to address both these questions by comparing visible pore space at different scales (core, macro, sub-macro and micro aggregate) from the same soil. To do so we scanned soil samples at different scales with high resolution X-ray CT which was followed by image analysis and the effect of image resolution on pore network properties was evaluated. The assessment of water retention curve (WRC) data on the same soil cores that were scanned with X-ray CT allowed comparison of total porosity and pore neck size distributions (PND) between WRC data and X-ray CT image analysis.

2.2 **Material and methods**

2.2.1 *Soil sampling and soil characteristics*

At a depth of 30 cm, 16 undisturbed soil cores (Ø=5 cm; h=5 cm) were sampled from an arable silt loam soil (33% S, 14% C, 53% L) with C and N content of 1.1±0.3% and 0.26±0.09%, respectively, located in Heestert, Belgium (50°48' N; 3°25' E) (Figure 2-1). Three undisturbed soil cores were analyzed for their total C and N content with a Variomax CNS analyzer (Elementar Analysesysteme, Germany). Five undisturbed soil cores were mixed to a composite samples to determine soil texture by the pipette sedimentation method (Gee & Bauder, 1986).
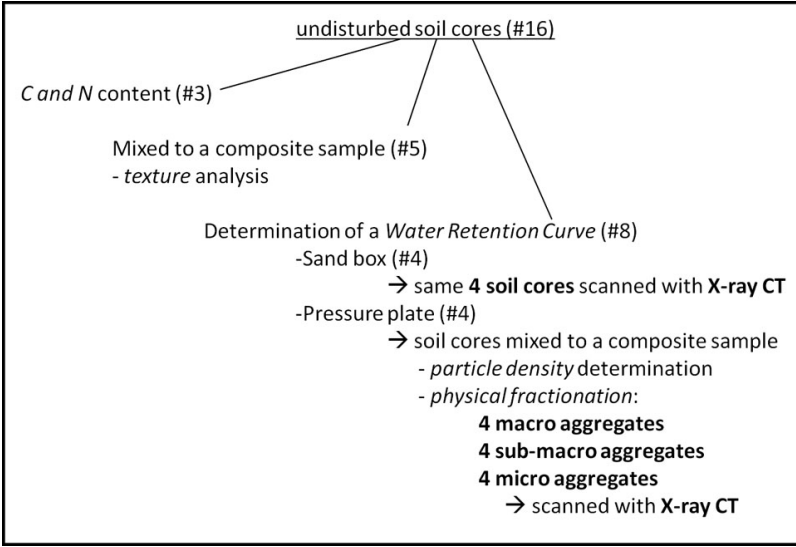
Figure 2-1: Division of 16 undisturbed soil cores among soil analyses for chemical and physical soil properties and selection of samples for X-ray CT scanning.

The remaining eight undisturbed soil cores were used to construct a WRC. Four undisturbed soil cores were places on the sand box (Eijkelkamp Agrisearch Equipment, the Netherlands) to measure volumetric moisture content at matric potentials of -1, -3, -7, -10 kPa. These four soil cores were then scanned with X-ray computed tomography (see 2.2.2). Four other undisturbed soil cores were placed on a pressure membrane (Soil Moisture Equipment, USA) to measure volumetric moisture content at the lower water tensions (-25, -150 and -1500 kPa). Afterwards air-dried soil of these four soil cores was combined to a mixed sample and was physically fractionated and used for determination of soil particle density with the pycnometer method (Blake & Hartge, 1986) to be used in porosity calculation. Bulk density of all eight soil cores was determined from the oven dry mass (105°C) of the undisturbed soil cores and the volume of the soil core. The van Genuchten (1980) water retention function was fitted to the desorption data:

$$\theta = \theta_r + \frac{\theta_s - \theta_r}{[1 + (\alpha * h)^n]^m}$$ Eq. (2)

where θ_r and θ_s are the residual and the saturated soil water content, respectively (m^3 m^{-3}), h is the soil water tension (cm), and α, n and m = 1-1/n are parameters obtained by fitting Eq. (2) to the measured water retention data. Effective pore neck sizes and PND were estimated from the soil water pressures using the capillary rise equation (Jury *et al.*, 1991).

Physical fractionation of a mixed soil sample was based on a modified scheme of the micro aggregate isolation method proposed by (Six *et al.*, 2000). Ten grams of mixed sample was consecutively wet-sieved on a 2 mm and a 0.5 mm sieve. Aggregates passing the 0.5 mm sieve were then immersed in deionised water on top of a 250 µm mesh screen and gently shaken with 50 steal beads (Ø=5 mm). Continuous and steady water flow through the device ensured that micro aggregates were immediately flushed onto a 53 µm sieve and were not exposed to any further disruption by the beads. After all 2 mm-aggregates were broken up, the material on the 53 µm sieve was rinsed with water to ensure that isolated aggregates >53 µm were water stable. Afterwards, four macro aggregates (Ø=2-3 mm), four sub-macro aggregates (Ø≈500 µm) and four micro aggregates (Ø≈ 250 µm) were randomly selected for X-ray CT scanning. The terms soil core, macro, sub-macro and micro aggregate used in this study may not be in accordance with other studies, but are used here simply to distinguish the four sample levels.

2.2.2 X-ray computed tomography and image processing

X-ray CT scanning

All the scans were performed with an in-house developed high resolution microfocus X-ray CT system (see 1.5.4). The acquisition was performed with an in-house developed acquisition framework (Dierick *et al.*, 2010) and the raw data were processed and reconstructed using the in-house developed reconstruction software package Octopus (Vlassenbroeck *et al.*, 2007). The soil cores were scanned using the directional target X-ray source (Hamamatsu L9181) and flat-panel detector (Varian Paxscan 2520). With a tube voltage of 130 kV, 255 µA tube current and 1 mm Aluminum filtration material 1000 projection images of 700 ms per projection were acquired, resulting in a dataset of 1500x1500x1500 voxels with a voxel pitch of 27.7 µm. All aggregates were scanned using the transmission target X-ray source (Hamamatsu L10711) and CCD camera with Gadox-coated fibre optic taper (Photonic science VHR). With a tube voltage of 80 kV and 50 µA tube current, 800 projection images of 800 ms per projection were acquired, resulting in a dataset of 1400x1400x1400 voxels with a voxel pitch of 10.0 µm for macro aggregates and a dataset of 700x700x700 voxels with a voxel pitch of 0.6 µm for the sub-macro aggregates. With a tube voltage of 80 kV and 30 µA tube current, 800 projection images of 1500 ms per projection were acquired, resulting in a dataset of 650x650x650 voxels with a voxel pitch of 0.3 µm. All datasets were converted to 8 bit data before image processing.

X-ray CT image processing

Scan data for all soil samples (Figure 2-2) were subjected to a similar image processing procedure to calculate porosity and distribution of PND with the in-house developed software package Morpho+ (Brabant *et al.*, 2011). Pore necks represent local minimum cross-sectional areas of the pore space. In each of the 16 datasets (4 levels*4 replicates), five cubes were randomly selected for image processing. The cube side lengths were 400, 200, 100 and 100 voxels for the soil cores, the macro, sub-macro and micro aggregates, respectively. Image analysis of these 80 squares was done following four steps: 1) single grey value threshold segmentation of the pore space with Otsu's method (Otsu, 1979), 2) two binary operations to remove foreground or background voxels that were erroneously classified during the segmentation step, 3) distance map calculation of the pore space, and 4) watershed-based separation of the pore space based on the distance map calculation resulting in a PND. For each dataset, the number of voxels classified as pore space was added for all five squares so that porosity was finally determined on a volume of $320*10^6$, $40*10^6$, $5*10^6$ and $5*10^6$ voxels for the soil cores, the macro, sub-macro and micro aggregates, respectively. Total porosity, calculated as the ratio of voxels segmented as pore space over the total number of voxels, is termed visible porosity (VP) referring to the fact that only porosity larger than the image resolution is visible on X-ray CT images. Pore volume per pore neck class for X-ray CT samples was expressed in cm^3 and multiplied by the ratio of the sample volumes for WRC determination and X-ray CT imaging to allow direct comparison of absolute X-ray CT and WRC derived pore volumes. The segmentation process was evaluated through a sensitivity analysis where VP was calculated at the threshold grey value (T) calculated by Otsu's algorithm, T-5 and T+5. Relative increase or decrease of VP was calculated as the ratio of VP at (T-5) or (T+5) to VP at T.

2.2.3   Representative elementary volume (REV) analysis

The representative elementary volume (REV) is the minimum volume of a soil sample from which a giving parameter becomes independent of the size of the sample (Bear, 1988) The method of Clausnitzer & Hopmans (1999) was applied on a single sample for each level to experimentally determine the size of a REV for assessment of porosity. Soil core 1, macro aggregate 3, sub-macro aggregate 2 and micro aggregate 3 were selected for REV analysis. The core sample was chosen randomly but the specific aggregate samples were chosen because their shape was most symmetric around their center point compared to other samples
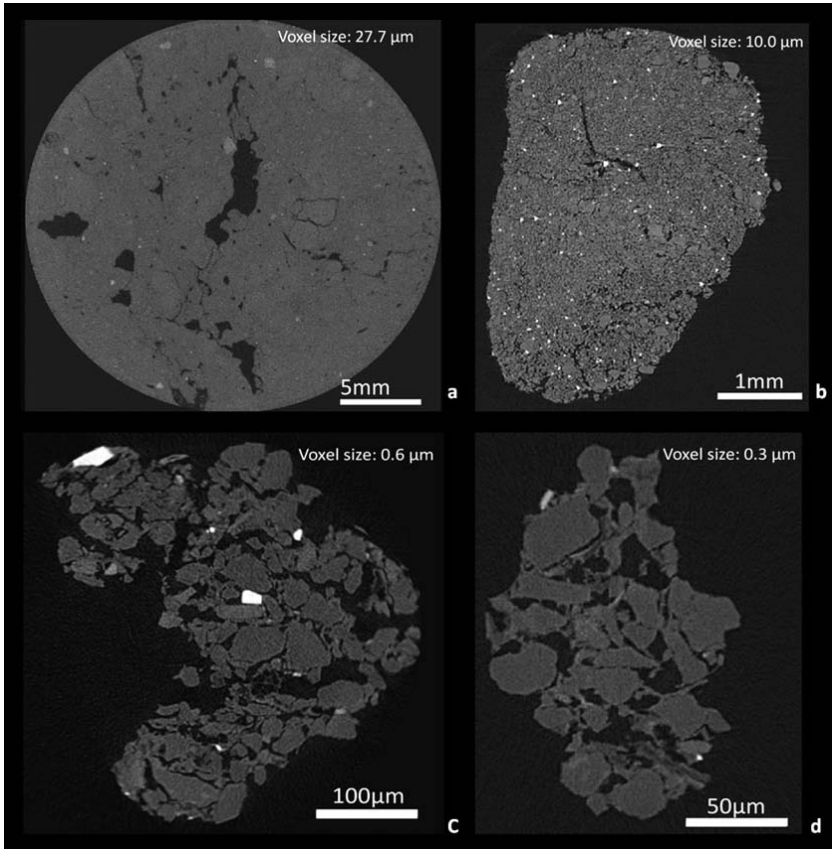
Figure 2-2: Grey-scale image in 2D of four sample levels: (a) undisturbed soil core, (b) macro aggregate, (c) sub-macro aggregate and (d) micro aggregate.

of the same level. REV analysis for these samples was performed by computing porosity of different volumes increments starting with a cylindrical volume centered at the center of the image. Two cubes were extracted per sample in the centre of the image: one centered in the pore phase, the other in the mineral phase. Initial cube sizes were 10x10x10 voxels for each sample level. Starting from these cubes, the volume was then expanded gradually by increments in all directions and for each expanded cube the porosity was recalculated. Incrementing cube side lengths were 10 voxels for soil core 1 (0.274 mm) and macro aggregate 3 (0.119 mm) and five voxels for sub-macro 2 (3.8 µm) and micro aggregate 3 (1.9 µm) with voxels sizes 27.4, 11.9, 0.76 and 0.38 µm, respectively, at each step. Porosity values for all sample cubes were obtained after segmentation at the same threshold value that was calculated during image processing earlier for the entire image (see 2.2.2). Porosity was computed and plotted for each volume increment. REV size was expressed as the ratio of the

cube side length and the average equivalent sphere diameter (Ø_{eq}) of the pores, because REV size is dependent on the dimension of the object of interest. In this study, REV sizes were determined based on the first concurrence of the two porosity curves although damping oscillation existed at higher REV sizes (see Figure 2-5).

2.2.4 Calculation of pore network properties

Several pore body and pore neck properties were calculated following image processing. First VP was calculated as the number of segmented voxels divided by the total amount of voxels in the image. Second, open porosity was the portion of porosity that is connected to the borders of the sample (Brabant *et al.*, 2011). Third, Ø_{eq} was calculated for each pore, i.e. the diameter of a sphere with the same volume as the pore (Brabant *et al.*, 2011). Fourth, connectivity was calculated as the ratio between the amount of voxels of the largest pore and the total amount of pore voxels that were segmented, before watershed-based separation of the pore space. Fifth, pore neck diameter was expressed in maximum opening, i.e., the smallest diameter of a sphere fitting in the opening of the pore neck and the adjacent pore bodies (Brabant *et al.*, 2011). Sixth, sphericity was calculated as the ratio between maximum opening and minimum closing of each pore (Brabant *et al.*, 2011). Seventh, the number of neighbouring pores was determined by counting the pores that are separated by the watershed transform from the object under consideration (Brabant *et al.*, 2011).

For each sample level, a local PND was calculated from the X-ray CT images for a number of pore neck size classes between a lower and upper boundary based on image resolution of that level. In addition, another PND was calculated from the WRC data. The PNDs were expressed as pore volume (cm^3) per pore neck class. The lower neck size boundary was equal to the voxel size, except at the sub-macro aggregate level. Upper boundaries were selected so that no pore neck size class was empty for the four repetitions of each sample level. Eventually, the local PNDs for the four sample levels had a range of 0.7-7, 2-8, 20-100 and 56-700 µm for micro, sub-macro, macro aggregates and soil cores, respectively.

2.3 **Results and discussion**

2.3.1 *Soil porosity and water retention curve*

The average bulk density at sampling was 1.56±0.03 g cm^{-3} and the average particle density, derived from pycnometer measurements, was 2.69±0.02 g cm^{-3}. Individual bulk densities and particle density measurements were used for total porosity calculations (TPV). An average WRC was modeled based on measurements of four replicate soil cores (Figure 2-3). Calculated TPV was 0.416±0.010 whereas the modeled average water content at saturation (θ_s) from the WRC was 0.405±0.013 m^3 m^{-3}. Based on the capillary rise equation, effective pore neck sizes were estimated from the soil water pressures (Jury *et al.*, 1991) and pore volume in pore neck size classes 0.7-7, 2-8, 20-100 and 56-700 µm was 10.2±0.7, 8.1±0.6, 5.5±1.1 and 1.6±1.4 cm^3 cm^{-3}, respectively.
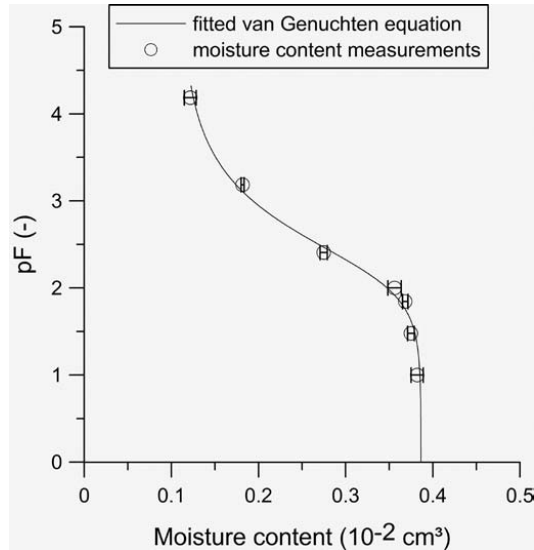
Figure 2-3: Average water retention curve of four soil cores from an arable silt loam soil, modeled by the van Genuchten equation. Horizontal error bars represent standard deviations of moisture content.

2.3.2   Segmentation procedure and sensitivity analysis

Over all sample levels, the relative decrease of VP at T-5 was smaller than the relative increase of VP at T+5 (VP -38±9, -31±5, -12±3 and -14±3% for T-5, and VP +61±99, +49±5, +16±6 and +22±13% for T+5 for core, macro, sub-macro and micro aggregates, respectively). The larger sensitivity of VP at T+5 was caused by the overestimation of VP by Otsu's algorithm during segmentation (Figure 2-4). The sensitivity of VP to the selection of the threshold value T was highest for the soil core and macro aggregate levels (area of A+B in Figure 2-4).

The use of Otsu's algorithm to segment the pore space in all soil samples resulted in an objective choice of a threshold value T allowing the comparison of measured pore network properties over all sample levels. Indeed, visual inspection of the threshold value on the histograms for four samples suggested that the pore space segmentation was acceptable (Figure 2-4). In comparison, when we tested manual segmentation, T was usually placed at the minimum frequency between two peaks on the histogram, and this resulted in slightly smaller VP values for all sample levels compared to Otsu-based segmentation.

The histograms derived from the grey scale images of the four sample levels, contained two clear distinct peaks, except for the macro aggregate level. The pore space and mineral peak maxima occurred at grey values of 34 vs. 79, 16 vs. 68 and 22 vs. 56 for soil cores, sub-macro and micro aggregates, respectively. The absence of a separate peak for pore space in the histogram of macro aggregates appears to be due to the low pore space/solid phase CT contrast at this macro aggregate level.
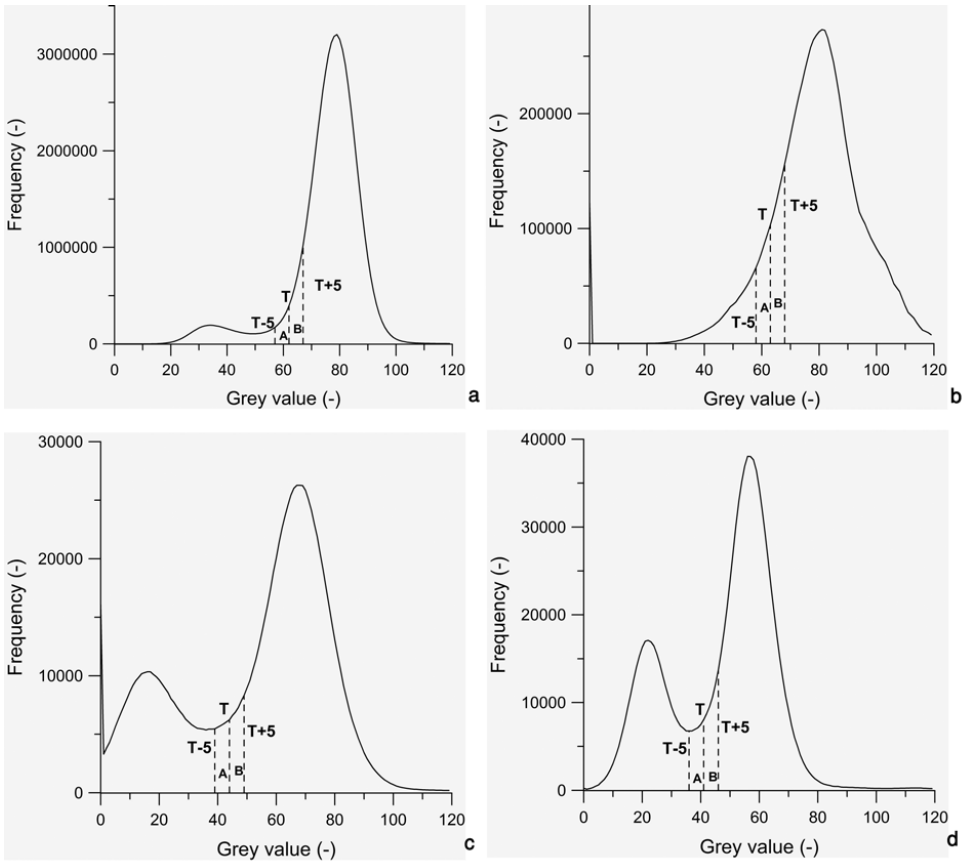
Figure 2-4: Sensitivity analysis of porosity by changing Otsu's threshold value (T), visualized on image grey value histograms of (a) soil core 3, (b) macro aggregate 4, (c) sub-macro aggregate 4 and (d) micro aggregate 4 of which a grey scale image in 2D is shown in Figure 2-2. Overestimation of T by Otsu's method causes a larger sensitivity of porosity (area B>area A) when T+5 was chosen over T-5.

A comparison between original and REV cube side length, each divided by the average pore $\emptyset_{eq}$ at the sample level of interest (Table 2-1) suggested that the initially chosen cube side lengths (400, 200, 100 and 100 voxels for soil cores, macro, sub-macro and micro aggregates, respectively) were sufficiently large for porosity measurements in soil cores and sub-macro aggregates. For macro aggregates and micro aggregates, the ratio of original cube side length and $\emptyset_{eq}$ was smaller than the REV cube side length/$\emptyset_{eq}$ ratio and this indicates that the chosen cube side lengths during image analysis were too small for porosity measurement at these sample levels.

To comply with the conditions of the REV analysis at the macro and micro aggregate level, a possibility is to increase the cube side length during image analysis to minimum 233 and 200 voxels, respectively (e.g. macro aggregates: (REV*average $\emptyset_{eq}$)/voxel size=(37x63 µm)/10 µm=233). A second option is to select a range of pore sizes (expressed as $\emptyset_{eq}$) which can be quantified adequately according to the REV analysis. For example, on the X-ray CT images of macro aggregate 3 we could quantify pores with $\emptyset_{eq}$ between 4.3 and 881 µm, but according to the REV size of 37, only pores with a maximum $\emptyset_{eq}$ of 54 µm should be taken into account (e.g. minimum $\emptyset_{eq}$=(cube side length*voxels size)/REV=(200 voxels*10 µm)/37=54 µm). Although the REV analysis suggested that our cube side length was too small for the macro and micro aggregate levels, we selected five cubes per sample for image processing. The results of the five cubes were summed and this should also have reduced the location dependence of the porosity results.

Table 2-1: Pore network properties of the four sample levels.

Sample level	Soil core	Macro aggregate	Sub-macro aggregate	Micro aggregate
Sample properties				
Sample diameter (mm)	50	2	500×10^{-3}	250×10^{-3}
Voxel size length (µm)	27.7	10.0	0.6	0.3
Original cube side length (voxels)	400	200	100	100
Cube volume	$(11080 \ \mu m)^3$	$(2000 \ \mu m)^3$	$(60 \ \mu m)^3$	$(30 \ \mu m)^3$
Porosity measurements				
Average visible porosity±stdev (%)	6.8±1.6	11.1±4.4	30.4±1.5	27.6±5.1
Proportion of open porosity	0.88	0.82	1.00	1.00
Proportion of open porosity/ Cube side length	0.22	0.41	1.00	1.00
Connectivity	0.74	0.62	0.98	0.96
Pore body properties				
Nr. of pores	15858	12922	368	290
Pore density (per mm³)	2	1113	309595	1539426
Minimum $\emptyset_{eq}^A$ (µm)	56	20	1.13	0.7
Average $\emptyset_{eq}^A$±stdev (µm)	190±184	63±39	7±5	5±4
Sphericity	0.63	0.61	0.53	0.48
Nr. of neighbours	0.4	0.6	2.5	1.8
Neighbour density (per mm³)	5.7×10^{-14}	1.6×10^{-11}	2.0×10^{-6}	9.5×10^{-6}
Pore neck properties				
Nr. of necks	2184	2231	237	126
Smallest neck maximum opening (µm)	56	20	1.13	0.7
Average neck maximum opening ±stdev (µm)	152.8±130.5	31.6±8.8	3.4±2.3	2.3±1.8
REV[B] analysis				
Original cube side length/ average $\emptyset_{eq}^A$±stdev	58.7±4.5	29.8±11.0	7.9±0.4	7.2±1.1
REV[B] cube side length/$\emptyset_{eq}^A$	21	37	6	12

[A] $\emptyset_{eq}$, equivalent sphere diameter

[B] REV, representative elementary volume
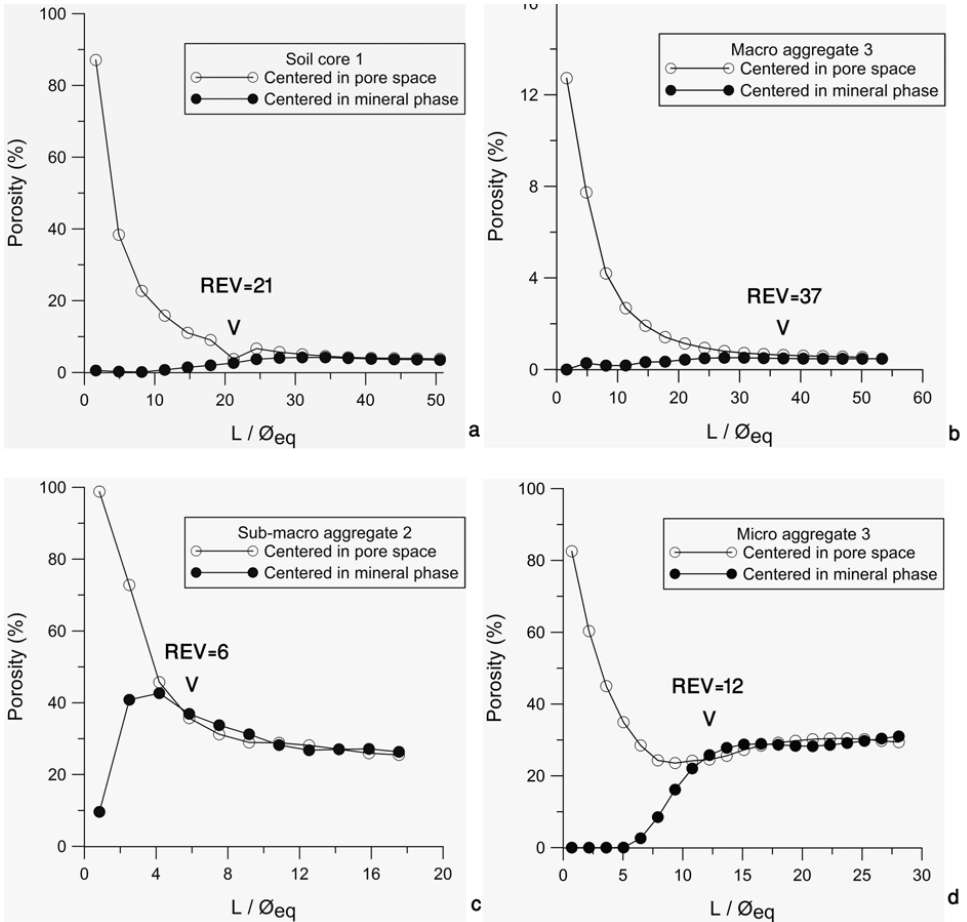
Figure 2-5: Soil porosity estimated for four sample levels: a) soil core 1, b) macro aggregate 3, c) sub-macro aggregate 2 and d) micro aggregate 3. Per sample level porosity of cubes with increasing size (L/Ø$_{eq}$) was calculated twice, once with the initial cube centered in pore space and once in the soil mineral phase (L=cube side length; Ø$_{eq}$=equivalent sphere diameter of pores).

2.3.3 Resolution dependence of sample and pore properties

Resolution dependence of sample properties

X-ray CT scanning of four sample levels resulted in **four different image resolutions**. Voxel size lengths were 27.7, 10.0, 0.6 and 0.3 µm for soil cores, macro, sub-macro and micro aggregates, respectively (Table 2-1). **Average VP** was negatively correlated with voxel size (r=-0.725; P<0.01). Adderley *et al.* (2001) also observed higher porosity in thin sections with voxel size of 30 µm compared to X-ray CT images with voxel size of 100 µm of soil sediments. In our study, ANOVA with a Tukey's posthoc test with sample level as fixed factor and four samples per level as random factor showed that VP was significantly different between the sample levels, except between the core and macro aggregate level and between the sub-macro and micro aggregates.

Proportion of open porosity and connectivity decreased with sample size (r=-0.479 and r=-0.448, respectively; both P<0.01). However, as pore network properties with large dimensions cannot be visualized at small scale, the cube side length was differently set per sample level. The negative relationship between voxel size and open porosity was probably caused by a decreasing cube side length with decreasing voxel size. Dividing open porosity by the voxel side length for each sample level still resulted in a strong negative relationship between open porosity and resolution (r=-0.916; P<0.01). According to Smucker *et al.* (2007), higher fractions of open porosity enhance the exchange of water and gases between inter-aggregate and the intra-aggregate pore volumes and thus also trigger biophysical processes in the aggregate interior. Open porosity was highest at the 250-500 µm aggregate scale, with implications for microbial decomposition processes that are depending on exchange of water and gases.

Resolution dependence of pore properties

All pore properties were significantly correlated with voxel size or sample level (Table 2-1). **Number of pores** and **number of necks** decreased both with decreasing voxel size (r=0.865 and r=0.689, respectively; both P<0.01). **Pore density** and **number of pore neighbours** per image volume increased with decreasing voxel size (r=-0.571 and r=-0.764, respectively; P<0.05 and P<0.01, respectively). This was probably caused by decreasing pore $\emptyset_{eq}$ with decreasing voxel size (r=0.982; P<0.01). Indeed, pore density and pore $\emptyset_{eq}$ were negatively correlated (r=-0.546; P<0.05).

Sphericity and voxel size were positively correlated (r=0.775; P<0.01) but this relationship was probably caused by the positive correlation between pore size and sphericity (r=0.661; P<0.01). Object shape can have consequences for object detection during image analysis. Ketcham (2005) found that spherical objects need approximately three voxel widths in diameter to be reliably identified and measured, while a fracture may be detectable even if it's within less than one voxel. As a consequence, if small pores are circular in shape, they may be more difficult to detect during image segmentation compared to elongated pores. Therefore, such small circular pores would be wrongly classified as noise which is most often deleted during pre-processing binary image operations, i.e. removal of isolated foreground or background voxels, eroding, dilating, opening, closing, and hole filling operations (Brabant *et al.*, 2011).

2.3.4 *Comparison of X-ray CT derived pore neck size distributions (PND) with water retention curve data (WRC)*

We compared PNDs retrieved from WRC data and X-ray CT image analysis. The PND calculated from WRC is based on the capillary law stating that at a certain pressure head, a water-filled pore with certain pore neck diameter will be drained. Capillarity depends not on the cross-sectional surface of the pore neck, but rather on its maximum opening. Therefore, we expressed pore neck dimensions from X-ray CT images as maximum opening, i.e. the smallest diameter of a sphere fitting in the opening of the pore neck to enable a comparison of PNDs calculated from WRC data and X-ray CT images.

The comparison of VP derived from X-ray CT and WRC data (Figure 2-6) is only meaningful at the soil core level where X-ray CT followed by image processing slightly overestimated the pore volume between 56-700 µm. A better comparison between X-ray CT-measured macro porosity (>1000 µm) and WRC data was found by Rachman *et al.* (2005).

The three aggregate levels were subsamples of a complete undisturbed soil core and the proportion of macro, sub-macro and micro aggregates in the original soil cores was unknown. Therefore, a comparison of pore volume between aggregate samples scanned with X-ray CT and soil cores from which WRC data were determined, is not completely justified. At the macro aggregate level, X-ray CT derived pore volume in the 50-100 µm class was slightly lower than WRC derived pore volume. X-ray CT derived pore volume of the other pore neck classes at the aggregate level was overestimated compared to WRC data. This general overestimation of X-ray CT pore volume compared to WRC derived pore volume can be explained by the selection of the threshold value that was slightly overestimated during image segmentation.
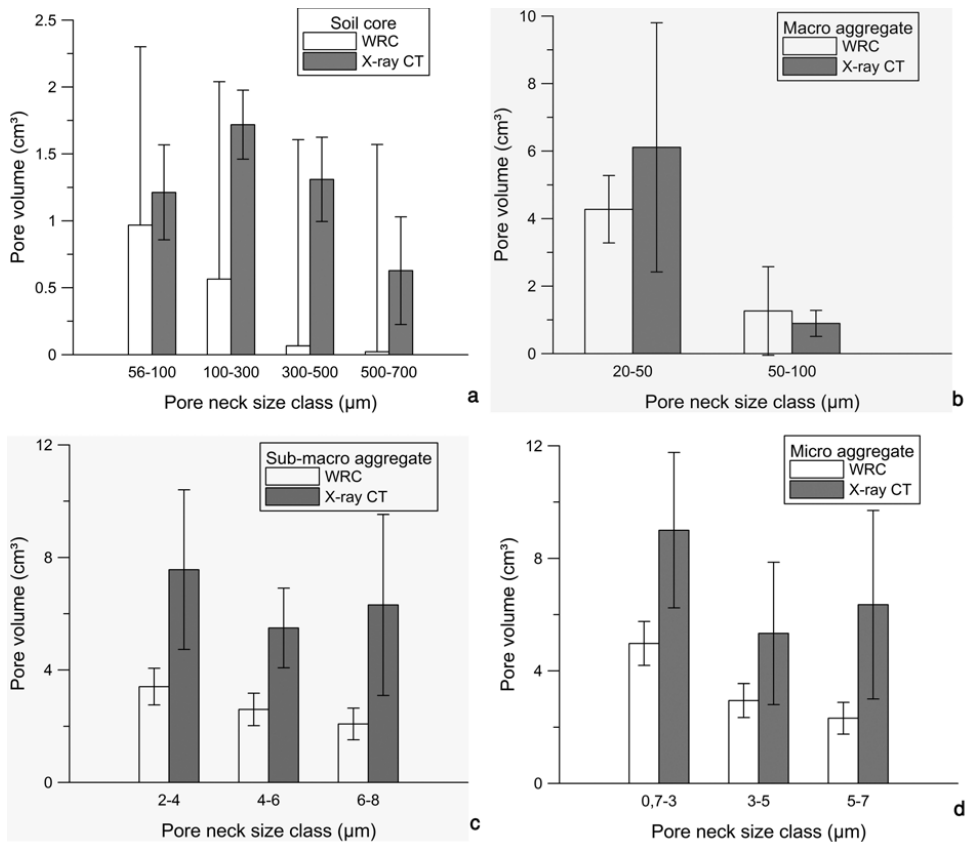
Figure 2-6: Comparison of local pore neck size distributions (PNDs, expressed as pore volume in cm³) calculated from the water retention curve and X-ray computed tomography images of four (a) soil cores, (b) macro aggregates, (c) sub-macro aggregates and (d) micro aggregates.

2.3.5   Implications for the use of X-ray CT for studying soil processes at different scales

The soil core level

At the soil core level pores with an average $\emptyset_{eq}$ of 190 µm and minimum neck diameter of 56 µm (resolution twice the voxel size, following De Gryze (2004), could be distinguished by X-ray CT. Pores with these dimensions are likely mainly useful for the study of soil water flow processes. Jarvis *et al.* (2007) also identified pores with $\emptyset_{eq}$ larger than about 0.3-0.5 mm relevant to water flow and solute transport in macro pores. Besides pore size, also pore continuity and tortuosity control the occurrence of macro pore flow (Beven & Germann, 1982). The ideal pores for water flow would be straight-sided continuous fissures and cylindrical macro pores without tortuosity (Jarvis *et al.*, 2007). Such geometrical pore characteristics could be assessed by processing X-ray CT images at this level. For example, Elliot *et al.* (2010) estimated saturated hydraulic conductivity from 3D pore characteristics (volume, surface area, and tortuosity) of intact soil cores (Ø=6.5 cm; h=7.6 cm) measured with X-ray CT. The predicted saturated hydraulic conductivity exhibited a positive correlation, indicating the potential use of X-ray CT scans at the soil core level for obtaining soil hydraulic properties.

The dimension of the soil pores visualized by X-ray CT at the soil core level is also relevant for the investigation of soil structure changes by soil fauna. Capowiez *et al.* (2011) mentioned that zones resulting from bioturbation by earthworms can be detected due to differences in grey levels on X-ray CT images. Also the resorting of soil particles by ants or termites in the construction of their nests could be visualized at this level. Measurements of macro porosity sized classes and identification of the orientation of macro porosity, constructed by soil fauna or not, are possible applications of X-ray CT at the soil core level.

The macro aggregate level

The resolution of 10.0 µm at the macro aggregate level allowed visualization of pores with an average $\emptyset_{eq}$ of 63 µm and an average pore neck diameter of 31.6 µm. The smallest identified pore neck diameter was 20 µm.

The average pore $\emptyset_{eq}$ of 63 µm at this level is highly relevant for soil biological processes like for instance C mineralization. Strong *et al.* (2004) found that soils with larger volumes of pores with necks between 15-60 µm supported faster rates of C decomposition as determined by the loss of ^{13}C from labeled wheat husks following incubation. Strong *et al.* (2004) used the moisture characteristic to calculate a PND. The present study shows that X-

ray CT images of 2-3 mm sized samples could be used as an alternative to assess pore neck size classes larger than 20 µm diameter. At this scale, X-ray CT furthermore provides pore structure information faster and more directly compared to WRC data. The pore dimensions that are visible on X-ray CT images at this level also correspond to the habitat of micro to meso fauna. Hassink *et al.* (1993) found a positive correlation between pores with necks ranging between 30-90 µm and the nematode biomass. Jones & Thomasson (1976) stated earlier that nematodes are restricted to pores with diameter >30 µm (because of their body dimensions) and <120 µm (because larger pores are mostly air-filled and are thus a barrier for nematode movement). The grazing hypothesis, stating that mineralization by bacteria is enhanced when predators are present (Hassink *et al.,* 1993), is very operative at this scale. Some studies have used the moisture characteristic to add bacteria (Wright *et al.*, 1995) or to add substrate solution (Killham *et al.*, 1993; Ruamps *et al.*, 2011) to targeted pore size classes. Ruamps *et al.* (2011), however, have acknowledged that the relationship between matric potential and the maximal neck diameter of water-filled pores is based on the assumption that the pore system can be approximated by a network of tubes, which is a simplification of reality. The validity of this relationship has never been evaluated in practice by directly visualizing the location of the substrate in the soil pore network. At this level, X-ray CT might serve as an alternative to evaluate the exact location of the added substrate in the pore system.

The sub-macro and micro aggregate level

At the sub-macro and micro aggregate level, pores had an average $Ø_{eq}$ of 7.2 and 4.8 µm and the minimal identified pore neck diameter were 1.13 and 0.7 µm, respectively. Although voxel size at the micro aggregate level was half of that at the sub-macro aggregate level, little more pore space was visualized at the micro aggregate level. Image resolution at these levels allows the investigation of physical stabilization of SOM. SOM included in aggregates is physically protected because aggregation limits substrate accessibility (Van Veen & Kuikman, 1990; Six *et al.*, 2002). Besides limited accessibility of substrate, aggregation may also influence other factors. For example, oxygen concentrations decrease towards the center of aggregates (Sexstone *et al.*, 1985), and this may also limit respiration even if substrate is accessible (Sollins *et al.*, 1996). SOM can also be stabilized through the compartmentalization of microbial biomass and grazers (Elliot *et al.*, 1980). Based on their diversity in body dimensions, different organisms reside in different pore size classes. Since there is an approximately 3:1 ratio between the diameter of pores and the body diameter of bacteria (Kilbertus, 1980), a large proportion of bacteria may occupy pores of less than 2.4

µm diameter (Rutherford & Juma, 1992). Indeed, Hassink *et al.* (1993) found a positive correlation between bacterial biomass and the volume of pores with diameters between 0.2-1.2 µm. Consequently, Rutherford & Juma (1992) called the pore space between 0.75-2 µm 'protected' pore space for bacteria because pores with a diameter of 2 µm were the lower limit of porosity available for protozoan inhabitation. All three mechanisms of physical stabilization of SOM can be studied with X-ray CT at the sub-macro or micro aggregate level.

SOM stabilization also occurs at a finer scale. Because most bacteria reside in pores with volumes larger than 0.2 µm diameter, SOM that is located in pores smaller than 0.2 µm should be protected from decomposition (Elliot *et al.*, 1980). Indeed Strong *et al.* (1999) executed a correlation analysis between soil pore size volumes and N concentrations and found an accumulation of N in pores with necks <0.6 µm, which they attributed to physical protection of organic N form microbial decomposition. Later on, a similar correlation analysis between soil pore volumes and native C content showed that C accumulated in pores with neck diameter <4 µm due to biodegradation (Strong *et al.*, 2004). Unfortunately, pores with dimensions around 0.5 µm or less could not be visualized on X-ray CT images at the sub-macro and micro aggregate level in this study.

2.4 <u>Conclusion</u>

Quantification of soil pore and network properties with X-ray CT at different levels in this study clearly suggests the potential of the technique for supporting the study of a variety of soil processes. X-ray CT data acquired at the soil core level would be useful in the study of soil processes like water flow and the alteration of the soil structure by earthworms and other soil fauna. The application of X-ray CT at the aggregate level (macro, sub-macro or micro) is more useful for the visualization of the physical environment in which microbes and their grazers operate and shows potential for investigating the mutual interaction between soil structure and SOM decomposition through visualizing the habitat of soil organisms. In conclusion, X-ray CT can support scientists in interpreting the significance of soil physical organization with respect to biological functioning. However, sample level and the concomitant image resolution do influence the results retrieved from image analysis such as pore properties and pore network architecture. The performance of a sensitivity analysis to determine the representative elementary volume for the variable of interest should always precede X-ray CT image analysis to retrieve results that are independent of the chosen sample level or image resolution.

Chapter 3:

Integrated use of X-ray CT
in soil biological experiments

Abstract

Combination of X-ray CT analysis with measures of soil microbial functioning would provide a powerful tool for revealing the influence of soil pore structure on soil organic matter (SOM) decomposition. However, soil cores with sufficient small dimensions are required for experiments that include X-ray CT scanning because a trade-off exists between sample size and X-ray CT resolution but sample size itself could affect assessment of soil processes like C mineralization. Secondly, the effect of X-ray CT scanning on microbial community structure and C mineralization has never been tested before. In order to extend the use of X-ray CT to investigate biological processes in soil rather than only physical properties, we investigated these two practical constraints.

Incubation of soil during 38 days at different sample sizes (3.5, 10 and 44 g) was found to yield different measurements of cumulative C mineralization, microbial biomass C and dehydrogenase activity. It would appear that the observed differences between the sample size were a result of deviation in the water distribution in soil after rewetting of different sized soil cores used in the incubation. There also existed an interaction between the established soil water content and this sample size effect, with a relatively smaller effect of sample size on soil biological parameters at lower moisture content. In conclusion, soil biological experiments with very small soil cores (e.g. 1 to 5 g soil) should be interpreted with caution, because sample size may affect microbial processes.

The effect of X-ray CT scanning on the microbial community and on C mineralization was investigated for the first time. Irradiation significantly affected dehydrogenase activity and PLFA biomarkers for Actinomycetes after one day. However, this effect was short-lived because after three weeks no influence was observed anymore on any of the soil biological parameters and processes (β-glucosidase and dehydrogenase activity, microbial biomass quantified by total PLFA and C mineralization). The fact that C mineralization was unaffected while there was an initial shift in microbial community structure can be explained by redundancy in microbial functions (Garcia-Pausas & Paterson, 2011). Although effects of irradiation cannot be excluded completely, this study showed that usage of X-ray micro-CT is compatible with soil biological experiments.

3.1 <u>Introduction</u>

X-ray CT has been widely used to study soil architecture, but no attempts have been made to integrate X-ray micro-CT in soil biological experiments. Combination of X-ray CT analysis with measures of soil microbial functioning would provide a powerful tool for revealing the influence of soil pore structure on SOM decomposition. However, the use of X-ray CT at a scale relevant to soil biological experiments may be limited by practical constraints. Firstly, when studying soil biological processes, CT image resolutions should match the scale at which those processes take place. Therefore, soil cores with sufficient small dimensions should be used for X-ray CT scanning because a trade-off exists between sample size and resolution (see 1.5.1). Soil processes like C mineralization and the assessment of soil biological properties such as enzyme activities may, however, be influenced by sample size. Secondly, X-radiation during X-ray micro-CT scans could possibly harm the soil microbial community and its function. However, the dose of ionizing radiation, estimated to be 10 Gy for the micro-CT scans mentioned in this chapter, is relatively low compared to the high radiation-tolerance of many soil organisms (in particular for fungi and bacteria which is about 5000 Gy, McNamara *et al.*, 2003). Consequently, there appears to be scope for using X-ray micro-CT with minimal impact on soil biological activity, but the effect of X-ray CT scanning on for example microbial community and C mineralization has never been tested before. In general we aimed to explore the possibility of using X-ray CT to investigate biological processes in soil rather than only physical ones. With the present study we aimed to (i) elucidate the feasibility of running biological experiments on an X-ray CT compatible scale and (ii) investigate whether assessment of biological parameters is possible following X-ray CT scanning.

Firstly, we investigated the effect of three different sample sizes on the assessment of C mineralization, microbial biomass and dehydrogenase activity for 20 soils at two moisture levels. Secondly, the impact of X-ray micro-CT scanning on C mineralization, enzyme activities and microbial community structure (by phospholipid fatty acid (PLFA) analysis) was evaluated for the first time.

3.2 Effect of sample size on microbial biomass function

3.2.1 Material and methods

Forty small (Ø=1.2 cm, h=2.8 cm), 40 medium (Ø=1.5 cm, h=5.3 cm) and 40 large (Ø=2.8 cm, h=6.9 cm) plastic cylinders were filled with 3.5, 10 and 44 g of 20 air-dried arable soils, respectively (Table 3-1). The 20 arable soils covered coarse to medium textures (sand to silt loam) and varied in C and N content ($1.1\pm0.4\%$ C and $0.10\pm0.04\%$ N) and pH (5.7 ± 0.7) (Table 3-1). All soils were brought to a bulk density of 1.3 g cm^{-3} by compaction and were brought to two different moisture contents (40 or 60% water-filled pore space (WFPS)) by adding water drop-wise to the surface of the repacked soil cores. All soil cores were incubated at 20°C for 42 days without lab replicates in plastic containers (Ø=2.8 cm, h=4.8 cm for small; Ø=5.2 cm, h=10 cm for medium; Ø=5.2 cm, h=10 cm for large soil cores), closed airtight with a lid and septum (Figure 3-1).
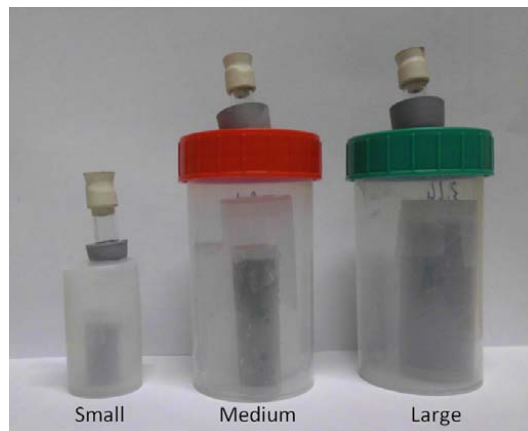
Figure 3-1: Three sample sizes (small-medium-large) were used to study the effect of sample size on measurement of biological functioning during a 42-days incubation at 20°C. Soil cores were kept in plastic containers closed airtight with a lid and septum for gas chromatography based determination of soil respiration.

We chose to work with 20 different soils without lab replicates rather than investigating fewer soils with different lab replicates to acquire a representative selection of the soil type population. Selecting 20 soils without lab replicates lead already to a drastic decrease (around 33%) of a type II error, i.e. accepting a null hypothesis that is actually false, compared to a selection of four soils with five lab replicates.

Table 3-1: Characteristics of 20 arable soils.

Sample	Sand %	Silt %	Clay %	C %	N %	C/N -	pH$_{KCl}$[A] -
Sand							
1	87	10	3	2.30	0.21	11.0	5.1
Loamy sand							
2	83	13	4	0.80	0.07	11.5	4.7
3	79	17	4	1.49	0.12	12.4	5.9
4	79	17	4	1.75	0.12	14.1	5.1
5	78	15	7	1.10	0.08	13.6	5.3
6	76	20	4	0.89	0.08	11.2	5.4
7	53	40	7	0.94	0.09	10.1	6.7
Sandy loam							
8	69	26	5	1.02	0.10	10.6	5.8
9	54	36	10	1.17	0.11	11.1	7.1
10	51	42	7	0.70	0.06	12.5	5.2
11	50	44	6	0.87	0.08	10.4	5.6
12	49	45	6	1.15	0.10	11.8	6.1
Loam							
13	51	40	9	0.64	0.06	11.7	6.0
14	46	44	10	1.58	0.11	13.8	5.9
Silt loam							
15	23	66	11	0.78	0.07	11.2	5.3
16	34	58	8	1.04	0.10	10.8	7.2
17	27	63	10	0.97	0.10	10.0	5.5
18	25	64	11	1.00	0.10	10.1	6.3
19	23	66	11	0.78	0.07	11.2	5.3
20	20	68	12	1.65	0.16	10.2	4.9

[A]measured at 1:2.5 ratio

To maintain similar soil headspace air volume ratios over all sample sizes, two cylindrical plastic objects (Ø=1.5 cm, h=5.3 cm and Ø=3.2 cm, h=7.4 cm) were added to the medium sized containers. To minimize water loss during incubation, the air humidity in the incubator was kept at 80% relative humidity level. Carbon mineralization was monitored by sampling the headspace in the incubation containers, using a 250 µl syringe, at days 2, 3, 6, 9, 14, 22, 31 and 38 and measuring the CO_2 concentration with a gas chromatograph fitted with ECD detector (Thermo Electron Trace GC Ultra). Because CO_2 concentration in the headspace of the incubation container was at all times <1%, we assume that C mineralization was not limited by CO_2 concentrations (Chen *et al.*, 2010). During incubation, soil moisture content was monitored by weighting the samples on day 6 and 22 for the 40% WFPS treatment (40.7±1.4% WFPS and 40.8±1.2% WFPS, respectively) and on day 8, 15 and 20 for the
60% WFPS treatment (60.6±1.3% WFPS, 60.3±1.3% WFPS and 60.9±1.4% WFPS, respectively) and no large moisture losses were observed.

A parallel first- and zero-order kinetic model was fitted to the C mineralization data for each soil core, assuming that SOM can be divided into two components, an easily decomposable fast pool (f) and a more stable slow pool (s):

$$C(t) = C_f*(1-e^{-kf*t})+k_s*t \qquad \text{Eq. (3)}$$

with C(t), the cumulative amount of substrate (i.e., C) mineralized in mg C kg^{-1} at time t (in days), C_f the size of the fast pool in mg C kg^{-1}, k_f the first-order C mineralization rate constant of the fast SOM pool (day^{-1}) and k_s the zero-order C mineralization rate constant of the slow soil organic matter (SOM) pool (mg C kg^{-1} day^{-1}) (Sleutel *et al.*, 2005). The parameters C_f, k_f and k_s of this first- and zero-order kinetic model were determined through non-linear regression using the Levenberg-Marquardt algorithm in SPSS 15.0. Soil 17 was excluded from the analysis of C mineralization because of its extremely high 38-days cumulative C mineralization (C$_{cum,38}$) of the medium soil core (104.7 mg kg^{-1} exceeded the average of 43.4±20.0 mg kg^{-1}).

C mineralization was measured until day 38 but all soil cores were further incubated until day 42, when destructed samples were taken for measurement of microbial biomass C (MBC) and dehydrogenase activity. MBC was determined by using the fumigation-extraction technique (Vance *et al.*, 1987). For each soil, 1 g of both fumigated soil and non fumigated controls were extracted with 10 ml 0.5 M K$_2$SO$_4$ for all sample sizes. Immediately after extraction, the extracts were analyzed for their organic C contents with a TOC analyzer

(TOC-V$_{CPN}$, Shimadzu Crop., Kyoto, Japan). For conversion from organic C contents in the extracts to MBC in the soil a k$_{EC}$ value of 0.45 was assumed (Joergensen, 1996). Soil 12 was excluded from further statistical analysis of MBC data based on its extreme value for large soil cores (2026 mg g^{-1} exceeded the average of 586±369 mg g^{-1}).

Dehydrogenase activity was determined on all samples according to a procedure by Casida *et al.* (1964) modified for small sample sizes. One, 1 and 5 gram of moist soil were weighed in glass vials, and 0.5, 0.5 and 2 ml 3% solution of triphenyltetrazolium chloride and 0.5, 0.5 and 2 ml Tris buffer pH 7.8 were added to the moist soil of the small, medium and large soil cores, respectively. Soil suspensions were incubated in the dark for 24 h at 37°C. After incubation, 5, 5 and 20 ml of methanol was added to each vial of the small, medium and large soil cores, respectively, and the vials were shaken in the dark for 2 h on a linear shaker (125 rev min^{-1}). Filtrates were collected in 10 (small and medium soil cores) or 25 ml (large soil cores) volumetric flasks. To extract all produced triphenyl formazan, the remaining soil in the vials was washed twice with methanol, following which filter papers were also washed twice. Filtrates in the volumetric flasks were made up to 10, 10 or 25 ml with methanol. Absorbance of the filtrates at 485 nm was measured with a Hitachi 150-20 spectrophotometer. All measurements were carried out including one blank.

Pearson's correlation coefficients were calculated between C$_{cum,38}$, MBC and the dehydrogenase activity using SPSS (SPSS version 15.0, SPSS Inc., Chicago). Analysis of variance and Tukey's posthoc test were used to compare means of C$_{cum,38}$, MBC and dehydrogenase activity between the three sample sizes and two moisture treatments (40 and 60% WFPS).

3.2.2 Results

C mineralization

Overall, after an initial peak mineralization, the C mineralization rate stabilized after the first two weeks of incubation for the 40% WFPS treatment soils only, while it gradually kept on decreasing during the entire 38 days of incubation for the 60% WFPS treatment soils (Figure 3-2a,b). In general, the R^2 values of the fitted first- and zero-order kinetics model were close to one for all the treatments, implying that the selected model described the mineralization process appropriately (Figure 3-2c,d). C$_{cum,38}$ was significantly higher at 60% WFPS compared to 40% WFPS, for small ($P<0.01$), medium ($P<0.01$) and large soil cores ($P<0.05$) (Figure 3-2e). At 60% WFPS, C$_{cum,38}$ was significantly higher ($P<0.01$) for the

medium soil cores (82.2 ± 22.9 mg kg^{-1}) than for the small and large soil cores (52.6 ± 18.9 and 48.2 ± 12.4 mg kg^{-1}, respectively). At 40% WFPS, $C_{cum,38}$ was significantly lower ($P<0.01$) for the large soil cores (36.00 ± 11.1 mg kg^{-1}) than for the medium soil cores (49.5 ± 15.4 mg kg^{-1}) but was not different with small soil cores (40.5 ± 14.6 mg kg^{-1}).

Microbial biomass Carbon

Moisture content had a strong effect on MBC. At 60% WFPS, MBC was significantly higher compared to 40% WFPS for all sample sizes ($P<0.01$). An effect of sample size on MBC was observed at both moisture contents, although the nature of the effect was different (Figure 3-3). At 60% WFPS, MBC was significantly lower for the medium soil cores (284 ± 159 mg g^{-1}) than for the large (596 ± 377 mg g^{-1}; $P<0.05$) and small (774 ± 486 mg g^{-1}; $P<0.01$) soil cores. At 40% WFPS, MBC was significantly higher for large soil cores (110 ± 91 mg g^{-1}) than the medium (55 ± 54 mg g^{-1}; $P<0.05$) and small soil cores (29 ± 55 mg g^{-1}; $P<0.01$).

Dehydrogenase activity

The effect of sample size on dehydrogenase activity was different between moisture contents (Figure 3-4). Dehydrogenase activity was similar between sample sizes at 60% WFPS. In contrast, dehydrogenase activity at 40% WFPS was significantly ($P<0.05$) different between all three sample sizes and increased from small (4.7 ± 3.1 µg PNP g^{-1}) to medium (10.6 ± 5.9 µg PNP g^{-1}) and large (15.0 ± 5.3 µg PNP g^{-1}) soil cores. The effect of moisture content on dehydrogenase activity was different between sample sizes. For small soil cores, dehydrogenase activity was significantly ($P<0.01$) higher at 60% WFPS compared to 40% WFPS. In contrast, dehydrogenase activity was significantly ($P<0.01$) lower at 60% WFPS compared to 40% WFPS for large soil cores. For medium soil cores, no significant influence of moisture content on dehydrogenase activity was observed.
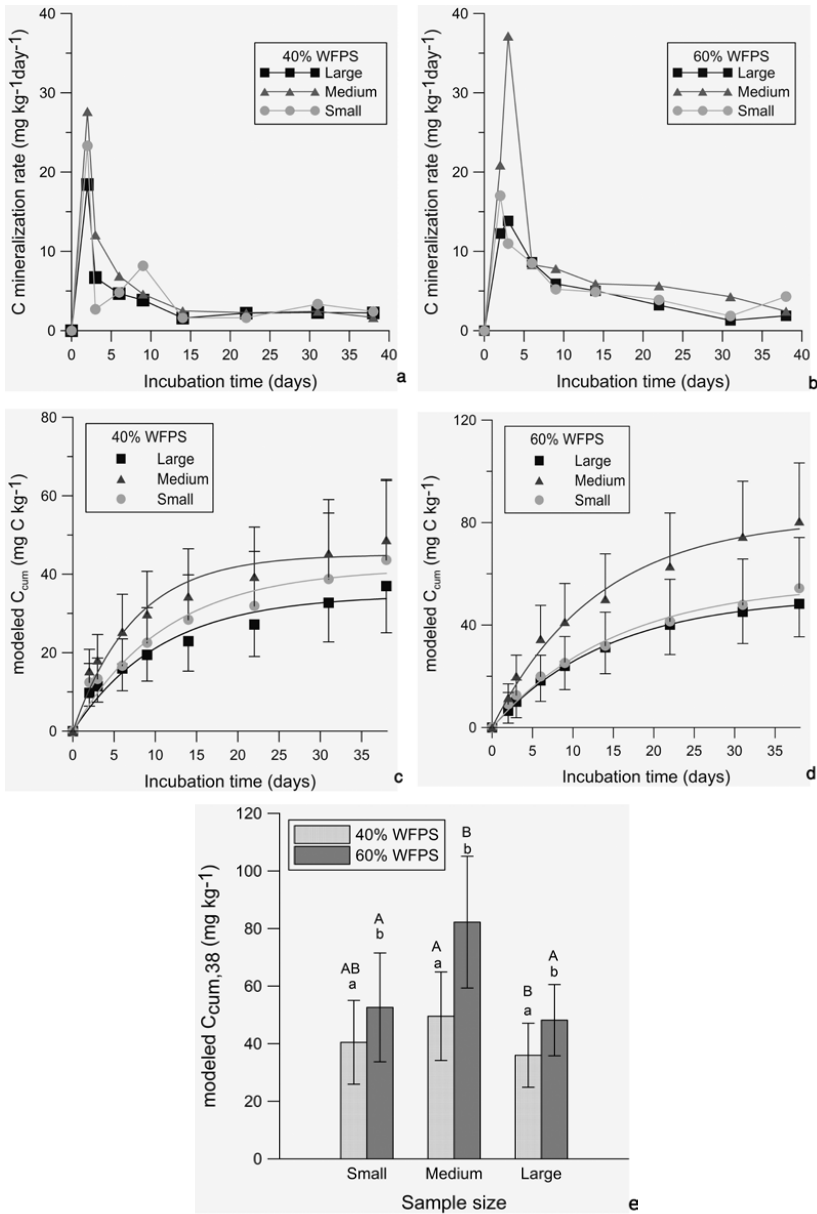
Figure 3-2: (a,b) Evolution of measured soil C mineralization during 38 days, **(c,d)** modeled time evolution of the cumulative C mineralization (C_{cum}) (error bars are standard deviations) and **(e)** modeled total cumulative C mineralization after 38 days ($C_{cum,38}$) for three sample sizes (small-medium-large) and two moisture contents (40% and 60% water-filled pore space (WFPS), respectively). Statistically different moisture treatments are indicated by different lowercase letters. Statistically different sample size treatments are indicated by different capital letters.
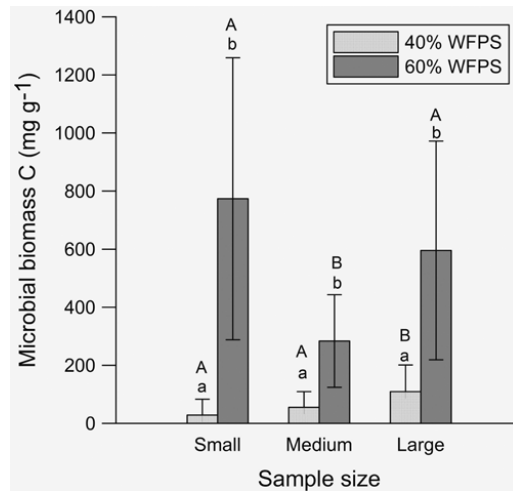
Figure 3-3: Microbial biomass carbon C for three sample sizes (small, medium and large soil cores) and two moisture contents (40 and 60% water-filled pore space (WFPS)). Statistically different moisture treatments are indicated by different lowercase letters. Statistically different sample size treatments are indicated by different capital letters.
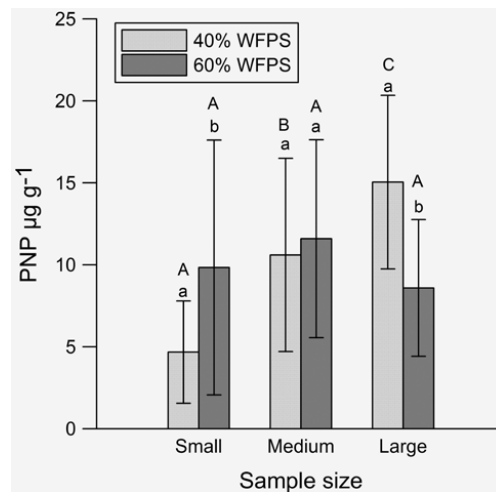
Figure 3-4: Dehydrogenase activity (PNP, p-nitrophenol) at day 42 of incubation for three sample sizes (small-medium-large) and two moisture contents (40 and 60% water-filled pore space (WFPS)). Statistically different moisture treatments are indicated by different lowercase letters. Statistically different sample size treatments are indicated by different capital letters.

3.2.3 Discussion

The difference in average $C_{cum,38}$ for all treatments and sample sizes between 40% and 60% WFPS was relatively smaller (30%) than findings (60%) by Linn & Doran (1984). High C mineralization rates during the first week of incubation at both moisture contents were probably caused by biomass-C released by a less negative water potential and desiccated biomass-C (Birch, 1958; Soulides & Allison, 1961; Sorensen, 1974; Kieft *et al.*, 1987). The difference of peak magnitude of soil respiration between sample sizes during the first week suggests that sample size has an effect on C mineralization rate in early stages of incubation. At 40% WFPS, C mineralization rate of the small and medium soil cores was on average 1.7 times higher for days 2, 3 and 6 compared to C mineralization rate of the large soil cores. At 60% WFPS, C mineralization rate of the medium soil cores was 1.8 and 1.7 times higher than in the small and large soil cores, respectively. Possibly, the differences in soil core dimensions could have caused different water distribution between sample sizes. In this study, water was added to dry soil in repacked soil cores, and logically the distribution of water to the bottom of soil cores with larger dimensions could take more time compared to smaller soil cores. In line with this hypothesis, maximum mineralization rates at the beginning of the incubation should occur faster for small soil cores compared to larger ones. At 60% WFPS, this is indeed the case, namely the large and medium soil cores reach their maximum C mineralization rate at day 3 while C mineralization in the small soil cores already peaked earlier at day 2 (Figure 3-2b). But no such time differences in maximum mineralization rates between sample sizes were found at 40% WFPS (Figure 3-2a). It is possible that soil cores at 40% WFPS already reached their maximum mineralization rates before day 2 when no measurements were taken yet. Logically, with less water to be distributed, the problem of delay in water distribution would also become smaller at 40% WFPS. These differences in C mineralization flush between sample sizes in the first week of the incubation determined largely the outcome of $C_{cum,38}$. At day 6 of incubation, on average $43\pm8\%$, $52\pm10\%$, $40\pm10\%$ of total $C_{cum,38}$ for small, medium and large soil cores was already mineralized.

At 40% WFPS, both MBC and dehydrogenase activity were found to increase with increasing sample size (only significant for MBC of largest soil cores and all significant for dehydrogenase activity). Surprisingly, $C_{cum,38}$ did not follow the same trend as MBC and dehydrogenase activity with sample size, because $C_{cum,38}$ was lowest for the large soil cores. Consequently, $C_{cum,38}$ did not correlate with MBC nor with dehydrogenase activity at 40% WFPS. The same trend of MBC and dehydrogenase activity with sample size was confirmed

by a linear correlation analysis (r=0.440; P<0.01). Dehydrogenase is an intracellular enzyme participating in the processes of oxidative phosphorylation of micro organisms (Alef & Nannipieri, 1995) and is thus linked with microbial respiratory processes (Moeskops *et al.*, 2010). According to Rice *et al.* (1996), the magnitude of MBC may indicate potential rate of C flux. Moreover, Wang *et al.* (2003) hypothesized that MBC is the main determinant of soil respiration when temperature and/or moisture level are not ideal (in our case, at 40% WFPS). All these findings indicate that $C_{cum,38}$ should be correlated somehow with MBC and dehydrogenase activity. On the contrary, Franzluebbers *et al.* (1996a; b) found only a strong positive correlation with CO_2 flush when MBC was determined after fumigation-chloroform extraction. In contrast, a poor relationship between CO_2 flush and MBC was determined with the classical fumigation-chloroform incubation method (meaning that an incubation precedes the extraction). Wang *et al.* (2003) found similar results and concluded that a larger available C pool in the air-dried samples caused a closer relationship between MBC and the CO_2 flush following rewetting of dry soil, in contrast to when the soil is pre-incubated. In our experiment, the initial CO_2 flush had disappeared by the time MBC was determined (on day 42 of incubation) by the fumigation-extraction method. In line with the findings of Franzluebbers *et al.* (1996a; b) and Wang *et al.* (2003), we found a very weak linear correlation between MBC and $C_{cum,38}$ at 40% WFPS (r=-0.112).

At 60% WFPS, MBC and dehydrogenase activity did not follow similar trends with sample size and consequently both variables did not correlate significantly. However, at 60% WFPS, $C_{cum,38}$ did correlate with both MBC (r=-0.406; P<0.01) and dehydrogenase activity (r=0.468; P<0.01). Although substrate availability and not MBC is the principal determinant to soil respiration under favorable temperature and moisture conditions according to Wang *et al.* (2003), our results show otherwise. The moisture level of 60% WFPS was considered to be a favorable condition for soil respiration in our study based on the findings of Linn & Doran (1984) who found maximum aerobic microbial activity at 60% WFPS for laboratorial incubated soil. Thus at 60% WFPS, the decrease in $C_{cum,38}$ for small and large soil cores compared to medium soil cores was probably linked with a decrease in dehydrogenase activity even though MBC did not show this decrease.

Our hypothesis that the effect of sample size on C mineralization is actually caused by time differences in water distribution and that this problem increases with increasing moisture content, does not explain why the medium soil cores have higher mineralization rates during the entire incubation at 60% WFPS. Fact is that medium soil cores had a lower surface/soil

volume ratio (0.39) then small and large soil cores (0.48 and 0.98, respectively) but we expected rather a decline in C mineralization as a consequence of this; a larger surface/soil volume ratio could have limited gas diffusion such as oxygen supply or removal of CO_2 gas between the soil volume and its environment. Therefore, we can rule out the surface/soil volume ratio as a possible influence on C mineralization. We cannot, however, explain what caused the increased $C_{cum,38}$ of the medium soil cores at 60% WFPS.

3.2.4   Conclusion

Using different sample sizes for assessment of microbial regulated processes in soil may alter measurements of C mineralization, microbial biomass C and dehydrogenase activity. Largest differences were found at the highest moisture level (60% WFPS) and in the early stage of the incubation (first week). Differences in the time occurrence of the initial peak C mineralization might be explained by differences in time needed for diffusion of added water to these differently sized soil cores. Such effects could possibly be ruled out by comparing C mineralization after a pre-incubation period. Yet, still the experiments indicated inconsistent but significant differences in biological parameters (MBC, dehydrogenase activity) measured after 42 days at different sample levels. Still, at given sample size and experimental conditions, we can examine effects of different soil treatments (e.g. variation soil pore network structure, different soil moisture levels) on key soil biological parameters like soil respiration, microbial biomass C and enzyme activities. However, extrapolation of the outcomes to larger scales can only be done with care and this limits comparison with previous studies, most often carried out on larger soil masses.

3.3 Influence of X-radiation on microbial biomass function

3.3.1 Material en methods

Four arable fields and one forest site were sampled by taking 15 soil augerings in a cross pattern to a depth of 30 cm (Table 3-2).

Table 3-2: Characteristics of four arable soils (Vo, Ot, Be & Ma) and one forest soil (Go).

Soil	pH_{KCl}	Texture	Sand	Silt	Clay	OC[A]
			%	%	%	%
Vosselare (Vo)	5.91	Loam	46	44	10	1.0
Otegem (Ot)	6.25	Silt loam	25	64	11	1.1
Beernem (Be)	5.72	Silt loam	26	60	14	4.3
St-Margriet (Ma)	7.92	Sandy loam	63	22	15	1.2
Gontrode (Go)	2.95	Loamy sand	85	11	4	3.7

[A]OC, organic carbon

The soil was homogenized, dried at room temperature and then passed through a 2 mm sieve. Sixty soil cores (Ø=3.35 cm, h=4 cm) were repacked with these five soils to a bulk density of 1.3 g cm^{-3} and were moistened to 50% WFPS (equivalent to 0.21 g g^{-1} gravimetric moisture content). After a two-week pre-incubation, half of the soil cores (30, i.e. six replicates per soil) were scanned using the X-ray nano-CT set-up at the Ghent University Centre for X-ray Tomography (see 1.5.4) fitted with a directional target microfocus tube operating at 100 kV and 255 µA (25.5 W), using a 2 mm aluminium filter. The samples, placed at a distance of 124 mm from the X-ray source, were irradiated for 45 min. All cores were then stored overnight at 4°C. The next day (day 1), 15 irradiated soil cores and 15 controls were analysed for β-glucosidase and dehydrogenase activity (except for the Go soil), and microbial community structure by PLFA analysis as described in the next paragraph. The other 30 soil cores (15 irradiated and 15 controls) were incubated for 21 days at 20°C in airtight containers fitted with a septum. Carbon mineralization was monitored by sampling the headspace in the containers with a 250 µl syringe and by measuring its CO_2 concentration with a gas chromatograph (Thermo Electron Trace GC Ultra) fitted with an ECD detector, at day 1, 3, 6, 9, 13, 17 and 21. At the end of the incubation, the soil cores were analysed for the same parameters as on day 1 (Figure 3-5).
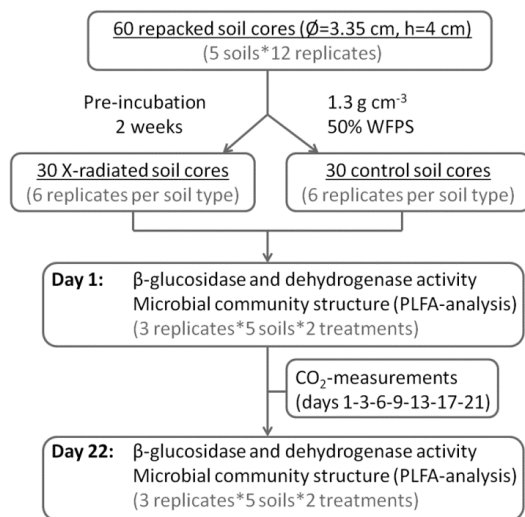
Figure 3-5: Schematic representation of incubated X-radiated and control soils, enzyme activity measurements and microbial community structure assessment on days 1 and 22 of incubation.

Determination of Phospholipid Fatty Acids (PLFAs) followed a procedure as described in Moeskops *et al.* (2010). Four gram freeze-dried soil was weighed in glass tubes. Then, 3.6 ml phosphate buffer pH 7.0, 4 ml chloroform and 8 ml methanol were added. The tubes were shaken for 1 hour and afterwards centrifuged for 10 min (2500 rev min^{-1}). The supernatant was decanted in new glass tubes and 3.6 ml phosphate buffer and 4 ml chloroform were added. Samples were left overnight for phase separation. The next day, the lipid layer was transferred to new tubes. The remaining phase was washed with 3 ml chloroform to remove any remaining lipids. The combined lipid fraction was dried under N_2. Phospholipids were separated from the lipid extracts by solid phase extraction, using silica columns (Chromabond, Macherey-Nagel GmbH, Düren, Germany). After discarding neutral and glycolipids by chloroform and acetone respectively, phospholipids were eluted using methanol. The methanol fraction was dried under N_2. The dried phospholipids were then dissolved in 1 ml methanol:toluene (1:1 vol:vol) and 1 ml 0.2M methanolic KOH. Samples were incubated at 35°C for 15 min to allow transesterification to methyl esters. After cooling to room temperature, 2 ml hexane:chloroform (4:1 vol:vol), 1 ml 1M acetic acid and 2 ml water were added to the tubes. After vortexing, the samples were centrifuged for 5 min (2000 rev min^{-1}). The hexane layer, containing the methylated PLFAs, was transferred to pointed tubes. The aqueous phase was washed twice with hexane:chloroform. The combined hexane phase was

dried under N_2. The fatty-acid methyl esters were finally dissolved in 0.3 ml of hexane containing methyl nonadecanoate fatty acid (C19:0) as an internal standard. PLFAs were determined by GC-MS on a Thermo Focus GC combined with a Thermo DSQ quadrupole MS (Thermo Fisher Scientific Inc., Waltham, USA) in electron ionization mode. Samples were injected on a Varian capillary column CP Sil 88 (100 m*0.25 mm i.d., 0.2 μm film thickness; Varian Inc., Palo Alto, USA).

3.3.2 Results and discussion

Soil, being a random factor in the ANOVA model, significantly affected all biological soil parameters ($P<0.01$). Activities of β-glucosidase and dehydrogenase were in the order Be>Ma>Ot>Vo both at day 1 (41.7±6.2, 32.9±2.6, 28.1±0.9, 14.4±0.6 and 7.9±1.2, 3.4±0.8, 0.8±0.2, 0.5±0.8 μg PNP g^{-1}, respectively) and day 22 (41.4±3.8, 30.1±0.9, 23.7±2.5, 12.8±1.2 and 22.7±3.1, 7.3±2.6, 1.7±0.8, 0.9±0.4 μg PNP g^{-1}, respectively). The average C mineralization rate was in the order Be>Vo>Go>Ot>Ma (3.0±1.2, 2.5±0.5, 1.2±0.4, 1.1±0.7 and 1.0±0.6 mg C kg^{-1} day^{-1}, respectively). Total PLFA contents were in the order Be>Ma>Go>Vo>Ot at day 1 (10.6±0.7, 8.0±0.2, 6.7±0.2, 5.5±0.0, 5.4±0.0 nmol g^{-1}, respectively) and in the order Be>Go>Ma>Vo>Ot at day 22 (10.2±5.1, 9.0±0.3, 8.3±0.8, 6.2±0.6, 5.7±0.4 nmol g^{-1}, respectively).

ANOVA for day 1 and day 22 separately, with irradiation as fixed factor and soil type as random factor, showed that β-glucosidase activity in soil cores one day after irradiation (29.7 μg PNP g^{-1}) was not significantly different from the controls (28.8 μg PNP g^{-1}). A small but significant decrease ($P<0.05$) of dehydrogenase activity at day 1 in irradiated samples compared to controls (2.8 and 3.5 μg PNP g^{-1} respectively) suggested some reduction in aerobic microbial activity (Alef & Nannipieri, 1995). However, this effect had disappeared by day 22, when activities of both β-glucosidase (27.7 and 26.1 μg PNP g^{-1}) and dehydrogenase (8.8 and 7.5 μg PNP g^{-1}) were not significantly different between control and irradiated samples, respectively. For the significant treatment effect on dehydrogenase activity, no significant interaction with the random factor soil was found. Moreover, a repeated measures model of ANOVA also showed no significant effect of irradiation on C mineralization rate. Stotzky & Mortensen (1959) also found no significant difference in CO_2 production in peat cores following γ-irradiation with doses up to 2.5 kGy, a dose which is several orders of magnitude higher than the average dose during X-ray micro-CT scanning (here about 5 Gy). The sensitive response of dehydrogenase activity (an endo-enzyme) to irradiation is in

agreement with the general high sensitivity of this enzyme to disturbances in soil (Moeskops *et al.*, 2010).

Total PLFA was not significantly different between irradiated soil cores and controls at both day 1 (7.3 and 7.1 nmol g^{-1}) and day 22 (7.5 and 8.3 nmol g^{-1}), respectively. ANOVA showed no significant differences in PLFA biomarkers between irradiated and control soils (Table 3-3), with the exception of those representative for the Actinomycetes group, which increased significantly one day after X-ray micro-CT scanning on average for all soil types ($P<0.05$). A change in microbial community structure not altering the C mineralization rate was also found by Garcia-Pausas & Paterson (2011) and was explained by redundancy in microbial functions, i.e. multiple populations mediating common processes. Principal Component Analysis (PCA) analysis of individual PLFAs showed no shift in microbial community following irradiation (Figure 3-6a). Most of the variation in the PLFA patterns was due to replicates in PLFA analysis explained by the first principal component (49.9% of total variation), where loadings 20:5, 15:0, a17:0 and 18:1ω9 all significantly differed between batches ($P<0.01$; Figure 3-6b). The two replicates of each treatment (five soils, irradiated vs. control treatment and 1 day vs. 22 days of incubation) were divided among two batches, so that variation between batches is actually variation in replicates. The second component (24.0% of total variation) separated PLFAs between the forest soil Go and the four arable soils, explained by higher relative abundances of 10Me16:0 and cy19:0 in the forest soil (9.0±0.7% and 3.7±0.3%; 7.2±0.7% and 4.3±0.4% for Go versus arable soils, respectively). The separation of PLFAs in time of incubation (day 1 vs. day 22), is explained by increasing values of 16:1ω7 ($P<0.01$), and 18:1ω3 (but not significantly; $P=0.076$) with time for Ma, Ot and Vo. The general lack of an irradiation effect on total PLFAs corresponds with the results of McNamara *et al.* (2003), although achieved with γ-irradiation, that only doses higher than 15 kGy and 20-70 kGy, would eliminate the fungi and Actinomycetes, and the bacteria populations, respectively.
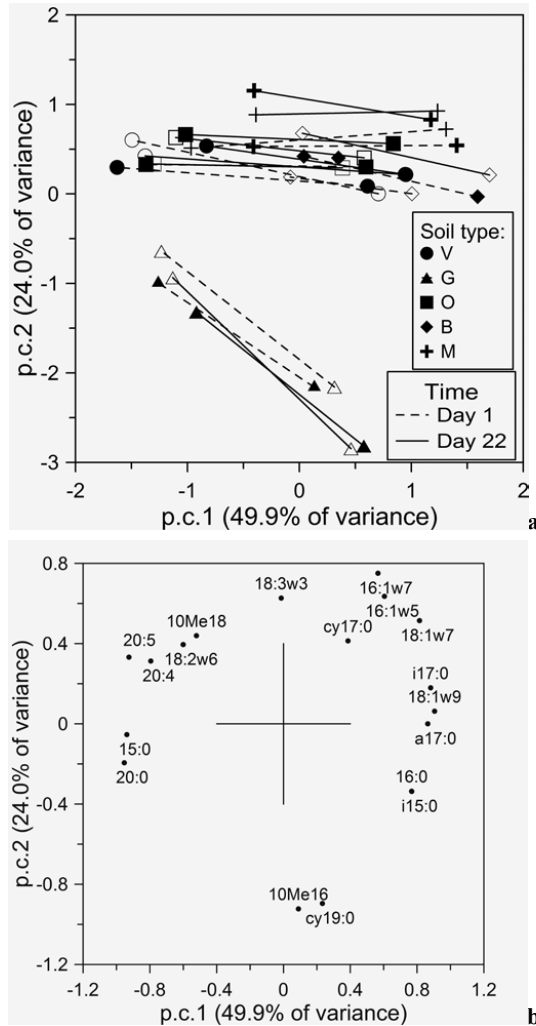
Figure 3-6: (a) Scatter plot of the first two principal components of a Principal Component Analysis on main extracted Phospholipid Fatty Acid Analysis (PLFA) (% of total PLFA>1.0%) of five soils (Vo, Go, Ot, Be & Ma), at two times (day 1 versus day 22 of incubation) following irradiation (solid symbols) or not (controls in transparent symbols), (b) plot of correlation of the primary loading PLFAs with p.c. 1 and 2.

Table 3-3: Average total Phospholipid Fatty Acid Analysis (PLFA) and biomarkers of five soils at two times (day 1 or day 22 of incubation) following X-ray micro-computed tomography scanning (X-ray) or not (C, control), means ± standard deviation.

Days after irradiation	Treatment	Total PLFAs (nmol g^{-1})	Biomarkers (% of total PLFA)				
			Gram+ bacteria	Gram- bacteria	Actinomycetes	Fungi	Protozoa
1 day	X-ray	7.32±2.21	16.03±1.78	8.07±1.15	7.87±1.97	5.97±0.68	1.46±0.31
	C	7.13±1.74	15.58±1.68	8.32±1.02	7.62±1.91	5.93±0.61	1.51±0.22
	5% LSD^A	2.26	1.26	0.82	0.23	0.20	0.13
22 days	X-ray	7.47±2.83	17.97±3.40	8.20±1.37	7.90±2.68	6.20±1.14	1.28±0.17
	C	8.32±3.33	17.83±2.64	7.82±1.58	7.92±2.19	6.24±1.12	1.31±0.26
	5% LSD^A	2.31	1.12	0.76	0.61	0.24	0.16
ANOVA							
Day 1 X-ray^B		N.S.	N.S.	N.S.	*	N.S.	N.S.
Day 22 X-ray^B		N.S.	N.S.	N.S.	N.S.	N.S.	N.S.
Day^B		N.S.	N.S.	N.S.	N.S.	N.S.	*
Day 1 X-ray x soil		N.S.	N.S.	N.S.	N.S.	N.S.	N.S.
Day 22 X-ray x soil		N.S.	N.S.	N.S.	N.S.	N.S.	N.S.

^{A} LSD = least significant difference

^{B} *Significantly different at the 5% significance level based on ANOVA *F*-test; N.S. not significantly different based on ANOVA *F*-test

3.3.3 Conclusion

The impact of X-ray micro-CT scanning on PLFA biomarkers for Actinomycetes and on dehydrogenase activity on day 1 was significant but (very) small, and the reasons behind it are unclear. However, this small impact was short-lived and had disappeared completely by the second sampling event (day 22). Although a safe radiation level does not exist, these results show that use of X-ray micro-CT is very well compatible with soil biological experiments. Based on this study, a time lag of three weeks between X-ray scanning and analysis of soil biological parameters is largely sufficient to rule out small effects of X-radiation even in such sensitive parameters like dehydrogenase activity. Three weeks is a substantial timescale for microbial activity and other overruling effects can take place than the ones caused by irradiation. For example, as mentioned above within this time bacteria can substantially mediate the soil physical structure and indirectly soil biology (Feeney *et al.*, 2006). Consequently, meaningful soil incubation experiments could follow shortly after X-ray CT scanning. This apparent compatibility of X-ray micro-CT with studies of soil biology and biochemistry is very promising and may very well open up a huge potential in evaluating the role of the soil pore network in regulating soil biological processes such as organic matter decomposition.

Chapter 4:

Examining the effects of artificially changed soil pore size distributions on C mineralization with X-ray CT

Abstract

Soil microstructure has a significant impact on soil processes by protecting micro-organisms from predation and by inducing spatial heterogeneity in moisture content and other soil variables. Because of the ever-present co-occurrence of a spectrum of factors influencing soil organic matter (SOM) decomposition, studying the complex relationship between soil pore network structure and SOM decomposition requires specifically designed experiments. Our objective was to investigate a number of artificial operations to manipulate soil pore size distribution for use in soil incubation studies focusing on the relationship between the soil pore structure and C mineralization. Grass and sawdust application to non-compacted soil (bulk density 1.0 g cm^{-3}) resulted clearly in increased substrate derived C mineralization. The strong effect of compaction on C mineralization after fresh substrate addition (the C mineralization relative to C content decreased by 53%) appears to have been related to a decreased pore volume of larger pores (>800 µm equivalent sphere diameter ($\emptyset_{eq}$)). Because native SOM is concentrated in smaller pores in the soils from which particulate OM was removed, C mineralization of the unamended soils was less influenced by soil compaction, which only reduced volumes of >800 µm pores. In general, the significant correlations observed between the substrate net C mineralization and the volume percentage of $\emptyset_{eq}$ pore class 10-200 µm (significantly negative for both treatments) and 610-800 µm (significantly positive for both treatments) and >800 µm (only significantly positive for the bulk density treatment) respectively, imply a profound influence of pores size distribution on C mineralization in both grass and sawdust amended soils. Explanations could involve changes in aeration, moisture availability, shift in habitable pore space, etc. A more in depth research is required to improve an insight on this matter, e.g. by the contribution of studies like this one with an analysis of the microbial community structure through Phospholipid Fatty Acid (PLFA) measurements. Controlled incubation studies in combination with X-ray CT and PLFA analysis would seem to be fit for this purpose.

4.1 <u>Introduction</u>

Distribution patterns of decomposer organisms in the soil do not generally match the allocation patterns of soil organic carbon (SOC) (Ekschmitt *et al.*, 2008). Soil organic matter (SOM) may be physically protected from microbial decomposition by its spatial separation from decomposers limited in their motility. For example, microfauna (i.e. mainly nematodes and protozoa) are bound to the water film covering soil, and mesofauna (mainly enchytraeids, springtails and mites) depend on existing macro pores in soil for movement (Ekschmitt *et al.*, 2008). Next to confinement of organisms to habitable pore spaces, the microstructure of soil has a significant impact on soil processes by protecting micro-organisms from predation, by inducing spatial heterogeneity in moisture content, pH and O_2 availability and by regulating the diffusion of substrate to and metabolites from microbial cells (Nunan *et al.*, 2005).

Ample research over the last decades has focused on interactions between soil structure dynamics and soil organic matter (OM) turnover (for example Elliot (1986) and Six *et al.* (2000)). Most research efforts have primarily relied upon physical separation of soil aggregates and associated OM into 'occluded' and 'free' fractions with differing conceptually allocated degrees of physical protection. However, narrowing down soil structure to soil aggregation is an oversimplification (Young *et al.*, 2001) and study of aggregates can only provide indirect information on the complex interactions between soil micro pore structure and OM turnover.

Because of the ever-present co-occurrence of a spectrum of factors influencing SOM decomposition, studying the complex relationship between soil pore network structure and SOM decomposition requires specifically designed experiments. Ideally, influence of variation in the soil pore structure should be studied in isolation, with all other factors influencing SOM decomposition being constant. To study the relationship between pore size distribution and OM decomposition, Strong *et al.* (2004) used natural spatial variation in both parameters by taking samples along a field transect. Hassink *et al.* (1993) compared pore size distributions and microbial biomass pools in grassland soils with different textures. However, this approach also yields unavoidable variation among samples in SOM composition and soil mineralogy. Several other authors (Franzluebbers, 1999; De Neve & Hofman, 2000) showed that compaction reduced C mineralization at different moisture levels and shifted the water-filled porosity at which C mineralization was maximized. Yet, compaction mainly reduces macro porosity (van der Linden *et al.*, 1989) and as such little work has been done on

relations between smaller pores and SOM decomposition. Thomsen *et al.* (1999) added clay to soil to study the influence of clay content on OM decomposition and, although unintended, by doing so they must have altered fine porosity as well. Other than this, we have no further knowledge of specific studies on OM decomposition with manipulation of smaller pores.

Our objective was to investigate a number of artificial operations to manipulate soil pore structure for use in soil incubation studies focusing on the relationship between the soil pore structure and C mineralization. We set up a controlled incubation experiment with a reconstituted and a reference sandy loam soil, which was also scanned afterwards by X-ray CT to quantify the pore size distribution. We looked into the influence of i) soil compaction or ii) artificial change in particle size distribution in combination with iii) application of distinct substrate types. Our hypothesis was that specific pore size classes may be targeted through different manipulations such as compaction and artificial change in particle size distribution. We also hypothesize that these different changes in pore size class volumes caused by these manipulations will affect C mineralization differently. Possible interactions between substrate type and artificial pore structure changes were also evaluated. In addition we set up the present C mineralization incubation experiments in such a way that possibly added substrate particles (at low bulk density and with removal of native particulate organic matter) would be visible in X-ray CT volumes to further investigate the location of added substrates and contact with the soil mineral phase.

4.2 **Material and methods**

4.2.1 *Experimental set-up*

The soil used for the incubations was a sandy loam soil (7% clay, 42% silt, 51% sand) with 0.797% SOC and 0.061% N, and a pH_{H2O} of 6.3. A 20 kg soil sample was taken from the 0-30 cm depth layer of a cropland field, situated in Lendelede (Belgium), with a spade. Particulate organic matter was removed as follows. The bulk soil was dry sieved on 2000, 200 and 53 μm sieves, then the >2000, >200 and >53 μm fractions were dispersed by shaking in 50 g l^{-1} sodium metaphosphate (1:3 w v^{-1} ratio). The dispersed slurries were passed once more on the respective sieves, then followed by extensive rinsing with deionized water. In this way three size fractions were obtained, namely coarse sand (CS: 200-2000 μm), fine sand (FS: 53-200 μm) and silt+clay (S+C: <53 μm). The coarse and fine sand fractions were placed in a muffle furnace at 500°C for 5 hours to remove the sand sized (particulate) organic matter. An

artificial soil with no particulate organic matter was then reconstituted by mixing these size fractions. In total nine different soil mesocosm treatments (each in three replicates) were constructed. The nine treatments were: a reference treatment, and treatments with i) compaction, and ii) artificial changes in soil texture (Figure 4-1) in combination with addition of two different substrates or no substrate applied at all.
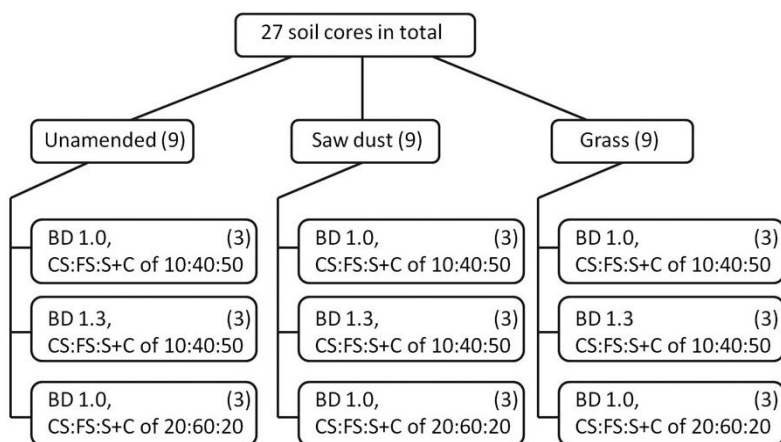
Figure 4-1: Overview of all treatments of the C mineralization experiment including combinations of addition of two different substrates (sawdust or grass) and manipulation of the soil pore size distribution (compaction or artificial texture changes); BD=bulk density and CS:FS:S+C=coarse sand, fine sand and silt+clay fractions.

The reference treatment had a coarse sand, fine sand and silt+clay (CS:FS:S+C) ratio of 10:40:50, 0.035% N and 0.448% C. The artificial texture treatment had a modified CS:FS:S+C-ratio of 20:60:20, 0.014% N, 0.179% C and pH 6.3. Twenty seven (nine treatments with three replicates) aluminium cylinders (Ø=1.2 cm; h=1.2 cm) were filled with 1.2 g of soil. Both the reference and manipulated texture treatments were compacted in a vertical plane with a cylinder to obtain a target bulk density (BD) of 1.0 g cm^{-3} (h=0.99 cm). The compaction treatment soil cores were compacted to obtain a target BD of 1.3 g cm^{-3} (h=0.81 cm). The removal of particulate organic matter prevented variation in the soil OM quality with the different ratios of CS:FS:S+C. There was always one unamended reference soil, one amended with ground sawdust and one amended with ground grass (both at a rate of 921 mg C kg^{-1}). Water content in all treatments was adjusted to 28% water filled pore space (WFPS) by adding deionized water (taking into account bulk density differences).

4.2.2 Soil incubation

The 27 pre-treated repacked soil cores were incubated at 20±1°C for 35 days to promote aggregation, and thus in pore network structure development. This approach was also used by Denef *et al.* (2002) and De Gryze *et al.* (2006) who incubated mixed dispersed soil to generate a variety in aggregate size distributions. Denef *et al.* (2002) (working with a silt loam Kastanozem) found that most macro aggregate formation occurred within a two week period and De Gryze *et al.* (2006) (working with sandy loam to clay loam Luvisols) found levelling-off of further aggregate formation after three weeks. Consequently, a 35-day lab incubation period was considered to be sufficient to achieve pore network development in the reconstituted soils.

4.2.3 X-ray CT derived pore size distribution and visualization of SOM

Two out of three replicates per treatment were scanned with a high resolution X-ray nano-CT tomography set-up (see 1.5.4) at the Ghent University Centre for X-ray Tomography (UGCT, www.UGCT.Ugent.be). The experimental conditions for the micro-focus CT scans consisted of a directional target microfocus X-ray tube operated at 100 kV and 80 µA (8 W), an amorphous silicium flatpannel detector (Varian Paxscan 2520) with 1400 ms exposure time per projection and 1400 projections per scan of 40 minutes. The raw data was reconstructed with the in-house developed reconstruction software Octopus (Vlassenbroeck *et al.*, 2007) to a dataset of 1500x1500x1500 cubic voxels with a 10 µm voxel pitch for each soil column. Automated sequential scanning of up to ten stacked soil cores was enabled by programmed movement of the rotational motor in a vertical plane and automated X-ray CT acquisition.

The scanned images (Figure 4-2) were analyzed for total porosity (TP) and pore size distribution (PSD) using Morpho+ (Brabant *et al.*, 2011), UGCT. The equivalent sphere diameter ($\text{\O}_{eq}$), i.e. the diameter of a circular sphere having the same volume as the pore, was calculated for each pore. A PSD resulted from the cumulative pore volumes of a number of $\text{\O}_{eq}$ classes. All 18 images were processed identically to allow comparison of the calculated PSDs. Firstly, a volume of interest (VOI) was selected to decrease image processing time. These VOIs of 350x300x300 voxels were then filtered twice by a 3D median (26x26x26) filter and once by a 3D bilateral (2,2) filter. Both filters reduced noise by replacing each voxel value by the average of nearby voxels, but the bilateral filter also preserves the edges of objects in the image. The objective of filtering images was to simplify the consecutive

segmentation step. A threshold value was selected based on histogram evaluation to separate pore space and soil matrix. Following segmentation, the binary image was then used as input for pore labeling, which assigns a label to every discrete object. Next, a distance map calculation of the pore space was then executed as the basis for a watershed-based separation of the pore space. A distribution of voxels according to $\emptyset_{eq}$ was then obtained and this was used to calculate the PSD. Total X-ray CT visible pore volume (%) was calculated from the ratio of the total volume (μm^3) of segmented pore voxels and total volume (μm^3) of the scanned CT volume.

4.2.4   C mineralization

The SOM and substrate derived C mineralization was monitored during incubation and was taken as a measure of biological activity. The CO_2 that evolved from soil was monitored by placing all soil cores in plastic containers, closed airtight with a lid and septum. Carbon mineralization was monitored by sampling the headspace above the soil cores. To this end, gas samples were taken periodically with a 50 or 250 µl syringe at days 1-3-5-7-15-21-29-35 and the CO_2 concentration was measured with a gas chromatograph fitted with ECD detector (Thermo Electron Trace GC Ultra). All measurements were corrected for ambient CO_2 initially present in the headspace by including two replicate empty containers.

A linear model was fitted to the C mineralization data for each soil core:

$$C(t) = k*t \qquad\qquad\qquad\qquad\qquad \text{Eq. (4)}$$

assuming that the C mineralization rate k is linear with time. The parameter k in this first-order model was determined through non-linear regression using the Levenberg-Marquardt algorithm in SPSS 15.0.

Moisture loss during incubation was controlled twice gravimetrically and water losses were added with a 10 ml syringe. A relative cumulative C mineralization was calculated by expressing 35-days cumulative C mineralization ($C_{cum,35}$) relative to the soil C content (C in soil organic matter and added substrate).
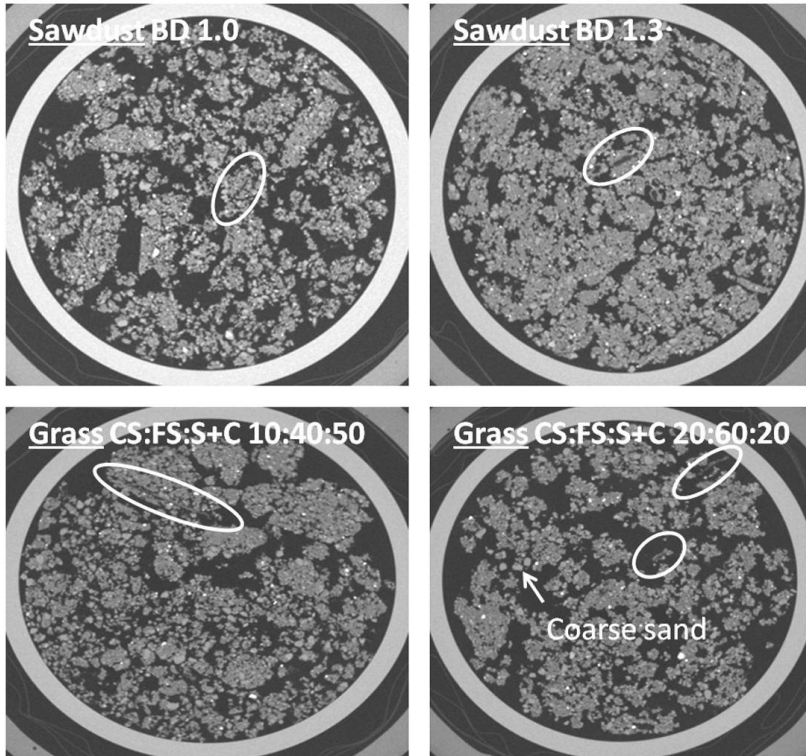
Figure 4-2: X-ray computed tomography images in 2D of sawdust amended soils at two different bulk densities (BD 1.0 and BD 1.3 g cm^{-3}) and grass amended soils at two different textures (coarse sand, fine sand and silt+clay fractions (CS:FS:C+S) of 10:40:50 and 20:60:20). White circles indicate added substrate particles, the white arrow indicates coarse sand particles.

4.2.5   Statistical analysis

By subtracting the C mineralization assessed from the unamended soil, net substrate C mineralization could be calculated. A one-sample *t*-test was applied to test if net C mineralization was significantly different from zero. Linear correlation analysis was carried out between total and net $C_{cum,35}$ and the percentage of pore volume of five pore size classes ($\varnothing_{eq}$ of 10-200, 210-400, 410-600, 610-800 and >800 µm) using Pearson's correlations in SPSS 15.0 (SPSS Inc., Chicago). Analysis of variance followed by multiple comparisons with Tukey's HSD post-hoc test was used to detect significant differences between means of net C mineralization and porosity at different bulk density and soil texture. Analysis of variance followed by Dunnett's post-hoc test was used to detect significant differences between means of net $C_{cum,35}$ at the bulk density treatment or the artificially changed texture treatment compared to the reference treatment for grass and sawdust amended soils.

4.3   **Results**

4.3.1   X-ray CT total porosity and pore size distribution

The X-ray CT calculated soil porosity was significantly lower in compacted soil (BD 1.3) than in the soil at BD 1.0 g cm^{-3}, independent from substrate addition ($P<0.05$) (Figure 4-3). Artificial change in soil texture from CS:FS:S+C from 10:40:50 to 20:60:20 decreased soil porosity significantly in the unamended and grass amended treatments (both $P<0.05$). Manipulation of soil texture did not change porosity in the sawdust amended soil.
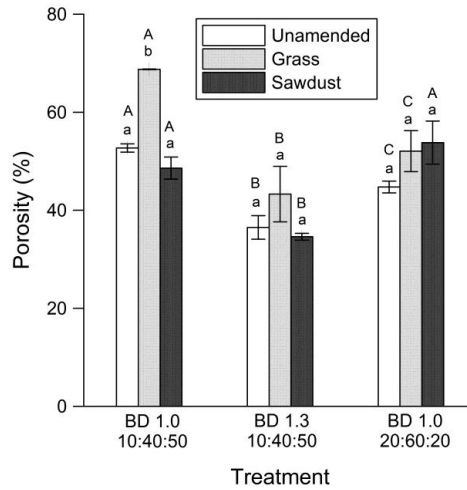
Figure 4-3: Total X-ray computed tomography visible porosity for all treatments (bulk density (BD) of 1.0 or 1.3 g cm^{-3}, coarse sand, fine sand and silt+clay fractions of 10:40:50 or 20:60:20 with or without grass or sawdust application). Statistically different substrate treatments are indicated by different lowercase letters. Statistically different bulk density and texture treatments are indicated by different capital letters.

X-ray CT derived pore volumes (expressed relatively as a volume%) of five pore $\varnothing_{eq}$ classes were calculated (Figure 4-4). Compaction significantly reduced the percentage of pore volume in the >800 µm class while the pore volume of the 200-400 µm class was significantly increased in the unamended soils. Soil compaction also reduced the percentage of pore volume in the >800 µm class when grass or sawdust were added, but only significantly for sawdust. Artificial change in texture did not significantly influence the pore volume in any $\varnothing_{eq}$ pore class for unamended, grass amended and sawdust amended soils, nor the summed volume of 210-800 µm classes.
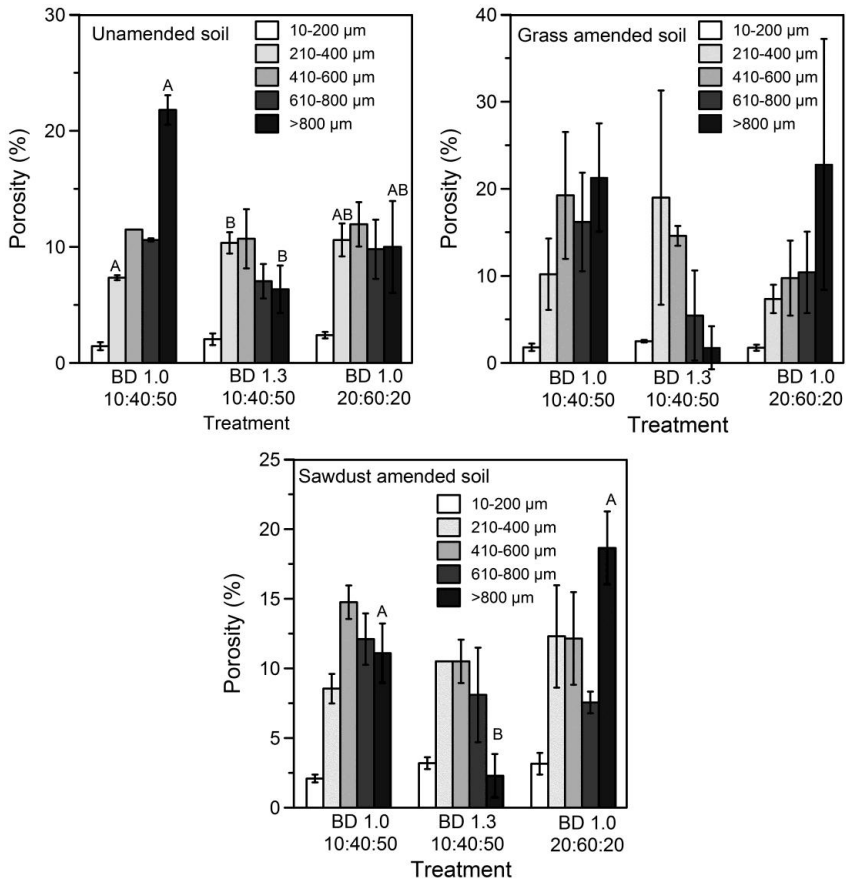
Figure 4-4: X-ray computed tomography derived absolute volume percentage of five equivalent diameter pore size classes (10-200, 210-400, 410-600, 610-800 and >800 µm) for unamended, grass or sawdust amended soil. Statistically different bulk density (BD of 1.0 or 1.3 g cm^{-3}) and texture treatments (coarse sand, fine sand and silt+clay fractions of 10:40:50 or 20:60:20) are indicated by different capital letters.

4.3.2 Carbon mineralization

The fitted parameter k of the linear model varied between different soil treatments (Table 4-1). In general, the R^2 values of this model were close to one for all the treatments, except for the reference treatment with grass application, implying that the selected model described the mineralization process appropriately (Figure 4-5).
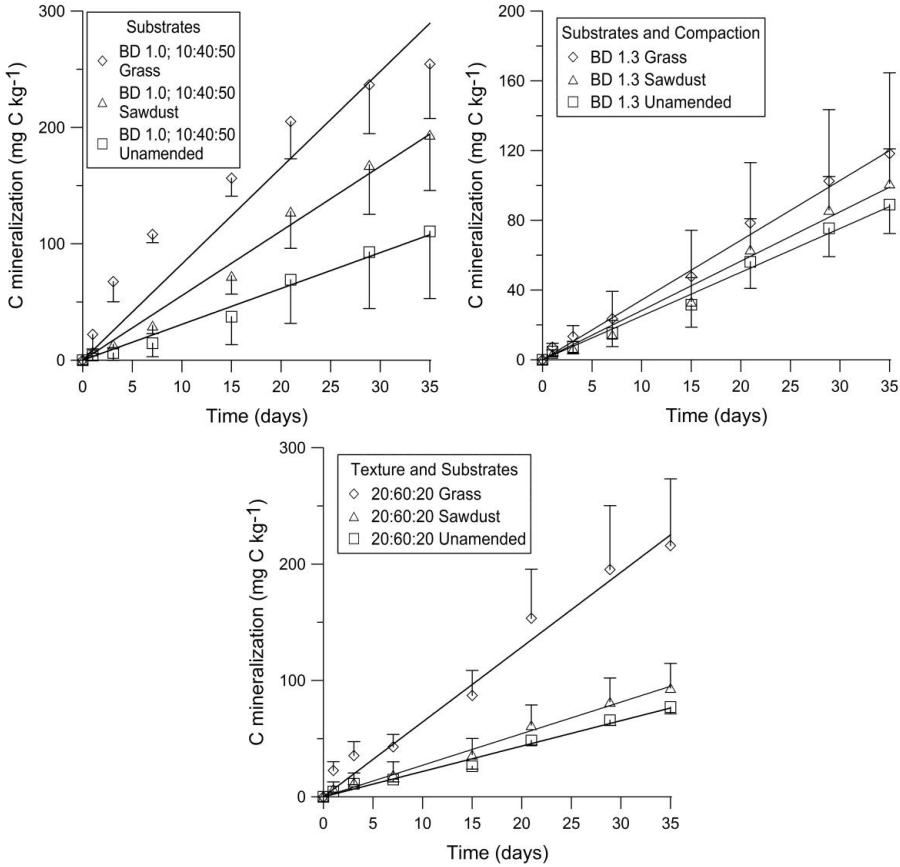
Figure 4-5: Time evolution of cumulative mineralized C after substrate addition (sawdust or grass), compaction (bulk density (BD) of 1.0 or 1.3 g cm^{-3}) and artificial change in soil texture (coarse sand, fine sand and silt+clay fractions of 10:40:50 or 20:60:20). Error bars represent standard deviations of three replicates.

Table 4-1: Estimated parameter *k* of the fitted linear model for all treatments (values are averages of three replicates) and total cumulative C mineralization over the 35-day incubation period (C$_{cum,35}$).

Treatment			k	R^2	C$_{cum,35}$	C$_{cum,35}$
			(mg C kg^{-1} day^{-1})	(-)	(mg C kg^{-1})	(% of C)[C]
BD[A] 1.0	10:40:50[B]	Unamended	3.08	0.987	108	2.4
BD 1.0	10:40:50	Grass	8.27	0.872	289	4.7
BD 1.0	10:40:50	Sawdust	5.55	0.990	194	3.6
BD 1.3	10:40:50	Unamended	2.51	0.992	88	2.0
BD 1.3	10:40:50	Grass	3.43	0.992	120	2.2
BD 1.3	10:40:50	Sawdust	2.83	0.987	99	1.8
BD 1.0	20:60:20	Unamended	2.18	0.986	76	4.2
BD 1.0	20:60:20	Grass	6.43	0.974	225	8.0
BD 1.0	20:60:20	Sawdust	2.71	0.988	95	3.4

[A] BD, bulk density

[B] 10:40:50 & 20:60:20 are ratios of coarse sand, fine sand and silt+clay fractions

[C] sum of C in native silt+clay sized SOM and C in the added substrate

In all three unamended treatments (BD 1.0 g cm^{-3}, BD 1.3 g cm^{-3} and CS:FS:S+C of 20:60:20) the mineralization rate *k* was smallest compared to the amended treatments. Among the amended treatments, the mineralization rate *k* of the grass application was higher than the sawdust application treatments (BD 1.0 g cm^{-3}, BD 1.3 g cm^{-3} and CS:FS:S+C 20:60:20). Among similar substrate addition treatments, the highest mineralization rate *k* was found in soils with a low bulk density (BD 1.0 g cm^{-3}) and CS:FS:S+C ratio of 10:40:50 over other combinations of bulk density and soil texture.

One-way ANOVA followed by Tukey's HSD post hoc test (Figure 4-6) revealed a significantly higher ($P<0.05$) C$_{cum,35}$ in the reference soil (BD 1.0 g cm^{-3}; CS:FS:S+C 10:40:50) with grass addition compared to the reference unamended soil. C$_{cum,35}$ was also higher in the reference soil with sawdust additions compared to the unamended reference soil, but not significantly. Substrate addition to soil compacted to BD 1.3 g cm^{-3} did not alter C mineralization compared to the unamended soil at BD 1.3 g cm^{-3}. However, C$_{cum,35}$ was significantly lower in soil at BD 1.3 g cm^{-3} than in non compacted soil (BD 1.0 g cm^{-3})

for both grass ($P<0.05$) and sawdust ($P<0.05$) treatments. Soil compaction from BD 1.0 to 1.3 g cm^{-3} had no effect on native SOM C mineralization.

Manipulation of soil texture by changing the CS:FS:S+C from 10:40:50 to 20:60:20 without application of a substrate had no significant effect on $C_{cum,35}$. When substrate was applied, $C_{cum,35}$ was consistently lower in the CS:FS:S+C 20:60:20 treatment compared to reference CS:FS:S+C 10:40:50 treatment, but this decrease was only significant for the sawdust amended soils ($P<0.05$). Among the CS:FS:S+C 20:60:20 treatments, $C_{cum,35}$ was significantly higher in the grass amended soil compared to the sawdust amended soils, in contrast to soils with CS:FS:C+S ratio of 10:40:50.
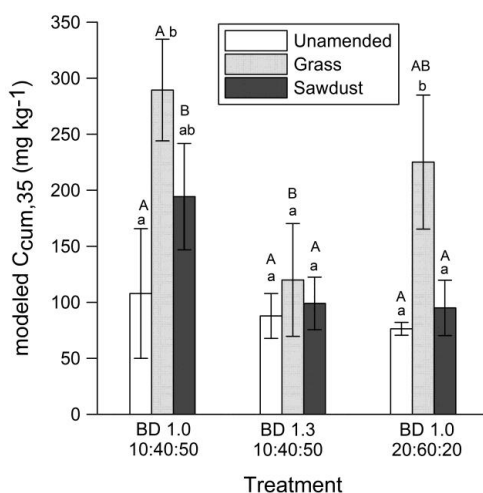
Figure 4-6: Total modeled C mineralization after 35 days of incubation ($C_{cum,35}$) for all treatments (bulk density (BD) of 1.0 or 1.3 g cm^{-3}, coarse sand, fine sand and silt+clay fractions of 10:40:50 or 20:60:20 with or without grass or sawdust application). Statistically different substrate treatments are indicated by different lowercase letters. Statistically different bulk density and texture treatments are indicated by different capital letters.

Compaction from BD 1.0 to 1.3 g cm^{-3} resulted in a significant reduction (both $P<0.05$) of net grass- and sawdust-derived $C_{cum,35}$ (Figure 4-7). Artificial change in texture did not affect net modeled $C_{cum,35}$ from grass while it significantly reduced ($P<0.05$) net $C_{cum,35}$ of sawdust compared to the reference sawdust amended soil.
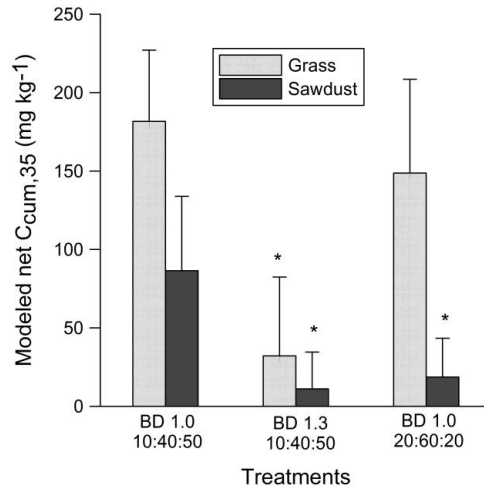
Figure 4-7: Net modeled substrate derived 35-days cumulative C mineralization ($C_{cum,35}$) for all treatments (bulk density (BD) of 1.0 or 1.3 g cm^{-3}, coarse sand, fine sand and silt+clay fractions of 10:40:50 or 20:60:20 with either grass or sawdust application). Treatments indicated by * have a statistically different ($P<0.05$) net C mineralization than the reference treatment (BD 1.0 g cm^{-3} with either grass or sawdust application) according to Dunnett's post hoc test).

4.3.3 Correlation maps

Correlation coefficients between the modeled $C_{cum,35}$ (mg C kg^{-1}) and the volume percentage of five different $\O_{eq}$ pore size classes, namely 10-200, 210-400, 410-600, 610-800 and >800 µm, were calculated (Figure 4-8). In unamended soil, $C_{cum,35}$ did not correlate with the volume percentage of any of the $\O_{eq}$ pore size classes. For grass and sawdust amended soils $C_{cum,35}$ correlated negatively with the volume of small $\O_{eq}$ pore size classes (10-200 µm).
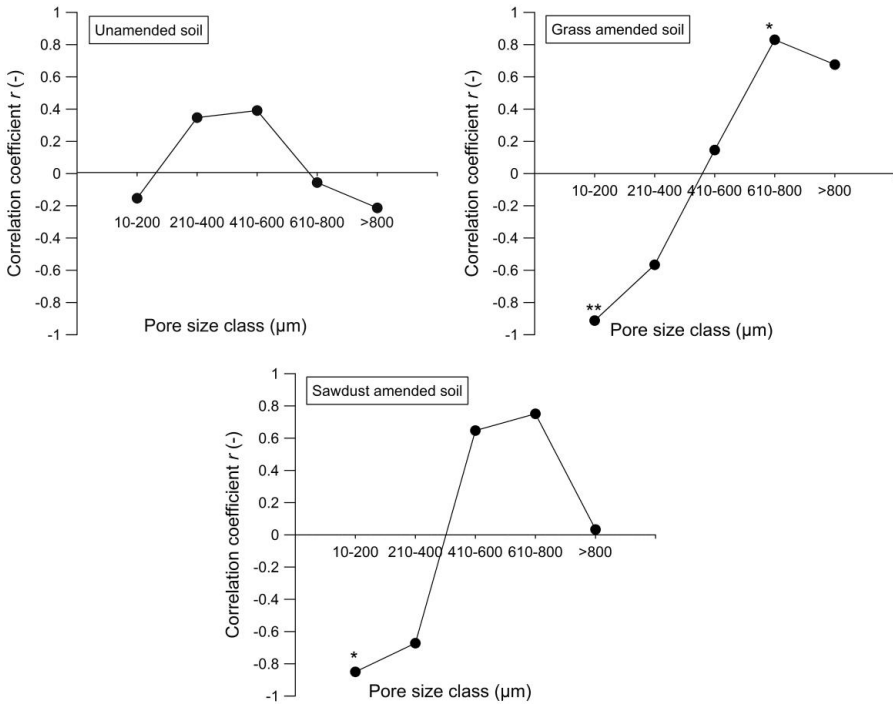
Figure 4-8: Pearson's correlation coefficients between modeled 35-days cumulative C mineralization and the X-ray computed tomography calculated pore class volumes plotted against the average equivalent diameter of that pore class for three substrate application treatment (unamended, grass or sawdust amended soil). * indicates a correlation at significance level *P<0.05* and ** at *P<0.01*.

For the grass amended soil, there was a significant positive correlation between the volume of $Ø_{eq}$ pore size class 610-800 µm and $C_{cum,35}$ ($P<0.05$). Positive correlations between $C_{cum,35}$ and the volume of the >800µm $Ø_{eq}$ pore size class in case of the grass amended soil and the volume of 410-600 and 610-800 $Ø_{eq}$ pore size classes in case of the sawdust amended soils were only significant at P=0.151, P=0.163, and P=0.085, respectively.

A final correlation analysis was performed between the volumes of $Ø_{eq}$ pore size classes and net modeled $C_{cum,35}$ from the added substrates (mg C kg^{-1}) (Figure 4-9). For both manipulation of soil pore network structure treatments (change of BD 1.0 to 1.3 g cm^{-3} and of CS:FS:C+S10:40:50 to 20:60:20), the correlation maps between net modeled $C_{cum,35}$ and percentage of pore volumes in pore size classes switched from negative to positive with increasing $Ø_{eq}$ of the pore size classes. For both treatments, net modeled $C_{cum,35}$ was negatively and significantly (both $P<0.01$) correlated with percentage of pore volume in the smallest pore size class (10-200 µm). For the bulk density treatment, positive correlations between net modeled $C_{cum,35}$ and percentage of pore volume in pore size classes 610-800 and >800 µm were significant ($P<0.01$ and $P<0.05$, respectively), while only the positive correlation between modeled net $C_{cum,35}$ and pore size class 610-800 µm was significant for CS:FS:C+S of 20:60:20.
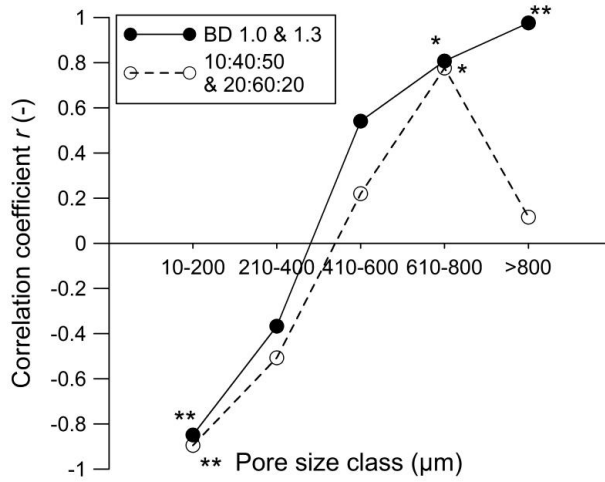
Figure 4-9: Correlation analysis between net 35-days cumulative C mineralization (i.e. C mineralization of grass or sawdust amended soil minus the average of unamended soil) and the X-ray computed tomography derived volumes of pore size classes plotted against the average equivalent diameter of each pore size class for bulk density (BD 1.0 or 1.3 g cm^{-3}) and texture treatments (coarse sand, fine sand and silt+clay fractions of 10:40:50 or 20:60:20). * indicates a correlation at significance level *P*<0.05 and ** at *P*<0.01.

4.4 **Discussion**

4.4.1 *Effect of soil compaction on C mineralization and soil pore structure*

There was no significant change in native SOM derived C mineralization when changing bulk density from 1.0 to 1.3 g cm^{-3}. This is in agreement with results obtained by De Neve & Hofman (2000) for a soil with similar texture after more severe compaction (1.2 to 1.6 g cm^{-3}). Sleutel *et al.* (2012) as well found only a small but insignificant decrease in C$_{cum,35}$ after soil compaction (BD of 1.3 to 1.6 g cm^{-3}) for the same soil used here. Soil porosity and PSDs were obtained from image analysis from the X-ray CT scans of 18 small soil cores (Figure 4-3 and Figure 4-4). The lower soil porosity in compacted soil (at BD 1.3 g cm^{-3}) was accompanied by changes in the PSD. Soil compaction was found to affect mainly the larger pores, namely the pore volume >800 µm was reduced by soil compaction for all substrate treatments. The comparatively high volume percentage of pores with Ø$_{eq}$ of 210-400 µm after soil compaction points to an increase in pores of this class (only significant for the unamended soil). Similar results were observed by Breland & Hansen (1996) who reported a shift in the PSD after soil compaction of a sandy loam soil towards a higher percentage of small pores (neck Ø<3 µm) and a lower percentage of large pores (neck Ø>30 µm). van der Linden *et al.* (1989) also observed a decrease in the volume of large pores (neck Ø>30 µm) and an increase in the volume of small pores (neck Ø<0.2 µm) upon compaction of a similar textured soil from 1.0 to 1.5 g cm^{-3}. Sleutel *et al.* (2012) as well found decreasing pore volume of pores with necks between 30-100 µm after soil compaction (1.3 to 1.6 g cm^{-3}) for a sandy loam soil. Native SOM was only present in the silt+clay size fractions and, which is mainly organized in smaller pores, which were not affected by the compaction treatment.

On the contrary grass and sawdust application to soil at BD 1.0 g cm^{-3} resulted clearly in an expectable surplus substrate derived C mineralization and soil compaction resulted in an almost 50% reduction of C mineralized after 35 days in the grass and sawdust amended soils. When expressed as a percentage of the C present in the soil, cumulative relative C mineralization decreased by more than 50% by upon compaction, demonstrating a strong effect of compaction on substrate derived C mineralization. De Neve & Hofman (2000) also found a significant decrease in C mineralization rate following compaction (1.2 to 1.6 g cm^{-3}) in soil added with fresh crop residues in a sandy loam soil. In contrast, van der Linden *et al.* (1989) found no effect of compaction on C

mineralization for a loamy sand soil after substrate addition, but they did find a decreased C mineralization following compaction in a silt loam soil (compaction from 1.0 to 1.5 g cm^{-3}). An observed increase in soil porosity after addition of grass in non compacted soils (BD 1.0 g cm^{-3}) can be related to improvement of soil structure by higher microbial activities. When fresh residue is incorporated into the soil, microbial activity increases and binding agents are produced that lead to the formation of macro aggregates (De Gryze, 2004). Also Feeney *et al.* (2006) have observed an increase in soil porosity (>4.4 μm) due to higher biotic activity following addition of roots to the soil. An increase in soil porosity after addition of grass in non compacted soils (BD 1.0 g cm^{-3}) could also have been caused by the physical presence of the substrate itself (50-200 μm sized OM particles). A similar increase in soil porosity was not observed after application of sawdust and the different respons compared to grass amendment may be associated to degradability of these materials. Grass addition more strongly favoured microbial activity than sawdust addition, as seen from the increased C mineralization, and this could have enhanced the formation of soil structure (De Gryze, 2004).

The effect of soil compaction on C mineralization in the amended soils might have been due to increased physical protection of the added substrates. During the initial decomposition stage, freshly added substrate will form part of free coarse of organic matter fraction (Hassink & Dalenberg, 1996) associated with larger pores (>800 μm Ø$_{eq}$). Soil compaction would reduce the accessibility of this coarse fraction of organic matter. More probably, the reduced C mineralization after compaction was caused by limited gas exchange due to a decrease in the volume of larger pores (>800 μm Ø$_{eq}$).

4.4.2 *Effect of artificial soil texture changes on C mineralization and soil pore structure*

Manipulation of soil texture from a CS:FS:C+S ratio of 10:40:50 to 20:60:20 considerably reduced C mineralization in the unamended soil, which is logical and not of interest here as the soil C content was lower in the latter treatment. When substrate was added a large and significant reduction in net substrate C mineralization was found only in the sawdust but not in the grass treatment. Overall these results point to a specific interactive effect from both soil pore network structure and substrate type.

Soil porosity was found to decrease significantly after artificial change of soil texture from CS:FS:C+S ratio of 10:40:50 to 20:60:20 in the unamended and grass amended soils, in spite the fact that all cores were brought to an initial BD of 1.0 g cm^{-3}. Although unintended, such a decrease in soil porosity during the incubations might be attributed to the combination of a very low initial reference BD (1.0 g cm^{-3}) next to low soil structural stability in the CS:FS:C+S 20:60:20 soils as a consequence of its high sand percentage (80%) and in case of the unamended soils also the low C content (0.18% C). A change in soil porosity during incubation of the same unamended CS:FS:C+S 20:60:20 soil was not observed by Sleutel *et al.* (2012) but they worked at a higher BD of 1.3 g cm^{-3}. Mainly, the combination of artificially changed texture and substrate addition resulted in lowered volumes of medium sized pores (400-800 Ø$_{eq}$ µm) and for the sawdust amended soils also in an increase of >800 µm pores.

In order to explain the observed reduced C mineralization after artificially changing soil texture of the amended soils it would seem logical to relate these observations to possible changes in water availability affected by this alteration of the pore structure. Changes in PSD due to varying texture may have altered microbial available water volume for decomposition in our study. A fixed water content (28% WFPS) was applied to all soil cores. From the WRC data of the same soil in Sleutel *et al.* (2012) we estimated that change in soil texture from CS:FS:C+S of 10:40:50 to 20:60:20 pores expanded the initial primordial presence of water only in pore necks <4.95 µm up to pores with necks diameters <11.95 µm. Thomsen *et al.* (1999) hypothesized that native SOC decomposition occurred at a faster rate in soils containing more clay because these soils hold a larger fraction of water available to microbial biomass (>0.2 µm). However, in the here substrate amended soils an expansion of the distribution of water to larger pores would be expected to have resulted in an increase instead of a decrease of substrate derived C mineralization. Hence, it would seem that distribution of water over these finer pore classes does not explain the observed differences in C mineralization between the CS:FS:C+S 10:40:50 and 20:60:20 treatments.

4.4.3   Relation between soil pore size distribution and C mineralization

A clear trend from negative towards positive correlation coefficients with increasing $\emptyset_{eq}$ pore size observed in both grass and sawdust amended soil points to a positive influence of larger pores (>410 µm) on C mineralization. Analogously, a negative relationship with the percentage volume of small pores (10-400 µm) suggests the opposite for smaller pores. In contrast to the unamended soils the volume percentage of the $\emptyset_{eq}$ classes 610-800 and >800 µm was positively correlated to the C mineralization (only significant for >800 µm). Enhanced soil aeration with increasing volumes of these larger pore size classes could be the main reasons for increased bulk soil C mineralization. However, as these larger pores are mostly air-filled, very fine water films (<10 nm; Or *et al.*, 2007) are the only water source available in these larger pores. Second, as the added grinded grass and sawdust materials had comparable size as these pores, C mineralization of the added substrates could have actually only occurred inside these pores. Significant negative correlations observed between $C_{cum,35}$ and the volume of the 10-200 µm $\emptyset_{eq}$ pore size class for grass and sawdust amended soils, may have been an indirect consequence of the inverse relation with the volume of >410 µm pores. Because the size of the added substrate particles primarily exceeded the dimensions of such pores it seems unlikely that microbial activity in these smaller pores contributed substantially to bulk soil CO_2 production.

In general, the significant negative and positive correlations observed between the substrate net C mineralization and the volume percentage of $\emptyset_{eq}$ pore class 10-200 µm (for both treatments) and 610-800 µm (for both treatments) and >800 µm (for the bulk density treatment only) respectively, imply a profound influence of PSD on C mineralization in the grass and sawdust amended soils. These results can be related to other research by Strong *et al.* (2004) where a rapid decomposition of the added plant material was observed in soil with relative large volume of pores with neck diameters class from 15-60 µm but low proportion of pores with neck $\emptyset$<4 µm. Similarly, Gregorich *et al.* (1991) observed more rapid OM decomposition in sandy soil than in clay soil and this difference was partly attributed to differences in volume of small pores. In case soil moisture is not limited, high C mineralization in larger pores (pores with $\emptyset_{eq}$>800 µm) can be related to the presence of favourable conditions for microbial activity such as adequate soil aeration and gas exchange (O_2, CO_2). In addition, physical support to accommodate most microorganisms

has been put forward as a factor through which the macro pore network structure affects biological activity in soil. The presence of nematodes and other fauna may enhance C mineralization through grazing effect on microbes as Hassink *et al.* (1994) estimated the faunal contribution to C mineralization to be 4-12% of the total C mineralization. Most (about 80%) of this faunal contribution to C mineralization would derive from an indirect positive effect on the growth rate of microbes. van der Linden *et al.* (1989) showed that protozoa and nematodes are excluded from pores <5 µm and <30 µm, respectively. However the substrates must have resided in pores larger than these diameters and should thus still be susceptible to decomposition or predation by these soil fauna. It also seems unlikely that the stimulating effect of larger pores (>800 µm) on substrate derived C mineralization was related to promotion of soil fauna because of the severe disturbance of soil upon removal of POM. With the exception of protozoa most fauna (e.g. arthropods, nematodes) have probably died off during repeated drying and sieving. Sleutel *et al.* (2012) used the exact same soil to investigate how soil compaction and artificial change in soil texture affected the microbial community structure via PLFA analysis. They found that artificial change in soil texture from a CS:FS:C+S ratio of 10:40:50 to 20:60:20 reduced the ratio of bacterial to fungal biomarkers, implying a relative increase in fungal biomass. In sawdust amended soil a considerable decrease in bacterial to fungal biomarkers ratio was observed and this was logically linked to the lignin content of wood material. Consequently, the combination of artificial change in soil texture and sawdust application would be expected to promote fungi and fungal controlled OM decomposition. In contrast to Sleutel *et al.* (2012), however, the present incubations were carried out at a lower bulk density (BD 1.0 g cm^{-3} instead of 1.3 g cm^{-3}) in order to enable visual detection of added substrates in the CT-scans. Fungal growth starting from the added silt and clay sized native SOM containing aggregates towards the sometimes even isolated sawdust particles at this high porosity (Figure 4-2) may have been restricted by the relatively large distances and low moisture availability. This would explain the strong reduction of sawdust derived C mineralization by changing the CS:FS:C+S ratio from 10:40:50 to 20:60:20. These same constraints, however, did not prevent decomposition of the ground grass substrate. Possibly, the combination of moisture stress with the good degradability of carbohydrate rich grass material was still attainable for microorganisms while a combination of moisture stress and the higher biochemical stability of lignin-rich sawdust was not.

In chapter 3, we have shown that a combined measurement of microbial functioning and quantification of the soil pore structure with X-ray CT is possible because X-radiation did not alter SOM decomposition and any short living effects on enzyme activity or microbial biomass disappeared completely three weeks after X-radiation. In future experiments, simultaneous measurements of the microbial community, C mineralization and visualization of OM and water in the pore space will facilitate interpretation of results of experimental incubation studies like the present one. Although the simultaneous visualization of OM and water in the pore space is very challenging, Van Loo *et al.* (2012) were able to successfully stain particulate OM in X-ray CT images of an artificial sand-particulate OM mixture. The enhanced X-ray CT contrast of the particulate OM compared to the pore space and the soil matrix in their study appears to be very promising for future separate visualization of SOM in soil cores.

4.5 <u>Conclusion</u>

The incubation experiments revealed that substrate derived but not native SOM derived C mineralization depends on the here quantified soil pore network structure measures. In both grass and sawdust amended soil, a clear trend of the correlation coefficients from negative to positive with increasing pore size class suggested a positive influence of macro porosity on C mineralization of freshly added substrates. The specific effect of this study's artificial modifications of the soil pore structure on substrate C mineralization was, however, found to be highly dependent on substrate quality. At this point the nature of these interactive effects between substrate quality and variations in pore size distribution on C mineralization can only be hypothesized. Explanations could involve changes in aeration, moisture availability, shift in habitable pore space etc. A more in depth research is required to improve an insight on this matter. Controlled incubation studies in combination with X-ray CT and PLFA analysis would seem to be fit for this purpose.

Chapter 5:

C mineralization and pore network structure in undisturbed soil cores

Abstract

Soil pore network effects on organic matter turnover have, until now, been studied indirectly because of lack of data on the 3D structure of the pore network. The application of X-ray computed tomography to quantify pore neck size distributions from undisturbed soil cores with simultaneous assessment of C mineralization, could establish a relationship between soil organic matter decomposition and soil pore network structure. Eighteen miniature soil cores (Ø=1.2 cm, h=1.2 cm), covering a range of bulk densities, were incubated at 20°C for 35 days. Respiration was modeled with a parallel first- and zero-order kinetic model. The cores were scanned at 9.44 µm resolution using an in-house developed X-ray CT scanner with a directional target micro-focus X-ray tube (Hamamatsu L9181) and an amorphous silicon flatpannel detector (Varian Paxscan 2520) . Correlation analysis between the slow pool C mineralization rate, k_s, and visible porosity for each pore neck class yielded significant positive correlations (*r* values and *p* values) for the 150-250, 250-350 and >350 µm pore neck classes. Because larger pores are most probably mainly air-filled, a positive relation with k_s was ascribed to enhanced aeration of smaller pores surrounding large pores. The weak and insignificant relationship between the smallest pore neck classes (<9.44 µm) and k_s could be explained by obstructed microbial activity and mobility or diffusion of exo-enzymes and hydrolysis products as a result of limited water availability, even at 39% water-filled pore space. The current study supports the hypothesis that the spatial organization of the soil pore network exerts a significant influence on soil microbial processes including C mineralization.

5.1 <u>Introduction</u>

The spatial distribution of soil organisms is not random (Nunan *et al.*, 2003; O'Donnell *et al.*, 2007; Young *et al.*, 2008), instead their location in the soil matrix depends, among other factors, on presence of substrate (Or *et al.*, 2007), soil water (Foster, 1988) and pore size distribution. The control of the pore size distribution on soil biological processes is two-fold: firstly, soil organisms are likely to reside in pores having a diameter thrice their body diameter (Kilbertus, 1980; Foster, 1988) and secondly, the pore size distribution controls gas exchange and water distribution in the soil matrix. Because soil pore structure has a profound impact on the microbial community structure, it potentially controls soil organic matter (SOM) decomposition (Sleutel *et al.*, 2012).

Several studies have tried to trace the location of SOM decomposition in the soil pore space indirectly. For example, Killham *et al.* (1993) introduced ^{14}C-labeled glucose into soil pores of two different size classes by adding a ^{14}C-labeled glucose solution, based on predetermined moisture release characteristics, to obtain a matric potential of -50 kPa or -10 kPa to predominantly fill pores with neck diameters of ca <6 µm and <30 µm, respectively. They found a greater [14]CO_2-production when the ^{14}C-labeled glucose solution was located in the larger pores and particularly when all pores with necks up to 30 µm diameter were water-filled, showing that turnover is affected by location both in terms of pore size and by the soil water matric potential under which turnover takes place. Ruamps *et al.* (2011) also introduced ^{13}C-labeled substrate in three different pore size classes (-100, -3.15 and -1 kPa) by the same method as Killham *et al.* (1993) and found evidence for significant variation in microbial community structure and C mineralization at the pore scale in undisturbed soil cores. Strong *et al.* (2004) correlated residue derived total C of added plant material after 90 days of incubation with pore size classes (<1.2 to >300 µm) and found different decomposition rates (deduced from residual native SOM after incubation) in differently sized pores: rapid decomposition rates of added plant material were found in soils with a relatively high volume of pores with neck diameters of 15-60 µm, while slow decomposition rates were found in soils with relatively high volume of pores with neck diameters <4 µm and 60-300 µm. Thomsen *et al.* (1999) found water to be the main factor controlling soil organic carbon (SOC) turnover and concluded that the effect of texture on SOM turnover is indirect: it is the soil structure determining the soil

pore size distribution that regulates water retention and thus also the water availability to the decomposer organisms. All these studies show the crucial role of the pore network and water distribution in C dynamics but detailed knowledge about their interdependence is lacking. The main reason for this knowledge gap remains the lack of data on the 3D structure of the pore network including spatial organization and information about its morphology in relation to C dynamics (Young *et al.*, 2001).

X-ray computed tomography (X-ray CT) provides non-destructive 3D visualisation and characterisation based on the variation of X-ray attenuation within objects. Warner *et al.* (1989) evaluated this technique as promising for investigating the soil pore structure and many others have used it for this purpose (Anderson *et al.*, 1990; Nunan *et al.*, 2006). In contrast, studies using X-ray CT to investigate the biological function of the physical organization of soil are far less abundant. In Chapter 3 (section 3.3) we demonstrated the compatibility of X-ray CT with incubation experiments, a conclusion derived from the fact that X-radiation did not alter soil microbial functions at a dose of order of magnitude of 5-10 Gy. De Gryze *et al.* (2006) found that microbial activity changed the porosity and pore morphology during an incubation of soil to which fresh residue was added. To our knowledge, no direct measurements of SOM decomposition have been related to the 3D pore network structure although many studies have concluded that the spatial organization of the habitat of micro-organisms should be taken into account when studying SOM dynamics (Six *et al.*, 2004; Nunan *et al.*, 2006; Young *et al.*, 2008).

The objective of this study was to relate soil respiration from undisturbed cores to the pore network structure. The idea of Strong *et al.* (2004) to perform a correlation analysis between pore network characteristics and SOM decomposition was the basis for our study. However, in contrast to previous studies, we here directly correlated cumulative C mineralization instead of residual C after incubation, with pore characteristics. We decided to hold chemical soil properties like pH constant, in order to receive meaningful data on the relationship between the pore network structure, microbial community structure and SOM decomposition. We harnessed natural variability in the pore size distribution to explicitly study its relation with SOM decomposition without co-variation of other factors such as soil C and N content and pH.

5.2 **Material and methods**

5.2.1 *Soil sampling and soil characteristics*

Our soil sampling was designed to obtain soil cores with similar pH_{KCl} (5.40±0.1), SOC and N content (4.5±0.5% SOC and 0.35±0.05% N) and similar C:N ratio (13.0±0.7) but with a variation in bulk density and pore neck size distributions (PNDs). Only C/N ratio was significant ($P<0.05$) smaller in silt loam and silt clay loam soils compared to loam soils, which demonstrates that the sampling approach was successful (Table 5-1).

We specifically used custom-built aluminium rings (Ø=1.2 cm, h=1.2 cm), with sharpened lower edge and a millimetre thickness for collecting the miniature soil samples, to obtain high resolution X-ray CT images following the incubation (see 1.2.3). Soil cores were sampled from a forest site located in Melle, Belgium (50°58'38''N; 3°47'34''E). The O-horizon (approximately 5 cm thick) was carefully removed and 18 undisturbed miniature (Ø=1.2 cm, h=1.2 cm) and six large (Ø=5 cm, h=5 cm) soil cores from the A-horizon (5-10 cm) were sampled by means of aluminium and steel rings, respectively. To achieve a gradient in bulk density among soil cores, samples were taken at three different locations (six miniature and two larger sized soil cores per location) spaced approximately ten meters apart which represented different bulk densities as revealed from a preceding survey of the site (1.06, 1.18 and 1.32 g cm^{-3}). The miniature soil cores were air-dried for two days and 0.01 M $CaSO_4$ was added drop wise. The water content of nine miniature soil cores was brought to 25% water filled pore space (WFPS), the other nine to 35% WFPS (equivalent to 0.16 and 0.23 g g^{-1} moisture content, respectively) with m_{water}= TPV*volume$_{cylinder}$*%WFPS and TPV=1-BD/ρ_s, taking into account the initial air-dried soil's water content (TPV=Total Pore Volume, BD=Bulk Density). Soil particle density (ρ_s) was determined with the pycnometer method (Blake & Hartge, 1986) and used in the porosity calculation. The soil cores were then wrapped in a single layer of gas permeable parafilm in order to minimize moisture losses. The bulk density at sampling was calculated from the dry soil weight and the volume of the larger cylinders, assuming that the cylinders were entirely filled. Bulk density was recalculated taking into account the actual soil volume at the end of the incubation experiment, which was determined from image analysis of X-ray CT volumes of the soil cores (see 5.2.3).

Table 5-1: Soil characteristics of 18 small undisturbed soil cores (Ø=1.2 cm, h=1.2 cm).

Soil core	SOC[A]	TN[B]	C:N	BD[C] Day 35	MC[D] Day 35
	(%)	(%)	(-)	(g cm^{-3})	(% WFPS)
Silt clay loam					
10	4.77	0.38	12.6	1.23	42
12	4.62	0.37	12.4	1.26	40
15	5.51	0.40	13.6	1.35	30
16	4.29	0.33	13.1	1.36	29
17	4.04	0.32	12.8	1.41	35
18	3.67	0.29	12.7	1.42	30
Average±Stdev	4.48±0.64	0.35±0.04	12.9±0.5	1.34±0.08	34±6
Silt loam					
3	4.10	0.32	12.7	1.10	49
5	4.58	0.37	12.5	1.15	64
8	4.65	0.38	12.4	1.18	58
9	4.33	0.34	12.9	1.20	42
11	4.25	0.35	12.3	1.25	41
13	4.43	0.36	12.2	1.30	45
Average±Stdev	4.39±0.21	0.35±0.02	12.5±0.3	1.20±0.07	50±9
Loam					
1	4.62	0.35	13.3	0.92	36
2	5.83	0.47	12.4	0.98	29
4	4.50	0.33	13.5	1.14	30
6	4.19	0.28	15.2	1.17	36
7	3.98	0.30	13.3	1.17	38
14	3.95	0.29	13.4	1.33	30
Average±Stdev	4.51±0.70	0.34±0.07	13.5±0.9	1.12±0.15	33±4

[A]SOC, Soil Organic Carbon content

[B]TN, Total Nitrogen content

[C]BD, Bulk Density

[D]MC, Moisture Content

The six large soil cores were used to determine a water retention curve (WRC) (two soil cores per sampling location) using the sand box method (Eijkelkamp Agrisearch Equipment, the Netherlands) for measuring volumetric moisture content at matric potentials of -1, -3, -5, -6 kPa, and the pressure membrane method (Soil moisture Equipment, USA) for measuring volumetric moisture contents at lower water tensions (-32, -100 and -1580 kPa). The water retention function of van Genuchten (1980) was fitted to the desorption data. Soil texture was measured by the pipette sedimentation method (Gee & Bauder, 1986) and pH_{KCl} was measured in 1:2.5 soil:1M KCl extracts with a glass electrode, for the three sampling locations on separate composite samples (one for each sampling location).

5.2.2   X-ray CT and reconstruction procedures

Soil cores were scanned after 35 days of incubation with a custom built high resolution nano-CT scanner at the Ghent University Centre for X-ray Tomography (see 1.5.4). The experimental conditions for the micro-focus CT scans consisted of a directional target micro-focus X-ray tube (Hamamatsu L9181) operating at 100 kV and 80 µA (8 W), an amorphous silicon flatpannel detector (Varian Paxscan 2520) with 1400 ms exposure time per projection and 1400 projections per scan of 40 minutes operated with in-house developed control software (Dierick et al., 2010). The raw data was reconstructed with the in-house developed reconstruction software Octopus (Vlassenbroeck et al., 2007) to a dataset of 1500x1500x1500 cubic voxels with 9.44 µm voxel pitch for each soil core (Figure 5-1a). Following X-ray CT scanning, the soil cores were air-dried and analyzed for their total C and N content with a Variomax CNS analyzer (Elementar Analysesysteme, Germany).

5.2.3   Image processing

Scan data for all soil cores were subjected to a similar image processing procedure to calculate total visible porosity (VP; i.e. porosity that is visible on X-ray CT images) and PND with the in-house developed software package Morpho+ (Brabant et al., 2011), in five steps: 1) selection of a region of interest in centre of the image without border artefacts, 2) applying twice a median filter (26x26x26 kernel) to remove noise and once a bilateral filter (Tomasi et al., 1998) to smooth the image (both filters preserved edges), 3) single grey value threshold segmentation of the pore space based on histogram evaluation, 4)

distance map calculation of the pore space, and 5) watershed-based separation of the pore space based on the distance map calculation resulting in a PND of the soil cores (see Appendix II). VP was calculated as the ratio of the number of segmented voxels to the total number of voxels in the image. The third step in this image analysis, segmentation, was the most subjective step in image processing according to Baveye *et al.* (2010). They found that calculated porosity from image segmentation can differ largely (12.9-72.7%) among researchers segmenting the same 8 bit image. To prevent subjective segmentation, all 16 bit images were rescaled to 8 bit images to synchronize the attenuation peaks of air (=pores). This allowed us to apply the same threshold value (65) to all 18 CT volumes based on histogram evaluation (Figure 5-1b). Finally, the outcome of VP assessed with this procedure was compared with WRC data to assure that our threshold procedure was objective. In addition, the sensitivity of the threshold value (T) to VP was calculated in a range of (T-10, T+10) for all 8 bit images as proposed by Baveye *et al.* (2010). Next, a PND was calculated with boundaries at 9.44-30-90-150-250-350 µm. Pore neck class boundaries were chosen arbitrarily. Pore neck size class <9.44 µm contains pores with small dimension without a visible pore neck on the X-ray CT images, but in reality these pores are probably connected to other pores by pore necks smaller than 9.44 µm. In this study, pore neck diameters were employed to define pore size classes because they determine pore water content at given matric potentials (Danielson & Sutherland, 1986) and control accessibility for micro-organisms (Wong & Griffin, 1976; van der Linden *et al.*, 1989; Van Veen & Kuikman, 1990). Pore neck diameters may describe water distribution and mobility of organisms better than for example equivalent sphere diameter (Sleutel *et al.*, 2008) or the number of voxels of the neck, which would overestimate the actual pore opening in case of convex pore necks. Therefore, pore size classes were calculated based on the diameter of the largest sphere fitting the pore neck and the adjacent pore volumes (Brabant *et al.*, 2011), resulting into a PND.
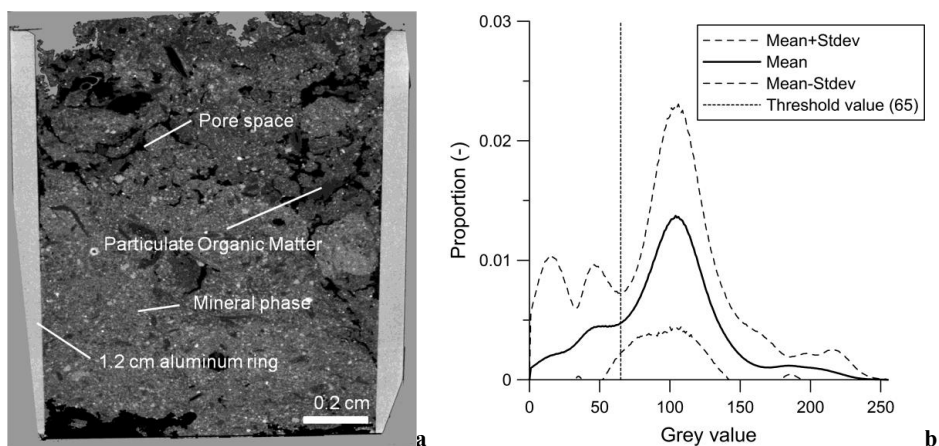
Figure 5-1: (a) Two-dimensional grey scale visualization of X-ray computed tomography attenuation of a miniature forest soil core; one voxel = 9.44x9.44x9.44 µm. (b) Mean (Stdev=Standard deviation) histogram of attenuation grey-values of 18 miniature soil cores and the chosen threshold value (65) used for image analysis of all soil cores.

5.2.4 C mineralization

All miniature soil cores were incubated at $20\pm1°C$ for 35 days in plastic containers (Ø=2.8 cm, h=4.8 cm), closed airtight with a lid and septum. Carbon mineralization was monitored by taking gas samples from the container with a 250 µl syringe at days 1, 3, 5, 7, 12, 19, 26 and 35. Containers were closed before each measurement between several hours or days, dependent on the expected CO_2 concentration, to capture the produced CO_2. CO_2 concentration in the gas sample was measured with a gas chromatograph fitted with ECD detector (Thermo Electron Trace GC Ultra). After each measurement, the containers were opened for oxygen supply. After incubation, soil cores were reweighed to determine the soil moisture content. All soil cores were then closed with caps to prevent further moisture loss and were kept in the fridge until scanning by X-ray CT.

A parallel first- and zero-order kinetic model was fitted to the C mineralization data for each soil core (see Eq. 3), assuming that SOM can be divided into two components, an easily decomposable fast pool and a more stable slow pool. The parameters C_f, k_f and k_s in this parallel first- and zero-order kinetic model were determined through non-linear regression using the Levenberg-Marquardt algorithm in SPSS 15.0.

5.2.5   Correlation analysis and statistics

A first linear correlation analysis was performed between soil characteristics (bulk density, moisture content, C and N content) and VP calculated from X-ray CT images with model parameters C_f, k_f and k_s. To establish a relationship between SOM decomposition and the soil pore network structure, a second linear correlation analysis was performed between the total VP per pore neck class (expressed in cm^3 cm^{-3}) and the mineralization rate of the slow C pool k_s. The parameter k_s was used rather than k_f and C_f because k_s is assumed to be less dependent on the inherent very large variation in labile SOM among the sampled cores, but instead relates to decomposition of a more stable C pool. Moreover, decomposition of this slow C pool dominated C mineralization during the last weeks of incubation at which time the fast C pool had been depleted, ensuring a temporal match with the soil pore size distribution data, which was derived from X-ray CT scanning and image processing at the end of the incubation. Pearson's correlations and non-linear regressions were carried out using the Gauss-Levenberg-Marquardt algorithm in SPSS (SPSS version 12.0, SPSS Inc., Chicago), except for samples 2 and 15 for which k_s was restricted to be >0 and the quadratic algorithm method was used instead. Stepwise multiple linear regression (probability of F to enter ≤0.05 and probability of F to remove ≥0.10) was executed for C_f to determine its relation to bulk density. An exceptionally high mineralization rate was observed for soil core 2 (383 mg C kg^{-1} day^{-1} on day 3 in comparison with the average of 78±86 mg C kg^{-1} day^{-1} for that day), which was therefore considered an outlier and excluded from the correlation analysis.

5.3 **Results and discussion**

5.3.1 *Soil sampling and soil characteristics*

Soil texture was measured on one composite sample per sampling location and was silt clay loam, silt loam and loam for the three sampling locations. WRC data were very similar among the three sampling locations (small standard deviations in Figure 5-2). The water content at saturation (θ_s) was on average 0.616 ± 0.012 cm^3 cm^{-3} and average soil particle density was 2.45 ± 0.02 g cm^{-3}.
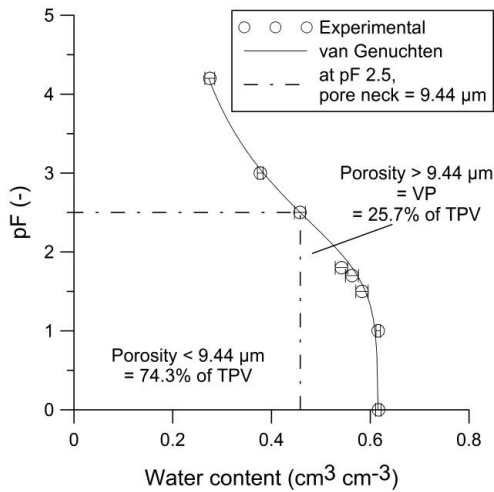
Figure 5-2: Average Water Retention Curve (n=6) of the three sampling locations (Error bars are standard deviations) shows the ratio of 1/4th between visible porosity (VP), i.e. pores visible on X-ray computed tomography images with a resolution of 9.44 µm, and total pore volume (TPV).

Despite wrapping the soil cores with parafilm, moisture loss occurred during the 35-days incubation and resulted in shrinkage of soil volumes, changing both bulk density and moisture content as compared to the initial situation. Bulk density of small soil cores increased (from 0.97 ± 0.14 g cm^{-3} at day 1 to 1.22 ± 0.14 g cm^{-3} at day 35), which led to a decrease in total pore volume (TPV) of small soil cores of 17% (from 0.604 ± 0.058 to 0.502 ± 0.056 cm^3 cm^{-3}). The initial TPV of small and large soil cores was only slightly different (0.604 ± 0.058 and 0.614 ± 0.005 cm^3 cm^{-3}, respectively) and the slightly lower TPV of the small soil cores was probably originated from a lack of macro porosity compared to large soil cores. Although small soil cores suffered water evaporation, water

contents expressed in % of water-filled pore space (WFPS) increased because of decreasing TPV. The original goal of creating a range in bulk density was still maintained, but the two original water contents of 25 and 35% WFPS changed unevenly and resulted in a range of water contents (29-64% WFPS, on average 39±10% WFPS) (Table 5-1). In further analysis, the bulk densities and water contents at the end of the incubation (day 35) were used. WRC measured on the large soil cores were only used relatively to validate the results of image segmentation (see 5.3.2).

5.3.2   Pore neck size distribution

In this study, VP designates total porosity calculated from image analysis of the scanned CT volumes (thus porosity >9.44 µm maximum opening of the pore neck), while the term Total Pore Volume (TPV) designates total porosity calculated from the bulk density of the miniature soil cores. X-ray CT quantified VP averaged 13.2±0.1% for all 18 miniature soil cores. Average TPV over the three sampling locations was 61.6±0.6%. From the average WRC data it was estimated that 25.7±0.5% of TPV has pore necks larger than 9.44 µm maximum opening (Figure 5-2). Thus, on average over all soil cores VP should be 13.0% (25.7% of the average TPV of 50.4%). VP and TPV were significantly and positively correlated (r=0.702, P<0.01).

No large overestimation in porosity was made during image segmentation, a common problem that was found in a round-robin test of Baveye $et\ al.$ (2010). Moreover, the sensitivity analysis of the chosen threshold value (T-value) showed only a small change in VP (+3.34%, -2.41%) when the segmentation process was repeated with (T+10, T-10). The similarity between VP measured by X-ray CT and the relative portion of porosity >9.44 µm found with WRC data and the sensitivity analysis both demonstrate the validity of the segmentation in pore space and mineral soil by X-ray CT in this study. The similarity between VP measured by X-ray CT and the relative portion of porosity >9.44 µm found with WRC data was also seen in correlation analysis. VP and bulk density at day 35 were significantly negatively correlated (r=-0.702, P<0.01). As both variables were retained independently from each other, this shows that VP results based on image analysis, are in line with traditional porosity measurement of TPV based on bulk density. As a remark, the ratio of VP:TPV was negatively correlated with bulk density (r =-0.533, P<0.05) because larger pores are more likely visualized and segmented through

thresholding and evidently there is always a shift towards larger pores with decreasing bulk density; more porosity is thus visible via X-ray CT at low bulk density.

The average VPs were 0.64±0.27, 0.55±0.31, 2.10±0.94, 1.66±0.71, 2.12±0.94, 1.84±1.00 and 4.28±4.27%, for the <9, 9-30, 30-90, 90-150, 150-250, 250-350 and >350 µm pore neck classes, respectively (Figure 5-3). In each pore neck class at least a 3-fold range in porosity existed among the soil cores. This range was largest for the >350 µm (30-fold) pore neck classes compared to an average 5-fold range in other pore neck classes. The original goal to create substantial variation in bulk density and volume percentage of several of the pore neck size classes was successful. VP of each pore neck class decreased with increasing bulk density but only for the 30-90 and >350 µm pore neck classes a significant correlation with bulk density was found (Table 5-4).
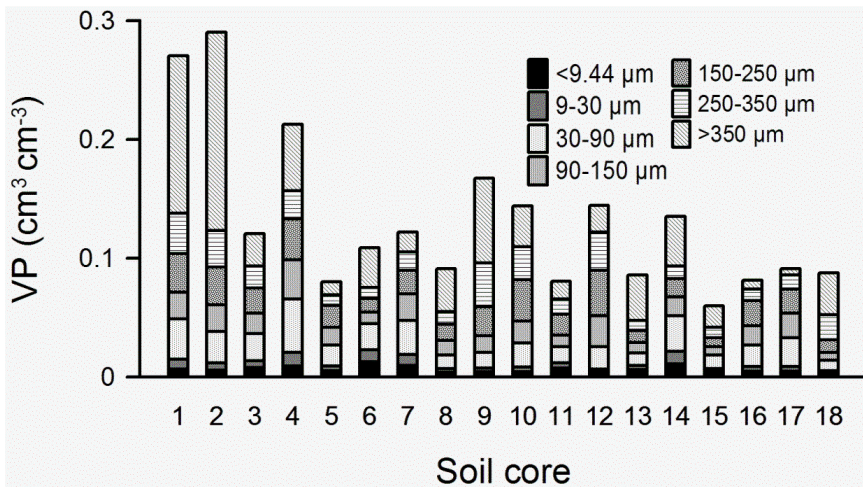
Figure 5-3: X-ray computed tomography visible porosity (VP, at resolution 9.44 µm) divided into seven pore neck classes for 18 miniature soil cores (Ø=1.2 cm, h=1.2 cm) ordered from left to right according to increasing bulk density.

Because sufficient variation of VP per pore neck class among soil cores existed, a correlation analysis with the slow pool C mineralization rate k_s was possible (see 5.3.4). A lack of sufficient ranges in porosity per pore neck class could have covered up existing correlations with other variables. Strong *et al.* (2004) also executed a correlation analysis based on a minimum 2-fold range of porosity per pore neck class using a similar sampling procedure over a natural gradient in texture, although with very large co-variation in SOC and N content. Even larger variation in pore neck class volumes was achieved in Chapter 4 were we manipulated soil pore distributions by remixing different soil fractions, with however substantial disturbance of the 'natural' pore network structure. Our choice for sampling undisturbed soil cores appeared sufficient for pore size class ranges without the risk of influencing microbial community structure.

5.3.3 C mineralization

Overall, the C mineralization rate was highly variable among the soil cores and was highest at days 1 and 3 (73 and 78 mg C kg^{-1} day^{-1}, respectively) and steeply decreased thereafter (Table 5-2). This brief pulse of respiration represents biomass-C released by water potential increase and desiccated biomass-C when a dry soil is rewetted (Kieft *et al.*, 1987). The cumulative C mineralization after 35 days ($C_{cum,35}$) ranged from 0.3 to 5.2% of SOC (data not shown). The parallel first- and zero-order kinetic model fitted well to $C_{cum,35}$ for all soil cores ($R^2 \geq 0.98$). Average mineralization rate of the slow C pool k_s (4.6±3.6 mg C kg^{-1} day^{-1}) was slightly lower than average mineralization rate at day 35 (5.4±3.8 mg C kg^{-1} day^{-1}). This could indicate that at the end of the incubation the fast degradable C pool was not depleted. However, the contribution of the fast degradable C pool to C mineralization was small (15%) and mineralization rate at day 35 and k_s correlated strongly (r=0.968, P<0.01).

The significant negative relationships between C_f and k_s on one hand and bulk density on the other in a first correlation analysis (Table 5-3), demonstrated a clear connection between biological processes such as SOM decomposition and soil structure. In contrast, De Neve & Hofman (2000) found that variation in bulk density (1.2-1.6 g cm^{-3}) did not significantly influence native SOM mineralization in an arable soil. However, they did find an influence of bulk density on C mineralization from added crop residues (0.92-1.42 g cm^{-3}) and this situation probably much better resembles our studied forest soil with 4.3% C and particulate OM or plant residues that were visible on X-ray CT images.

Moisture content at day 35 (in %WFPS) correlated significantly ($P<0.01$) and positively with C_f, but not significantly with k_s (Table 5-3). C_f represents the amount of easily degradable C-sources, such as particulate OM and dissolved OM. Particulate OM (POM) chiefly resides in large pores that are air-filled at lower moisture content, and consequently do not contribute substantially to soil C mineralization (Thomsen *et al.*, 1999). The large sensitivity of the fast pool C mineralization parameter C_f to moisture content could have resulted from this strong dependency of particulate OM decomposition on water availability in the larger pores, and thus on %WFPS. On the contrary, the slow C pool is probably constituted by finer mineral bound and aggregate occluded OM, less restricted to larger pore size classes and less dependent on moisture content. The latter could explain why k_s was only related to bulk density and not to moisture content, unlike C_f. So it appears that slow C pool mineralization primarily depended on differences in soil bulk density, and consequently on pore network structure. This is confirmed by linear modeling data where k_s was very strongly influenced by bulk density alone (adj. $R^2=0.588$, $P<0.01$). Abera *et al.* (2012) found that decomposition of the more recalcitrant fractions of added litter was more severely inhibited by moisture limitations (pF 3.9 vs. pF 2.5) than the labile fractions. This influence of chemical composition of OM on the relationship between water content and OM decomposition when the location of both substrates can be considered similar (as the addition was), suggests to interpret the slow and fast C pools in Eq. 3 not only in terms of their chemical composition, but also in terms of their location in the soil matrix. Indeed, both pools can include labile and recalcitrant material and the different mineralization rates of both pools can be caused by other factors besides their chemical composition. The stronger relationship between mineralization rate of applied ryegrass with microbial available water (>0.2 µm pore neck diameter) compared to total volumetric water content in Thomsen *et al.* (1999), shows that freshly added POM is mainly located in larger pores compared to native SOM. Moreover, Killham *et al.* (1993) found that turnover of added ^{14}C-labeled glucose was higher in 6-30 µm pores than in <6 µm pores, and this difference in [14]CO$_2$ production between pore size classes became even larger when all pores with necks up to 30 µm were water-filled. Thus, the decomposition of OM located in larger pores is more subjected to changes in soil water content than OM located in smaller pores. Similarly, Scott *et al.* (1996) found %WFPS to affect litter decay differently from the mineralization of native soil C but in contrast to our findings, a stronger correlation existed between WFPS and native SOM ($R^2=0.77$) compared to

Table 5-2: C mineralization rate after 1, 2, 5, 7, 12, 15, 26 and 35 days of incubation, calculated 35-days cumulative C mineralization ($C_{cum,35}$) and parameters C_f, k_f and k_s of the first- and zero-order kinetic C mineralization model for 18 undisturbed soil cores (Ø=1.2 cm, h=1.2 cm).

Soil core	Mineralization rate (mg C kg⁻¹ day⁻¹)								$C_{cum,35}$ (mg C kg⁻¹)	C_f (mg C kg⁻¹)	k_f (day⁻¹)	k_s (mg C kg⁻¹ day⁻¹)
	day 1	day 3	day 5	day 7	day 12	day 19	day 26	day 35				
1	134.0	153.9	50.6	46.0	17.6	13.5	10.8	10.2	1169	808±20	0.233±0.010	10.27±0.73
2	287.1	382.8	262.1	190.3	190.1	28.2	12.9	14.9	4111	4378±1240	0.096±0.027	0.00±32.51[A]
3	60.6	79.6	38.6	36.1	22.4	15.8	10.4	8.1	857	590±21	0.125±0.005	7.87±0.62
4	71.6	64.7	72.9	26.4	9.8	6.7	7.9	7.9	719	515±52	0.190±0.010	5.54±1.01
5	131.4	84.5	84.4	40.5	18.2	9.8	6.6	5.7	999	805±29	0.191±0.009	10.27±0.71
6	46.3	132.9	23.1	26.1	7.5	9.0	4.2	5.6	655	501±53	0.155±0.019	7.74±1.79
7	82.1	79.7	35.4	27.6	11.0	6.8	5.8	7.0	683	480±9	0.197±0.030	5.60±1.81
8	109.6	94.2	52.9	41.8	22.2	12.8	11.2	9.8	1023	665±20	0.224±0.007	5.73±0.33
9	68.7	74.8	69.5	38.3	15.9	11.6	10.3	10.1	871	596±55	0.210±0.035	4.30±1.91
10	53.6	51.1	49.8	27.0	17.0	10.2	7.8	7.2	679	480±28	0.128±0.014	0.69±1.01
11	37.7	33.7	26.1	26.2	6.2	4.0	3.2	1.7	388	365±34	0.135±0.009	5.75±0.86
12	68.4	49.6	49.4	21.5	14.4	12.5	8.9	8.1	697	385±17	0.143±0.007	0.85±0.40
13	37.3	34.6	19.5	20.2	6.9	3.5	2.3	1.1	345	317±13	0.202±0.014	9.00±0.62
14	44.3	24.9	5.7	28.2	4.7	4.2	3.0	3.0	348	274±41	0.151±0.029	2.12±1.33
15	24.0	16.9	5.6	18.8	0.9	1.0	0.0	0.6	176	179±29	0.155±0.033	0.00±0.94[A]
16	14.4	15.8	6.6	6.1	1.8	1.4	1.0	0.3	125	100±2	0.203±0.005	0.73±0.05
17	22.6	7.3	37.7	3.1	3.0	2.4	1.2	1.9	199	163±29	0.204±0.011	0.50±0.15
18	16.8	22.9	2.6	9.7	1.0	1.4	0.6	0.5	142	124±4	0.179±0.046	0.98±1.00

[A]The restriction $k_s>=0$ was applied during non-linear regression

surface-applied plant litter, recalcitrant (R^2=0.57) or labile (R^2=0.45). However, the surface-applied litter remained moist throughout their incubation, so that a lower WFPS in the soil had only a small influence on litter decomposition. Therefore we hypothesize that the WFPS-dependence of the C pool C_f in contrast to the independence of mineralization rate k_s of the second pool suggests that the C pool C_f was probably located in larger pores, in comparison with OM that was mineralized at a slower rate k_s, the latter being less subjected to varying WFPS when located in smaller pores.

Table 5-3: Pearson's correlation coefficients between soil characteristics, X-ray computed tomography visible porosity (X-ray CT VP) and parameter estimates of the parallel first- and zero-order kinetic C mineralization model (r).

	C_f	k_f	k_s
SOC	0.193	-0.125	0.161
TN	0.195	-0.292	0.190
Bulk Density	-0.901**	-0.241	-0.783**
X-ray CT VP	0.518*	0.320	0.618**
Moisture Content	0.666**	-0.174	0.477

*,** denote 5% and 1% significance level according to Pearson's correlation.

5.3.4 C mineralization and pore network volume

Overall, the linear correlation coefficients between VP per pore neck class and k_s increased with increasing pore neck size class with the exception of the >350 µm pore neck class (Figure 5-4). Correlation coefficients were positive for all pore neck size classes except for the <9 µm pore neck class. Three correlations were significant between VP and k_s: for pore neck classes 150-250, 250-350 and >350 µm (P<0.05). All data were also plotted to check for possible non-linear relationships but no such correlations were apparent for any of the pore neck size classes.
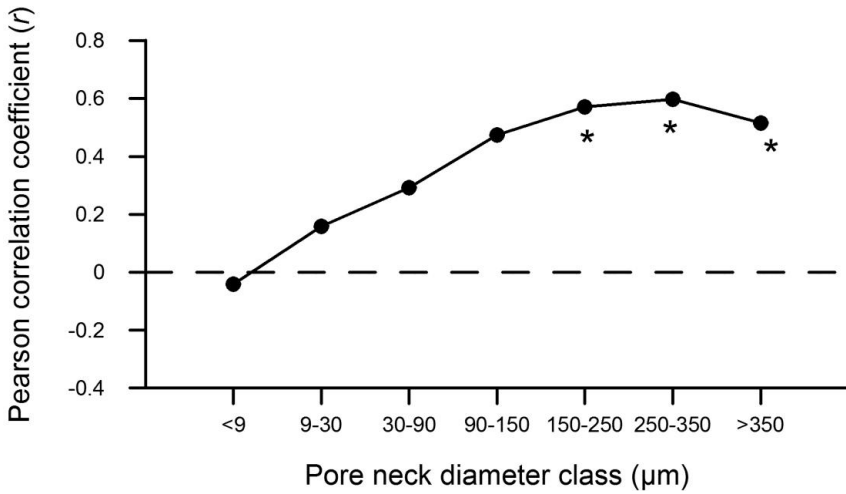
Figure 5-4: Correlation coefficients between X-ray computed tomography visible porosity per pore neck class and the zero-order C mineralization rate constant of the slow SOM pool k_s ($P<0.05$* or $P<0.01$** according to ANOVA's F-test).

The positive relationship between larger pore neck classes (>150 μm) and k_s could be caused by relationships between k_s and pore neck classes smaller than 9.44 μm pore neck, although these were not visible on the X-ray CT images. Strong *et al.* (2004) found an autocorrelation for larger (>300 μm) pore size classes and smaller ones (<4 μm), and both pore size classes were related to SOM protection. However, the autocorrelation of the pore size classes with each other actually made it difficult to separate the contributions of both pore size classes to SOM protection. Unfortunately, the spatial resolution in this study was too small to confirm that smaller pore size classes contribute to SOM protection, although the correlation map of VP per pore size class with k_s approached a more negative trend between <9.44 μm pore neck size class and k_s.

Table 5-4: Correlation analysis between the zero-order C mineralization rate constant of the slow SOM pool k_s, visible porosity (VP) in each pore neck class and porosity measurements (Pearson's correlation coefficients r).

	Porosity per pore neck class (boundaries in µm)							X-ray CT VP[A]	Bulk Density
	<9.44	9-30	30-90	90-150	150-250	250-350	>350		
k_s	-0.041	0.158	0.292	0.474	0.572*	0.598*	0.516*	0.618**	-0.783**
<9.44		0.901**	0.581*	0.139	-0.112	-0.278	0.078	0.199	-0.296
9-30			0.852**	0.456	0.182	-0.029	0.335	0.529*	-0.468
30-90				0.818**	0.562*	0.244	0.377	0.717**	-0.486*
90-150					0.845**	0.476	0.217	0.664**	-0.383
150-250						0.765**	0.356	0.726**	-0.440
250-350							0.639**	0.762**	-0.421
>350								0.857**	-0.660**
X-ray CT VP[A]									-0.702**

[A]VP, Visible Porosity in X-ray computed tomography (CT) images (= sum of all pore neck classes)

[B]*,** Correlation coefficient r was significantly different at 5% and 1% significance level according to Pearson's correlation

Based on WRC data, only pores with necks smaller than 0.04 or 3.6 μm could be water-filled at an average and maximum water content of 39 or 64% WFPS, respectively. The accessibility of POM located in the largest pores through the water phase would only be possible through water films (Or *et al.*, 2007). Unfortunately, the dimensions of these water films are too small (around 10 nm thickness at field capacity according to Or *et al.* (2007)) to be visible on the X-ray CT images. Thus, we cannot answer the questions we originally asked about the effects of water content and pore structure. Future advances in X-ray CT which result in a better signal-to-noise ratio, e.g. via increased X-ray flux, would enable semi-automized segmentation of water- and air-filled pore space to further investigate the nature of a presumed 'air-water interface'.

Ekschmitt *et al.* (2008) stated that distribution patterns of decomposer organisms in the soil do not generally match the allocation patterns of SOM, which may be physically protected from microbial decomposition by its spatial separation from decomposers, which are limited in their mobility. For example Kilbertus (1980) showed that soil organisms are likely to reside inside pores sized three times their body size. We could add that perhaps it is the unequal distribution of water, O_2 and OM in the soil matrix (e.g. particulate OM in larger air-filled pores), rather than physical barriers, which separates decomposers from their substrates. McCarthy *et al.* (2008) found that most of the OM resides in pores that could accommodate exo-enzymes and even bacteria. Consequently, in their view, protection of SOM against microbial decay arises from spatial and kinetic constraints imposed on the ability of microbial exo-enzymes to access and degrade the OM and on the delivery of hydrolysis products that can be assimilated by the microbes. In this study, we were unable to draw conclusions on the predominance of abiotic or biological constraints imposed on SOM decomposition. In this experiment, 74.3% of porosity had pore necks <9.44 μm and only 39% of TPV was water-filled. Thus, microbial activity and mobility or diffusion of exo-enzymes and hydrolysis products could have been obstructed in <9.44 μm neck diameter pores by limitations to water. Moreover, this pore neck class showed a weak negative correlation with k_s, suggesting protection of SOM. Thomsen *et al.* (1999) found that at moderate matric potentials, lack of O_2 may limit microbial activity in the inner part of aggregates in clay-holding soils. Such conditions were certainly met in this study's soils with clay contents of 11-31% and a well developed aggregation (undisturbed forest soil cores). In line, Killham *et al.* (1993) found a greater turnover of added C when the soil was held at a lower matric potential.

All findings combined lead to the conclusion that no single pore size class can be responsible for only SOM decomposition or protection from microbial decomposition. For example Young & Ritz (2000) found that the location of bacterial cells in the pore space depends on water content as they were found to be located in smaller pores in dry soils when compared to wet soils. In agreement with Thomsen *et al*. (1999), we hypothesize that it is the water distribution in soil, regulated by the soil pore size distribution, which primarily determines the location of SOM decomposition in the soil pore network. It is therefore only possible to identify certain pore classes as 'the' relevant ones for SOM decomposition for a very specific combination of soil pore size, water and OM distribution, such as may be generated in lab experiments but not for all soil types and circumstances.

5.4 Conclusion

There is a general consensus that the spatial organization of the soil pore network exerts a significant influence on soil microbial processes including C mineralization. Our study demonstrates the potential value of X-ray CT to study this spatial organization of soil, despite some difficulties during image processing due to sample size, observer-dependence and resolution. Combining X-ray CT with incubation experiments at the scale employed in this study can provide new insights in the study of SOM stabilization mechanisms, particularly when the pore network structure can be visualized in a spatially explicit manner as was the case here. We hypothesize that C mineralization is located at a moving zone of air-water interfaces in the 3D soil matrix, which is determined by soil moisture content and the pore size distribution. Consequently, no single pore size class may be responsible for neither C mineralization nor C protection. In combination with soil incubation studies, development of bench top X-ray CT visualization of both water- and air-filled pore space, for example by future hardware-driven increased X-ray flux, will open up new possibilities to study the interplay of soil pore space, water distribution and SOM location on SOM decomposition.

Chapter 6:

General Discussion and conclusions

6.1 <u>Introduction</u>

Despite the growing body of evidence showing the importance of micro-habitat structure for many microbial processes, little detail is known about the topology and distribution of soil pore networks at the micro-habitat scale (Nunan *et al.*, 2006). As elaborated in the introduction (Chapter 1) using soil aggregates as surrogates for soil structure is a gross oversimplification. Therefore, we considered the soil organization as a continuous soil pore system within the framework of the mineral matrix. Since the soil pore system constitutes the actual habitat of micro-organisms, which in turn mediate biological processes including SOM decomposition, it appears evident to establish causal relationships between SOM decomposition and soil pore network structure. The present study consists of two parts. In part 1, we developed and tested the use of X-ray CT in soil biological experiments that include the assessment of microbial activity. In part 2, X-ray CT was used for the first time in combination with incubation experiments employing miniature soil cores (approximately 1 g soil) for investigating the role of soil pore network structure on soil C dynamics.

6.2 <u>Applicability of X-ray CT in soil biological experiments</u>

A first objective (**objective 1**) was to develop a methodology for X-ray CT scanning and related image processing to quantify the soil pore space. Two software programs (Avizo Fire 6.2 and Morpho+) were compared for their ability to retrieve soil pore network information from X-ray CT images by applying a series of algorithms. Ideally the soil pore network should be quantified in such a way that it allows analysis of the real interactions between the soil pore network, the water distribution and the distribution of soil organisms within the pore space. Because water distribution and the location of soil organisms are determined by pore necks (van der Linden *et al.*, 1989; Van Veen & Kuikman, 1990), i.e. the entrance to the pores, pore necks were the basis for selecting a software program. In contrast to Avizo Fire 6.2 (www.vsg3d.com), Morpho+ (Brabant *et al.*, 2011) contains an algorithm called 'watershed-based separation' (see Appendix II), allowing the description of the soil pore structure based on pore necks. We expressed the size of the pore necks as 'maximum opening', i.e. the largest diameter of a sphere fitting in the smallest opening of the pore neck and the adjacent pore bodies (Brabant *et al.*, 2011). This measure may describe water distribution and mobility of organisms better than for example equivalent sphere diameter (Sleutel *et al.*, 2008) or the number of voxels of the neck, which would overestimate the

actual pore opening in case of convex pore necks. All analyses in this thesis were executed with Morpho+, whereas Avizo Fire was used for its excellent 3D rendering algorithms. Only in Chapter 4, soil pore network was retrieved based on pore equivalent sphere diameter, instead of maximum neck opening.

Results for porosity and other pore characteristics seemed highly dependent on the selected threshold value during segmentation in all chapters. The sensitivity of porosity quantification on the selection of a grey value could be evaluated by recalculating porosity at an increased or decreased threshold value with 5 or 10 units. In addition, image analysis of aggregates showed that the selection of a volume of interest in the centre of the sample was necessary to avoid edge effects during image analysis, e.g. large porosity overestimation due to similar grey values of porosity and background voxels. The visualization of organic matter in the soil pores was only possible for larger particles (>100 μm). The intimate association of organic matter and the mineral matrix resulted quite often in mixed voxel values due to the partial volume effect (see Appendix I) and could not be automatically separated from dark pore voxels. It was, however, possible to visually differentiate large organic matter particles from pores because of the rough surface texture of organic matter compared to pores and mineral particles.

A second objective (**objective 2**) was to investigate which soil pore network characteristics can be reliably quantified for a range of scales going from the micro aggregate level to the undisturbed soil core level. We found that visualization of pore properties was highly scale-dependent; along with decreasing object dimension, an increase in voxel size resulted in different observations and quantification of the pore space. Earlier, Nunan *et al.* (2006) already mentioned that porosity in natural undisturbed soils is often scale-dependent. Because calculations of porosity and other parameters depend highly on image resolution, Al-Raoush & Willson (2005) suggested carrying out a representative elementary volume (REV) analysis before the actual image processing to minimize errors as a consequence of the given resolution of the images. The results (Chapter 2) demonstrated the need for a REV analysis before analyzing the CT images for pore properties of interest. A REV analysis determines the minimum size of the volume of interest during image analysis that is required to retrieve porosity results independent from the location selection of the volume of interest in the soil sample. Based on the results in Chapter 2, we suggest minimal REV sizes for porosity measurements of approximately 21, 37, 6 and 12 (expressed as ratio between cube side length and average pore diameter) for soil samples with approximate diameter of 5 cm, 2 mm, 500

and 250 µm. Al-Raoush & Papadopoulos (2010) even suggested that a REV analysis should be carried out for every parameter calculated from X-ray CT, because the minimum REV size for porosity in their study was different from the REVs for other parameters such as particle size distribution, local void ratio and coordination number. Results of Chapter 2 showed that X-ray CT data acquired at the soil core level (Ø=5 cm) could be useful in the study of soil processes like water flow and the alteration of the soil structure by earthworms and other soil fauna. The application of X-ray CT at the aggregate level (Ø=250 µm to 2 mm) seemed more useful for the visualization of the physical environment in which microbes and their grazers operate and shows potential for investigating the mutual interaction between soil structure and SOM decomposition through visualizing the habitat of soil organisms.

The pore neck size distribution calculated from CT images and from water retention curve (WRC) data (Chapter 2) could only be compared meaningfully for macro porosity at the soil core level. Porosity at smaller scales (aggregate level) from both methods could not be compared because the aggregates were subsamples of a complete undisturbed soil core and the proportion of macro, sub-macro and micro aggregates in the original soil cores was unknown. In general, porosity measurements based on CT images are always limited by resolution, so that only a part of the pore size distribution can be quantified. Moreover, the similarity between the pore neck size distributions retrieved from X-ray CT images and WRC data is dependent on soil texture. In sandy soils, X-ray CT images will visualize a large part of the pore size distribution in contrast to clay soils, where most porosity has dimensions smaller than the resolution of CT images. For example, CT-based total porosity calculations for a soil with low clay content (Chapter 4) were $4/5^{th}$ of actual TPV values than for more clayey soil (Chapter 5) where only $1/4^{th}$ of porosity was visible. In chapter 2, the resolution of the X-ray CT images of the macro aggregates (10.0 µm) was similar to the ones in chapter 4 and 5 but the actual bulk density and thus TPV of the aggregates was not calculated. Based on TPV of the original undisturbed soil cores (0.42) before physical fractionation, $1/4^{th}$ of TPV was visible on the X-ray CT image of these silt loam macro aggregates. The magnitude of the VP:TPV ratio of the silt loam soil in chapter 2 and the silt clay loam, silt loam and loam soils in chapter 5 is similar, concomitant with their higher clay contents compared to the sandy loam soil in chapter 4.

A third objective (**objective 3**) was to investigate the usage of small sample sizes in soil incubation experiments in order to adapt biological assays to an X-ray CT compatible scale. In Chapter 3, incubation of soil at different sample sizes was found to yield different

measurements of cumulative C mineralization, microbial biomass C and dehydrogenase activity. It would appear that the observed differences between the sample size are a result of deviation in the water distribution in soil after rewetting of small (1-5 g) and commonly (>40 g) sized soil cores used in incubation. More experimental work is needed, however, to verify this hypothesis. There also exists an interaction between the established soil water content and this sample size effect, with a relatively smaller effect of sample size on soil biological parameters at lower moisture content. When differences in water distribution among different sample sizes were ruled out by only evaluating C mineralization rate during the last weeks of incubation, only a limited remaining effect of sample size was observed. In conclusion, soil biological experiments with very small soil cores (e.g. 1 to 5 g soil) should be interpreted with caution, because sample size may affect microbial processes. Still, for a given sample size one can study effects of different soil treatments (e.g. variation in soil pore network structure, different soil moisture levels) on soil biological parameters like soil respiration, microbial biomass C and enzyme activities. However, extrapolation of the outcomes to larger scales can only be done with care and this limits comparison with previous studies, most often carried out on larger soil masses.

The effect of X-ray CT scanning on the microbial community and on C mineralization was investigated for the first time (Chapter 3, **objective 4**). Irradiation significantly affected dehydrogenase activity and Phospholipid Fatty Acid (PLFA) biomarkers for Actinomycetes after one day. However, this effect was short-lived because after three weeks after no influence was observed anymore on any of the soil biological parameters and processes (β-glucosidase and dehydrogenase activity, microbial biomass quantified by total PLFA and C mineralization). The fact that C mineralization was unaffected while there was an initial shift in microbial community structure can be explained by redundancy in microbial functions (Garcia-Pausas & Paterson, 2011). Although effects of irradiation cannot be excluded completely, this study showed that usage of X-ray micro-CT is compatible with soil biological experiments. Based on this study, a time lag of three weeks between X-ray scanning and analysis of soil biological parameters seemed largely sufficient to rule out effects of X-radiation, even on such sensitive parameters like dehydrogenase activity. This apparent compatibility of X-ray micro-CT with studies of soil biology and biochemistry is very promising and opens up exciting new possibilities for studying the role of the soil pore network in regulating soil biological processes. Combining X-ray CT scanning and assessment of biological soil parameters on the same soil cores would help to explain the

outcome of correlation analyses between pore volume classes and C mineralization data (Chapters 4 and 5).

6.3 Combined use of X-ray CT in soil biological experiments to study the role of the pore network structure in SOM decomposition

A fifth objective (**objective 5**) was to use X-ray CT in lab scale incubation experiments to study the relationship between pore network structure and SOM decomposition. In a second part of this PhD, X-ray CT was for the first time used in combination with incubation experiments employing miniature soil cores to investigate the role of soil pore network structure on soil C dynamics. In a first study (Chapter 4), the soil pore network structure was artificially manipulated by combined treatments of soil compaction and artificial change of the soil texture with substrate addition. Correlation analysis revealed no significant relationships between C mineralization and the volumes of any of the considered pore size classes. At first sight, this outcome would suggest that pore network structure plays only a minor role in SOM decomposition. However, the lack of correlation between soil pore structure and SOM decomposition was perhaps not surprising. Indeed, all particulate OM (which by definition would reside in larger pores) was removed, and at the moisture level in this study (28% WFPS), water resides mainly in pores with <5 µm necks. Probably, native C mineralization was located in smaller pore size diameter classes (10-400 µm), which remained largely unaffected by the manipulations of the soil pore network structure. Contrary to the treatments without substrate additions, net C mineralization of freshly added substrates was significantly correlated to volumes of several individual pore size classes. This correlation analysis revealed the importance of macro porosity (>410 µm) for mineralization of freshly added substrates. The effect of the soil pore structure manipulations on substrate C mineralization was found to be highly dependent on substrate quality. While soil compaction (bulk density from 1.0 g cm^{-3} to 1.3 g cm^{-3}) decreased C mineralization of both grass and sawdust amended soils, a very strong inhibitory effect of artificial change to a coarser soil texture was only observed for the sawdust amended soil. The incubation experiments revealed that substrate derived C mineralization depends on the soil pore network structure. Soils were incubated at low bulk densities in this experiment (Chapter 4) in order to allow the visualization of particulate organic matter in the soil matrix. The purpose of this visualization was to explain the outcomes of the incubation study based on the observed differences in contact between organic matter and the mineral matrix. However, the level of contact between

organic matter particles and mineral particles could only be described qualitatively because of lack of contrast between both phases. Future improvements in image contrast in X-ray CT scans are expected to allow a quantitative description of the physical contact between organic matter and mineral particles. Moreover, assessment of the microbial community structure might help to explain the observed interaction effect between the influence of substrate quality and pore soil structure on C mineralization (Chapter 4), e.g. Sleutel *et al.* (2012) found an increased fungal/bacterial ratio after artificially changing soil texture to a higher sand fraction. Since X-ray CT scanning is compatible with measurements of soil biological parameters (Chapter 3), combined assessment of the microbial community structure with soil pore structure quantification will improve our insight in soil structural dependence of SOM decomposition (Chapters 4 and 5).

In a second study (Chapter 5) the influence of the soil pore network structure on native C mineralization in undisturbed soil cores collected in the field was studied. Here we relied on natural variation in texture and soil pore network structure instead of using artificial manipulations. In contrast to the first study, we used the volumes of pore neck size classes rather than pore diameter classes. Results once more revealed an important role of macro porosity (with pore neck diameter >150 µm) for native C mineralization. It would appear that the effect of macro porosity on native SOM derived C mineralization was indirect, by enhancing aeration and gas exchange with surrounding smaller pores. The role of macro porosity in C mineralization processes was mostly subordinate to the closely related volume of medium soil pores, as seen in previous studies (van der Linden *et al.*, 1989; Killham *et al.*, 1993; Wright *et al.*, 1995), but our findings are in line with other studies that also concluded the importance of oxygen for microbial activity in aggregates (Sexstone *et al.*, 1985; Sollins *et al.*, 1996). In agreement with Strong *et al.* (2004), native SOM C mineralization took primarily place in medium sized pores. The hypothesis that very fine pores protect OM from microbial decomposition (Marschner & Kalbitz, 2003) could not be verified at the scale of the X-ray CT images in our study. Most probably, C mineralization is regulated by air/water ratios in pores which are regulated by the soil structure and the pore size distribution. Because of the high temporal variation of soil water content and water distribution, the part of the pore size distribution that is water-filled or air-filled constantly changes. Therefore, we conclude that no single pore size class may be responsible for neither C mineralization nor C protection as the location of SOM decomposition changes along with the temporal variation in soil water distribution in the pores space.

6.4 <u>Further research</u>

The present PhD provides a basis for establishing X-ray CT as a valuable tool for elucidating the relationship between soil structure and SOM dynamics. Contrary to the continued emphasis on soil aggregates for studying the role of the soil structure on SOM dynamics, we considered the soil structure as a continuous pore space within the soil matrix.

In chapter 2 we observed some differences between PNDs retrieved from WRC data and X-ray CT images despite the fact that both are determined based on pore necks. However, deduction of PNDs from WRC data rely on Jurin's law which describes the relationship between soil pressure head (h) and pore dimensions that contain water at a certain value of h. This law is only an approximation of a very complex physical reality (pores are not straight capillary tubes and may be partly covered with microbial extracellular excretions and SOM). Furthermore, the water retention curve relies on extraction of water starting from saturation of soil cores. When rewetting a relatively dry soil core uniform spread over the entire core volume may well not be guaranteed. Such artifacts, which may be common in many classical incubation experiments, could be visually controlled by assessment of the actual physical distribution of water over the soil pore network by X-ray CT. Location of water in the soil pore space, with (Mooney & Morris, 2008) or without (Tippkötter *et al.*, 2009) the use of a contrast agents would provide direct evidence for the degree of similarity between the calculated PND based on WRC data and the actual location of soil water. Connected to this issue, the role of the propagation of water in the observed differences in C mineralization (Chapter 3) could be evaluated by repeated X-ray CT assessment of the water distribution (e.g. every 4 hours) of differently sized soil cores at different water levels. In combination with headspace analysis of CO_2 by gas chromatograph measurements at the same time intervals, we could unravel the real mechanism behind the C mineralization differences found in Chapter 3.

The compatibility of X-ray CT scanning with assessment of soil microbial functioning (chapter 3) opens up exciting possibilities for studying the relationship between the 3D soil structure, the microbial community functioning and SOM decomposition. Consequently, soil pore size distributions can be quantified on the same undisturbed soil cores where C mineralization, enzyme activities and microbial community structure are determined as well. Moreover, by repeatedly quantifying soil pore size morphology during incubation experiments, the direct influence of microbial activity on their habitat structure could be

investigated. The combination of X-ray CT with incubation and assessment of biological parameters at different moisture levels and pore structure could address the hypothesis that dry circumstances in soils are more favorable for fungi than bacteria because their hyphen can still reach smaller pores that are still water-filled at low soil water content.

The direct control of pore size distribution on SOM decomposition (through separation of SOM from its decomposers) and its indirect control via the regulation of water and air distribution may be investigated in future experiments by means of X-ray CT. Visualization of organic matter on X-ray CT images remains challenging because of poor contrast with air-filled pore space, water, or the mineral matrix. To date, heavy element-based stains have been successfully used in transition electron microscopy of clay sized organo-mineral soil particles (Chenu & Plante, 2006). The potential of chemical staining of OM to improve X-ray CT contrast of OM is promising and should be investigated. While the resolution limits in X-ray CT will not allow visualizing the majority of mineral bound OM, particulate OM or added substrates could probably be distinguished from mineral matter. With further developments of the X-ray CT scanning quality, driven by hardware and software improvements (increased X-ray flux enabled by actively cooled targets, high resolution detectors) water distribution and location of particulate OM may be visualized semi-automatically. In future, instead of qualitative and subjective manual identification, semi-automatic detection and quantification of OM would allow to determine the level of contact between OM and mineral matter (Chapter 4). For example, by measuring C mineralization at different soil moisture levels, the indirect promoting role of larger pores on C mineralization through their promotion of soil aeration to wetter finer pored parts of the soil matrix could be confirmed (chapter 4 and 5) via X-ray CT based visualization of water and substrates.

The strong interaction effect on SOM decomposition between SOM biochemistry and microbial biomass influenced in relation to the soil pore system (Chapter 4) could be further investigated by including microbial community structure measurements by PLFA analysis. For instance, lignin versus carbohydrate-rich materials may be expected to promote a fungal rather than a bacterial dominated decomposition and both groups may be expected to respond differently to moisture or oxygen availability.

Finally, there is a general consensus that the heterogeneity of SOM needs to be represented in models predicting SOM dynamics (Bosatta & Angren, 2003). Although a model structure with discrete pools offers advantages in case of practical use, its theoretical underpinning is weak. But the complexity and lack of verifiability of continuous structured

SOM models have limited the attempts to develop them. Because of the continuous nature of the data which will be compiled from CT scans of several studies, i.e. the pore size distribution representing soil structure and the distribution of the location of SOM within, studies like this provide directly usable data for such continuous SOM models.

Summary

The interactions between soil organic matter (SOM), soil structure and availability of water are very complex. Despite the growing body of evidence showing the importance of micro-habitat structure for many microbial processes, little detail is known about how the topology or distribution of the soil pore network steers microbial activity and SOM decomposition at the micro-habitat scale. X-ray computed tomography (CT), a non-destructive imaging technique, allows in combination with image analysis the 3D visualization and quantification of the internal architecture of soil pore space. The use of X-ray CT in combination with soil incubation experiments could have great potential for investigating the relationship between soil pore network structure and SOM decomposition.

The first part of this PhD focussed on the development and the testing of the use of X-ray CT in running soil biological experiments that include assessments of microbial activity. A micro-CT scanner that was developed at the "Centre for X-ray Tomography" of Ghent University was used for X-ray scanning of soils throughout this PhD research. A methodology was developed for the assessment of a pore *neck* size distribution from 3D grey scale X-ray CT images using the software program Morpho+. This was crucial as the water distribution and the location of soil organisms are determined by pore *necks*, i.e. the entrance to the pores. This methodology was applied on the X-ray CT datasets throughout the PhD thesis (except for Chapter 4).

A first study was aimed at investigating the scale dependence of X-ray CT derived information on the soil pore network and included scanning of soil samples with micro focus X-ray CT at four different scales. This resulted in different voxel (=pixel in 3D) sizes of 27.7, 10.0, 0.6 and 0.3 µm at the soil core (Ø=5 cm), macro (Ø=2 mm), sub-macro (Ø=500 µm) and micro aggregate (Ø=250 µm) level. Image analysis showed that quantification of pore properties was highly scale-dependent. A representative elementary volume (REV) analysis was executed to determine the minimum size of the volume of interest during image analysis that is required to retrieve porosity results independent from the location selection of the volume of interest in the soil sample. We suggest minimal REV sizes for porosity measurements of approximately 21, 37, 6 and 12 (expressed as ratio between cube side length and average pore diameter) for soil samples with approximate diameter of 5 cm, 2 mm, 500 and 250 µm. Comparison between the pore neck size distributions assays with X-ray CT and calculated from water retention curve data resulted mostly in overestimation of porosity by X-ray CT and this was largely determined by the image segmentation method. It was found that the selection of a threshold value for pore space segmentation can largely influence the

outcome of porosity measurements based on X-ray CT images, and we suggest inclusion of a sensitivity analysis in soil X-ray CT studies. The sensitivity of porosity quantification on the selection of a grey value can be determined by for example increasing/decreasing it with 5 or 10 units. For this in general it became apparent that porosity measurements based on X-ray CT image analysis will always be limited to a defined range in soil pore size classes by resolution. The results showed that X-ray CT data acquired at the soil core level (Ø=5 cm) could be useful in the study of soil processes like water flow and the alteration of the soil structure by earthworms and other soil fauna. The application of X-ray CT at the aggregate level (Ø=250 µm to 2 mm) enables the visualization of the physical environment in which microbes and their grazers operate and shows potential for investigating the mutual interaction between soil structure, the microbial community and SOM decomposition.

Due to a trade-off between sample size and X-ray CT resolution (approximate factor of 1000-1500), the use of X-ray CT for soil biological studies requires incubation experiments to be conducted with soil cores with sufficient small dimensions. In a second experimental study, soil sample size itself (3.5, 10 and 44 g) was found to affect the assessment of soil biological parameters like incubation derived C mineralization, microbial biomass C and dehydrogenase activity. It is hypothesized that the observed differences between the sample size are a result of deviation in the water distribution in soil after rewetting of small (1-5 g) and commonly (>40 g) sized soil cores used in incubation. Still, at given sample size and experimental conditions, the effects of different soil treatments (e.g. variation in soil pore network structure, different soil moisture levels) on key soil biological parameters can be examined. However, extrapolation of the outcomes to larger scales can only be done with care and this limits comparison with previous studies, most often carried out on larger soil masses.

In a next step, the effect of X-ray CT scanning itself on the microbial community and on bulk soil C mineralization was tested for the first time. C mineralization, enzyme activities and microbial community structure were assessed in repacked soil cores 1 day and 22 days after X-radiation. It was found that X-radiation only had a short-lived negative effect on dehydrogenase activity and a short-lived positive effect on the PLFA biomarkers for Actinomycetes. No differences were found in biological parameters between the X-radiated soil cores and the control soil cores at day 22. Consequently, a time lag of maximum three weeks between X-ray scanning and analysis of soil biological parameters seems largely sufficient to rule out small effects of X-radiation on the microbial community structure and its

activity. Although a safe radiation level does not exist, this study showed that usage of X-ray micro-CT is very well compatible with soil biological experiments.

The second part of this PhD research explored the use of X-ray CT in combination with running soil incubation experiments to investigate the role of the soil pore network structure on soil C dynamics. A first combined X-ray CT-incubation study revealed that substrate derived but not native SOM derived C mineralization in a sandy loam soil at 28% WFPS depends on quantified soil pore network structure measures. In substrate amended soils, we found a clear trend between substrate derived C mineralization and the volume of pore size classes from negative to positive correlation coefficients with increasing equivalent sphere pore size diameter. This trend suggested a positive influence of macro porosity on C mineralization of freshly added substrates (grass or sawdust particles). The specific effect of included artificial modifications of the soil pore structure on substrate C mineralization was found to be highly dependent on substrate quality. While compaction reduced C mineralization derived from the decomposition of both added substrates, an artificially introduced change to a more sandy soil texture (80% instead of 50%) reduced C mineralization from sawdust, but not from grass. The X-ray CT derived pore size distribution data could not explain this interaction effect. It appears that information on substrate location within the soil matrix (contact with soil particles, inclusion in aggregates), would provide relevant additional information. However, the CT image phase contrast of organic matter and other soil phases was too small to allow for such a quantitative analysis and only a first qualitative, manual evaluation was possible.

In a second combined X-ray CT-soil incubation study we relied on natural variation in texture and soil pore network structure of loam soils instead of using artificial manipulations. In line with the first sandy loam soil incubation experiment, the important role of macro porosity (neck diameter >150 µm) on decomposition was confirmed as available water was restricted to smaller pores at the established soil moisture level (39% WFPS). It would appear that the stimulating effect of macro porosity on native SOM derived C mineralization was indirect, i.e. more specifically by enhancing aeration and gas exchange of surrounding smaller pore space. The effect to which soil pore network structure influences SOM decomposition is indirectly, i.e. by determining the water distribution in soil, could not be quantified from both studies. A further in depth analysis including similar controlled incubation studies in combination with X-ray CT and crucially with assessment of the microbial community structure and activity will be required.

This PhD work forms a basis for the use of X-ray CT in soil biological studies. By a combined use of X-ray CT in soil incubation studies, the dependence of soil C mineralization on soil structure was confirmed, although the direct or indirect nature of this relationship was not clear. However, future studies in which the tested X-ray CT incubation approach is combined with biological assays would provide a powerful means to further investigate the interaction effect of soil pore network structure and the microbial community on SOM decomposition. We do conclude that no single pore size class is responsible for neither C mineralization nor C protection as the spatial location of microbial activity and SOM decomposition changes along with the temporal variation in soil water distribution in the pore space.

Samenvatting

Verbanden tussen bodem organische stof (BOS) afbraak, de bodemstructuur en de beschikbaarheid van water zijn zeer complex. Er zijn toenemende bewijzen dat microbiële processen grotendeels afhankelijk zijn van de ruimtelijke opbouw van de bodem poriën ruimte, hun microhabitat. Desondanks is onze kennis betreffende de sturing van deze microbiële processen en BOS afbraak door de porie netwerkstructuur op microschaal beperkt. Aan de hand van X-stralen tomografie (X-stralen CT), een niet-destructieve beeldtechniek, kan in combinatie met beeldanalyse de driedimensionale (3D) interne structuur van de porieruimte gevisualiseerd en gekwantificeerd worden. Een gecombineerd gebruik van X-stralen CT met bodem incubatie-experimenten werd tot op heden niet gerealiseerd maar zou veelbelovend kunnen zijn voor het onderzoek naar de afhankelijkheid van BOS afbraak van de bodemporie netwerkstructuur.

Het eerste deel van dit doctoraat focust zich op de ontwikkeling en het uittesten van het gebruik van X-stralen CT in bodembiologische experimenten, waarin ook microbiële activiteit wordt opgemeten. Een micro-CT scanner die ontwikkeld werd door het "Centrum voor X-stralen Tomografie" van de Universiteit Gent werd gebruikt voor alle bodem X-stralen CT scans binnen dit doctoraatsonderzoek. Een methodologie werd vooreerst ontwikkeld voor de kwantificering van een porie*neck*grootte verdeling uit 3D grijswaarden X-stralen CT beelden met behulp van het computer programma Morpho+. Dit was een cruciale stap aangezien de waterverdeling en de ruimtelijke verdeling van micro-organismen gereguleerd worden door porie*necks*, de porieopeningen. Deze methodologie werd toegepast op alle X-stralen CT datasets doorheen de doctoraatsthesis (behalve in Hoofdstuk 4).

In een eerste onderzoek testten we de schaalafhankelijkheid van informatie over het porienetwerk dat werd verkregen uit X-stralen CT beelden. Hiertoe werden bodemstalen van vier verschillende afmetingen gescand met microfocus X-stralen CT op vier verschillende beeldresoluties. Dit resulteerde in verschillende voxel (=pixel in 3D) resoluties van respectievelijk 27.7, 10.0, 0.6 en 0.3 μm op het niveau van een bodemkolom (Ø=5 cm), een macro aggregaat (Ø=2 mm), een submacro aggregaat (Ø=500 μm) en een micro aggregaat (Ø=250 μm). Beeldanalyse toonde aan dat de kwantificering van porie-eigenschappen schaalafhankelijk was. De minimum afmetingen van een beeldvolume dat bij analyse resultaten geeft die representatief zijn voor het ganse beeld en ook onafhankelijk zijn van de locatie van het beeldvolume in het bodemstaal werd bepaald door middel van een representatieve eenheidsvolume-analyse (REV-analyse). Wij stellen minimale REV groottes voor van 21, 37, 6 en 12 (uitgedrukt in de verhouding tussen lengte van de zijde van een

139

kubusvormig REV en de gemiddelde poriediameter) voor bodemstalen met diameters van ongeveer 5 cm, 2 mm, 500 en 250 µm. De vergelijking van porie*neck*grootte verdelingen verkregen uit X-stralen CT beelden enerzijds en verdelingen berekend op basis van de vochtkarakteristiek anderzijds resulteerde meestal in een overschatting van de porositeit bepaald uit de X-stralen CT beelden. Deze overschatting bleek grotendeels het gevolg te zijn van de geselecteerde segmentatiemethode. De keuze van een drempelwaarde voor de identificatie van voxels die behoren tot de porieruimte bepaalt grotendeels de correctheid van de porositeitmeting op basis van X-stralen CT beelden en uit dit onderzoek kan dan ook besloten worden om steeds een gevoeligheidsanalyse uit te voeren bij toepassing van X-stralen CT binnen bodemonderzoek. De gevoeligheid van de segmentatiemethode kan begroot worden door de grijswaarde van de drempelwaarde met 5 of 10 eenheden te vermeerderen of te verminderen en hierbij telkens de porositeit opnieuw te bepalen. Vervolgens bleek dat ten gevolge van de beeldresolutie porositeitmetingen gebaseerd op X-stralen CT beeldanalyse altijd gelimiteerd zijn tot een beperkt bereik in porie-groootteklassen. Deze studie toonde aan dat op het niveau van bodemkolommen X-stralen CT beelden toepasbaar zijn in het onderzoek naar bodemprocessen zoals waterbeweging en veranderingen in bodemstructuur ten gevolge van aardwormen of andere bodemfauna. X-stralen CT op bodemaggregaat niveau laat de visualisatie toe van de fysieke leefwereld van bacteriën, fungi en hun begrazers en vertoont dus potentieel voor het bestuderen van de wederzijdse interactie tussen bodemstructuur, de microbiële gemeenschap en BOS afbraak.

Doordat de X-stralen CT beeldresolutie van een staal en de staalgrootte omgekeerd evenredig zijn met elkaar (met factor 1000-1500), vereist de toepassing van X-stralen CT in biologisch onderzoek voldoende kleine staaldimensies. In een tweede onderzoek (Hoofdstuk 3) bleek echter dat de staalgrootte zelf (3.5, 10 of 44 g bodem) de meting van biologische bodemparameters zoals C mineralisatie, microbiële biomassa C en dehydrogenase activiteit kan beïnvloeden. Onze hypothese stelt dat de waargenomen verschillen tussen de staalgroottes het resultaat zijn van een variërende waterverdeling in de bodemstalen na het herbevochtigen voor incubatie van kleine bodemstalen (1-5 g) en standaard bodemstalen (>40 g). Niettemin, kan bij een gegeven staalgrootte en bepaalde experimentele omstandigheden dan nog steeds de invloed van verschillende bodembehandelingen (bv. variatie in de structuur van het porienetwerk, verschillende vochtgehaltes) op bodembiologische parameters bestudeerd worden. De extrapolatie van de resultaten naar grotere schaal moet echter

omzichtig gebeuren en dit beperkt de vergelijking met voorgaande studies die doorgaans werden uitgevoerd met grotere bodemmassa's.

In een volgende stap werd voor het eerst de invloed van X-stralen CT bestraling op de microbiële gemeenschap en C mineralisatie nagegaan (Hoofdstuk 3). C mineralisatie, enzym activiteiten en de samenstelling van de microbiële gemeenschap werden gemeten van opgevulde bodemkolommen, 1 en 22 dagen na al dan niet X-bestraling. De dehydrogenase activiteit en het gehalte aan fosfolipiden vetzuren (PLFA) biomarkers voor de actinomyceten ondervonden enkel een korte termijn effect (respectievelijk negatief en positief effect na 1 dag) ten gevolge van de X-bestraling. 22 dagen na de X-bestraling vertoonde geen enkele biologische bodemparameter nog een invloed van de X-bestraling. Bijgevolg blijkt een periode van drie weken tussen X-bestraling en het opmeten van biologische bodemparameters voldoende om kleine effecten op de samenstelling en activiteit van de microbiële gemeenschap uit te sluiten. Ondanks het feit dat een veilige bestralingsdosis niet bestaat, toont dit onderzoek aan dat X-stralen CT combineerbaar is met biologische experimenten.

In een tweede deel van dit doctoraatsonderzoek werd X-stralen CT toegepast in combinatie met biologische experimenten om de rol van de porie netwerkstructuur op de C dynamiek na te gaan. Een eerste incubatie-experiment betrof de opvolging van C mineralisatie in een zandleembodem bij 28% watergevuld poriegehalte (WFPS) waaraan twee substraten werden toegediend en waarvan de porieruimte structuur werd gemanipuleerd. De mineralisatie van toegediend substraten bleek afhankelijk te zijn van de bodemporie netwerkstructuur, in tegenstelling tot de C mineralisatie van BOS welke onafhankelijk bleek. Er werd een trend gevonden tussen C mineralisatie afkomstig van het substraat en het volume van verschillende porie grootteklassen, waarbij de correlatiecoëfficiënten tussen beiden van negatief naar positief varieerden met toenemende equivalente bol diameter. Deze trend suggereerde dat macroporositeit een positieve invloed had op de C mineralisatie van toegediend organisch materiaal. De specifieke invloed van een artificiële wijziging van de poriënstructuur op de C mineralisatie van het substraat bleek sterk afhankelijk te zijn van de substraatkwaliteit. Terwijl compactie de C mineralisatie van twee uiteenlopende substraten (gras en zagemeel) negatief beïnvloedde, daalde enkel de C mineralisatie van zagemeel en niet van gras wanneer de bodemtextuur artificieel werd gewijzigd naar een meer zandige textuur (80% in plaats van 50%). De verschillen in de porie grootteverdelingen verkregen uit de X-stralen CT beelden konden dit interactie effect niet verklaren. Mogelijks zou bijkomende informatie omtrent de ruimtelijke verdeling van het substraat in de bodemmatrix (contact met

141

bodemdeeltjes, omsluiting in aggregaten) relevant zijn. Echter, het contrast tussen X-stralen attenuering van organisch materiaal en andere bodemfasen was te beperkt om een kwantitatieve analyse van de CT beelden mogelijk te maken waardoor slechts een eerste kwalitatieve evaluatie mogelijk was.

In een tweede incubatie-experiment werd gebruik gemaakt van natuurlijke variatie in textuur en porie netwerkstructuur in een reeks ongestoorde kolommen van een lichte klei bodem, in plaats van artificiële manipulatie daarvan (Hoofdstuk 5). Gelijkaardig aan het eerste experiment (Hoofdstuk 4), werd het belang van macroporiën (*neck*diameter >150 μm) in BOS afbraak bevestigd. Aangezien water beperkt was tot kleinere poriën bij het vastgelegde vochtgehalte (39% WFPS) was de stimulerende invloed van macroporositeit op bodem C mineralisatie waarschijnlijk indirect, meer bepaald via de promotie van lucht- en gasuitwisseling van omliggende kleinere poriën. De indirecte beïnvloeding van BOS afbraak door de porie netwerkstructuur via regulatie van de waterverdeling, kon niet bevestigd worden. Dit vereist een verdere uitbreiding van de experimentele opstelling (incubatie-experiment in combinatie met X-stralen CT) met de bepaling van de samenstelling en activiteit van de microbiële gemeenschap.

Dit doctoraat vormt een basis voor de toepassing van X-stralen CT in bodembiologische experimenten. Door X-stralen CT te combineren met incubatie-experimenten van bodems werd de afhankelijkheid van BOS afbraak door de bodemstructuur bevestigd, al kon de directe of indirecte aard van deze relatie niet worden achterhaald. Toekomstige experimenten waarin X-stralen CT wordt gecombineerd met biologische metingen kunnen een krachtige basis vormen voor onderzoek naar de interactie-effecten tussen de bodem porie netwerkstructuur, de samenstelling van de microbiële gemeenschap en BOS afbraak. Tot besluit kan gesteld worden dat geen enkele porieklasse specifiek verantwoordelijk is voor BOS afbraak of BOS bescherming. Dit doordat de ruimtelijke verdeling van microbiële activiteit en BOS afbraak voortdurend veranderen met de temporele variatie van de verdeling van water en lucht in de bodem porieruimte.

References

G. Abera, E. Wolde-Meskel & L.R. Bakken. 2012. Carbon and nitrogen mineralization dynamics in different soils of the tropics amended with legume residues and contrasting soil moisture contents. *Biology and Fertility of Soils*, **48,** 51-66.

W.P. Adderley, I.A. Simpson & G.W. Macleod. 2001. Testing high-resolution X-ray computed tomography for the micromophological analyses of archaeological soils and sediments. *Archeological Prospection*, **8,** 107-112.

J.K. Adu & J.M. Oades. 1978. Physical factors influencing decomposition of organic materials in soil aggregates. *Soil Biology & Biochemistry*, **10,** 109-115.

R. Al-Raoush & A. Papadopoulos. 2010. Representative elementary volume analysis of porous media using X-ray computed tomography. *Powder Technology*, **200,** 69-77.

R.I. Al-Raoush & C.S. Willson. 2005. Extraction of physically realistic pore network properties from three-dimensional synchrotron X-ray microtomography images of unconsolidated porous media systems. *Journal of Hydrology*, **300,** 44-64.

K. Alef & P. Nannipieri eds. 1995. *Methods in Applied Soil Microbiology and Biochemistry*. Academic Press, London.

S.H. Anderson & J.W. Hopmans. 1994. *Tomography of soil-water-root processes*. Soil Science Society of America, Madison, USA.

S.H. Anderson, R.L. Peyton & C.J. Gantzer. 1990. Evaluation of constructed and natural soil macropores using X-ray computed tomography. *Geoderma*, **46,** 13-29.

J. Balesdent. 1996. The significance of organic separates to carbon dynamics and its modelling in some cultivated soils. *European Journal of Soil Science*, **47,** 485-493.

P.C. Baveye, M. Laba, W. Otten, L. Bouckaert, P. Dello Sterpaio, R.R. Goswami, D. Grinev, A. Houston, Y. Hu, J. Liu, S. Mooney, R. Pajor, S. Sleutel, A. Tarquis, W. Wang, Q. Wei & M. Sezgin. 2010. Observer-dependent variability of the thresholding step in the quantitative analysis of soil images and X-ray microtomography data. *Geoderma*, **157,** 51-63.

J. Bear. 1988. *Dynamics of fluids in porous media*. Dover Publications, New York.

T.P. Beldini, K.L. Mcnabb, B.G. Lockaby, F.G. Sanchez & O. Navegantes-Cancio. 2010. The effect of Amazonian Eucalyptus plantations on soil aggregates and organic matter density fractions. *Soil Use and Management*, **26**, 53-60.

K. Beven & P. Germann. 1982. macropores and water-flow in soils. *Water Resources Research*, **18,** 1311-1325.

H.F. Birch. 1958. The effect of soil drying on humus decomposition and nitrogen availability. *Plant and Soil*, **10,** 9-31.

G.R. Blake & K.H. Hartge eds. 1986. *Particle density. In Methods of soil analysis, Part1, Physical and Mineralogical Methods Second Edition*. American Society of agronomy, Madison, Wisconsin, USA.

E. Bosatta & G.I. Agren. 2003. Exact solutions to the continuous-quality equation for soil organic matter turnover. Journal of Theoretical Biology, **224**, 97-105.

A. Bot & J. Benites. 2005. The importance of soil organic matter. In: *Soil bulletin*, p. 80. Food and agriculture organization of the united nations, Rome.

L. Bouckaert, D. Van Loo, N. Ameloot, D. Buchan, L. Van Hoorebeke & S. Sleutel. 2012. Compatibility of X-ray micro-Computed Tomography with soil biological experiments. *Soil Biology & Biochemistry* (In press).

L. Brabant, J. Vlassenbroeck, Y. De Witte, V. Cnudde, M.N. Boone, J. Dewanckele & L. Van Hoorebeke. 2011. Three-Dimensional Analysis of High-Resolution X-Ray Computed Tomography Data with Morpho+. *Microscopy and Microanalysis*, **17,** 252-263.

N.C. Brady & R.R. Weil. 2002. *The Nature and Properties of Soils*. Pearson Education, Inc New Jersey.

T.A. Breland & S. Hansen. 1996. Nitrogen mineralization and microbial biomass as affected by soil compaction. *Soil Biology & Biochemistry*, **28,** 655-663.

A. Bruand, I. Cousin, B. Nicoullaud, O. Duval & J.C. Begon. 1996. Backscattered electron scanning images of soil porosity for analyzing soil compaction around roots. *Soil Science Society of America Journal*, **60,** 895-901.

Y. Capowiez, S. Sammartino & E. Michel. 2011. Using X-ray tomography to quantify earthworm bioturbation non-destructively in repacked soil cores. *Geoderma*, **162,** 124-131.

R.F. Carsel & R.S. Parrish. 1988. Developing joint probability-distributions of soil-water retention characteristics. *Water Resources Research*, **24,** 755-769.

L. Casida, J. Johnson & D. Klein. 1964. Soil dehydrogenase activity. *Soil Science*, **98,** 371-376.

X. Chen, J. Tang, L. Jiang, B. Li, J. Chen & C. Fang. 2010. Evaluating the impacts of incubation procedures on estimated Q(10) values of soil respiration. *Soil Biology & Biochemistry*, **42,** 2282-2288.

C. Chenu & A.F. Plante. 2006. Clay-sized organo-mineral complexes in a cultivation chronosequence: revisiting the concept of the 'primary organo-mineral complex'. *European Journal of Soil Biology*, **57,** 596-607.

V. Clausnitzer & J.W. Hopmans. 1999. Determination of phase-volume fractions from tomographic measurements in two-phase systems. *Advances in Water Resources*, **22,** 577-584.

V. Cnudde. 2005. *Exploring the potential of X-ray tomography as a new non-destructive research tool in conservation studies of natural building stones,* Ghent University, Ghent.

N. Dal Ferro, P. Delmas, C. Duwig, G. Simonetti & F. Morari. 2012. Coupling X-ray microtomography and mercury intrusion porosimetry to quantify aggregate structures of a cambisol under different fertilisation treatments. *Soil & Tillage Research*, **119,** 13-21.

J.B. Dalrymple. 1957. Preparation of thin sections of soils. *Journal of Soil Science*, **8,** 161-165.

J.H. Dane & G.C. Topp. 2002. *The soil solution phase; In: Methods of Soil analysis, Part 4, Physical Methods*. Soil Science Society of America, Inc., Madison, Wisconsin, USA.

R.E. Danielson & P.L. Sutherland eds. 1986. *Porosity. In Methods of soil analysis, Part1, Physical and Mineralogical Methods Second Edition*. American Society of Agronomy, Madison, Wisconsin, USA.

S. De Gryze. 2004. *Soil aggregation: processes and modeling*. Katholieke Universiteit Leuven, Leuven.

S. De Gryze, L. Jassogne, J. Six, H. Bossuyt, M. Wevers & R. MerckX. 2006. Pore structure changes during decomposition of fresh residue: X-ray tomography analyses. *Geoderma*, **134,** 82-96.

S. De Neve & G. Hofman. 2000. Influence of soil compaction on carbon and nitrogen mineralization of soil organic matter and crop residues. *Biology and Fertility of Soils*, **30,** 544-549.

P.C. de Ruiter, A. Steenbruggen, S. Keesstra, G. Mol, J. Okx & A. Zaal. 2011. Soil Science in a changing world. In: *Wageningen Conference on Applied Soil Science* (eds. S, K. & G, M.), p. 11, Wageningen, The Netherlands.

H. De Wever, D.T. Strong & R. Merckx. 2004. A system for studying the dynamics of gaseous emissions in response to changes in soil matric potential. *Soil Science Society of America Journal*, **68,** 1242-1248.

A. Dechesne, C. Pallud, D. Debouzie, J.P. Flandrois, T.M. Vogel, J.P. Gaudet & G.L. Grundmann. 2003. A novel method for characterizing the microscale 3D spatial distribution of bacteria in soil. *Soil Biology & Biochemistry*, **35,** 1537-1546.

K. Denef, J. Six, R. Merckx & K. Paustian. 2002. Short-term effects of biological and physical forces on aggregate formation in soils with different clay mineralogy. *Plant and Soil*, **246,** 185-200.

M. Dierick, D. Van Loo, B. Masschaele, M. Boone & L. Van Hoorebeke. 2010. A LabVIEW (R) based generic CT scanner control software platform. *Journal of X-Ray Science and Technology*, **18,** 451-461.

F.A.L. Dullien. 1981. Woods metal porosimetry and its relation to mercury porosimetry. *Powder Technology*, **29,** 109-116.

S.O. Eching & J.W. Hopmans. 1993. Optimization of hydraulic functions from transient outflow and soil-water pressure data. *Soil Science Society of America Journal*, **57,** 1167-1175.

K. Ekschmitt, E. Kandeler, C. Poll, A. Brune, F. Buscot, M. Friedrich, G. Gleixner, A. Hartmann, M. Kastner, S. Marhan, A. Miltner, S. Scheu & V. Wolters. 2008. Soil-carbon preservation through habitat constraints and biological limitations on decomposer activity. *Journal of Plant Nutrition and Soil Science-Zeitschrift Fur Pflanzenernahrung Und Bodenkunde*, **171,** 27-35.

T.R. Elliot & R.J. Heck. 2007. A comparison of optical and X-ray CT technique for void analysis in soil thin section. *Geoderma*, **141,** 60-70.

T.R. Elliot, W.D. Reynolds & R.J. Heck. 2010. Use of existing pore models and X-ray computed tomography to predict saturated soil hydraulic conductivity. *Geoderma*, **156,** 133-142.

E.T. Elliot. 1986. Aggregate structure and Carbon, Nitrogen, and Phosphorus in native and cultivated soils *Soil Science Society of America Journal*, **50,** 627-633.

E.T. Elliot, R.V. Anderson, D.C. Coleman & C.V. Cole. 1980. Habitable pore-space and mirobial trophic interactions. *Oikos*, **35,** 327-335.

E.T. Elliot & D.C. Coleman. 1988. Let the soil work for us. *Ecological bulletins*, **39,** 23-32.

K. Eusterhues, C. Rumpel, M. Kleber & I. Kogel-Knabner. 2003. Stabilisation of soil organic matter by interactions with minerals as revealed by mineral dissolution and oxidative degradation. *Organic Geochemistry*, **34,** 1591-1600.

D.S. Feeney, J.W. Crawford, T. Daniell, P.D. Hallett, N. Nunan, K. Ritz, M. Rivers & I.M. Young. 2006. Three-dimensional microorganization of the soil-root-microbe system. *Microbial Ecology*, **52,** 151-158.

R.C. Foster. 1988. Microenvironments of soil-microorganisms. *Biology and Fertility of Soils*, **6,** 189-203.

A.J. Franzluebbers. 1999. Microbial activity in response to water-filled pore space of variably eroded southern Piedmont soils. *Applied Soil Ecology*, **11,** 91-101.

A.J. Franzluebbers, R.L. Haney, F.M. Hons & D.A. Zuberer. 1996a. Active fractions of organic matter in soils with different texture. *Soil Biology & Biochemistry*, **28,** 1367-1372.

A.J. Franzluebbers, R.L. Haney, F.M. Hons & D.A. Zuberer. 1996b. Determination of microbial biomass and nitrogen mineralization following rewetting of dried soil. *Soil Science Society of America Journal*, **60,** 1133-1139.

A. Freibauer, M.D.A. Rounsevell, P. Smith & J. Verhagen. 2004. Carbon sequestration in the agricultural soils of Europe. *Geoderma*, **122,** 1-23.

C.J. Gantzer & S.H. Anderson. 2002. Computed tomographic measurement of macroporosity in chisel-disk and no-tillage seedbeds. *Soil & Tillage Research*, **64,** 101-111.

J. Garcia-Pausas & E. Paterson. 2011. Microbial community abundance and structure are determinants of soil organic matter mineralisation in the presence of labile carbon. *Soil Biology & Biochemistry*, **43,** 1705-1713.

G.W. Gee & J.W. Bauder eds. 1986. *Particle-size Analysis. In Methods of soil analysis, Part1, Physical and Mineralogical Methods Second Edition*. American Society of Agronomy Madison, Wisconsin, USA.

E.G. Gregorich, R.P. Voroney & R.G. Kachanoski. 1991. Turnover of carbon through the microbial biomass in soils with different texture. *Soil Biology & Biochemistry*, **23,** 799-805.

A.S. Gregory, N.R.A. Bird, W.R. Whalley, G.P. Matthews & I.M. Young. 2010. Deformation and Shrinkage Effects on the Soil Water Release Characteristic. *Soil Science Society of America Journal*, **74,** 1104-1112.

M.C.J. Grevers, E. Dejong & R.J. Starnaud. 1989. The characterization of soil macroporosity with CT scanning. *Canadian Journal of Soil Science*, **69,** 629-637.

B.S. Griffiths & I.M. Young. 1994. The effects of soil-structure on protozoa in a clay-loam soil. *European Journal of Soil Science*, **45,** 285-292.

G.L. Grundmann & D. Debouzie. 2000. Geostatistical analysis of the distribution of NH4+ and NO2--oxidizing bacteria and serotypes at the millimeter scale along a soil transect. *Fems Microbiology Ecology*, **34,** 57-62.

G.L. Grundmann, A. Dechesne, F. Bartoli, J.P. Flandrois, J.L. Chasse & R. Kizungu. 2001. Spatial modeling of nitrifier microhabitats in soil. *Soil Science Society of America Journal*, **65,** 1709-1716.

P.J. Hanson, N.T. Edwards, C.T. Garten & J.A. Andrews. 2000. Separating root and soil microbial contributions to soil respiration: A review of methods and observations. *Biogeochemistry*, **48,** 115-146.

J. Hassink, L.A. Bouwman, K.B. Zwart, J. Bloem & L. Brussaard. 1993. Relationships between Soil Texture, Physical protection of Organic-Matter, Soil Biota, and C-mineralization and N-mineralization in grassland soils. *Geoderma*, **57,** 105-128.

J. Hassink & J.W. Dalenberg. 1996. Decomposition and transfer of plant residue C-14 between size and density fractions in soil. *Plant and Soil*, **179,** 159-169.

J. Hassink, A.M. Neutel & P.C. De Ruiter. 1994. C and N mineralization in sandy and loamy grassland soils: the role of microbes and microfauna. *Soil Biology & Biochemistry*, **26,** 1565-1571.

M.H.B. Hayes. 2006. Solvent systems for the isolation of organic components from soils. *Soil Science Society of America Journal*, **70,** 986-994.

T.M. Henriksen & T.A. Breland. 1999. Nitrogen availability effects on carbon mineralization, fungal and bacterial growth, and enzyme activities during decomposition of wheat straw in soil. *Soil Biology & Biochemistry*, **31,** 1121-1134.

R. Horn & A. Smucker. 2005. Structure formation and its consequences for gas and water transport in unsaturated arable and forest soils. *Soil & Tillage Research*, **82,** 5-14.

N. Jarvis, M. Larsbo, S. Roulier, A. Lindahl & L. Persson. 2007. The role of soil properties in regulating non-equilibrium macropore flow and solute transport in agricultural topsoils. *European Journal of Soil Science*, **58,** 282-292.

J.D. Jastrow, T.W. Boutton & R.M. Miller. 1996. Carbon dynamics of aggregate-associated organic matter estimated by carbon-13 natural abundance. *Soil Science Society of America Journal*, **60,** 801-807.

D.S. Jenkinson & J.N. Ladd. 1981. *Microbial biomass in soil: measurement and turnover*. Marcel Dekker, New York.

R.G. Joergensen. 1996. The fumigation-extraction method to estimate soil microbial biomass: Calibration of the k(EC) value. *Soil Biology & Biochemistry*, **28,** 25-31.

F.G.W. Jones & A.J. Thomasson. 1976. Bulk-density as an indicator of pore space in soils usable by nematodes. *Nematologica*, **22,** 133-137.

N.G. Juma. 1998. *The pedosphere and its dynamics: a systems approach to soil science*. Qualtity color press Inc, Edmonton, Canada.

W.A. Jury, W.R. Gardner & W.H. Gardner. 1991. *Soil physics*. John Wiley & sons, New York.

R.A. Ketcham. 2005. Three-dimensional grain fabric measurements using high-resolution X-ray computed tomography. *Journal of Structural Geology*, **27,** 1217-1228.

R.A. Ketcham & W.D. Carlson. 2001. Acquisition, optimization and interpretation of X-ray computed tomographic imagery: applications to the geosciences. *Computers & Geosciences*, **27,** 381-400.

T.L. Kieft, E. Soroker & M.K. Firestone. 1987. Microbial biomass response to a rapid increase in water potential when dry soil is wetted *Soil Biology & Biochemistry*, **19,** 119-126.

G. Kilbertus. 1980. Study of microhabitats in soil aggregates - relation to bacterial biomass and size of prokaryotes. *Revue D Ecologie Et De Biologie Du Sol*, **17,** 543-557.

K. Killham, M. Amato & J.N. Ladd. 1993. Effect of substrate location in soil and pore-water regime on carbon turnover. *Soil Biology & Biochemistry*, **25,** 57-62.

A. Klute. 1986. *Porosity. In: Methods of soil analysis, Part 1, Physical and Mineralogical Methods, second edition*. American Society of Agronomy, Inc., Madison, Wisconsin.

I. Kögel-Knabner, K. Ekschmitt, H. Flessa, G. Guggenberger, E. Matzner, B. Marschner & M. von Lutzow. 2008. An integrative approach of organic matter stabilization in temperate soils: Linking chemistry, physics, and biology. *Journal of Plant Nutrition and Soil Science*, **171,** 5-13.

M.J. Kooistra, D. Schoonderbeek, F.R. Boone, B.W. Veen & M. Vannoordwijk. 1992. Root-Soil contact of Maize, as measured by a Thin-Section Technique.2. Effect of Soil Compaction. *Plant and Soil*, **139,** 119-129.

W.L. Kutsch, M. Bahn & A. Heinemeyer. 2009. *Soil Carbon relations: an overview. In: Soil Carbon dynamics, An integrated Methodology*. Cambridge University Press, Cambridge, UK.

M.J. Kwiecien, I.F. Macdonald & F.A.L. Dullien. 1990. 3-Dimensional reconstruction of porous-media from serial section data. *Journal of Microscopy-Oxford*, **159,** 343-359.

J.N. Ladd, M. Amato & J.M. Oades. 1985. Decomposition of plant-material in australian soils. 3. Residual organic and microbial biomass-C and biomass-N from isotope-labelled legume material and soil organic-matter, decomposing under field conditions. *Australian Journal of Soil Research*, **23,** 603-611.

R. Lal. 2004. Soil carbon sequestration to mitigate climate change. *Geoderma*, **123,** 1-22.

R. Lal & M.K. Shukla. 2004. *Principles of soil physics*. Marcel Dekker, Inc., New York, Basel.

P. Lavelle, E. Blanchart, A. Martin, S. Martin, A. Spain, F. Toutain, I. Barois & R. Schaefer. 1993. A hierarchical model for decomposition in terrestrial ecosystems - Application to soils of the humid tropics. *Biotropica*, **25,** 130-150.

J. Letey. 1991. The study of soil structure - science or art. *Australian Journal of Soil Research*, **29,** 699-707.

W.B. Lindquist, A. Venkatarangan, J. Dunsmuir & T.F. Wong. 2000. Pore and throat size distributions measured from synchrotron X-ray tomographic images of Fontainebleau sandstones. *Journal of Geophysical Research-Solid Earth*, **105,** 21509-21527.

D.M. Linn & J.W. Doran. 1984. Effect of water-filled pore-space on carbon-dioxide and nitrous-oxide production in tilled and nontilled soils. *Soil Science Society of America Journal*, **48,** 1267-1272.

B. Marschner, S. Brodowski, A. Dreves, G. Gleixner, A. Gude, P.M. Grootes, U. Hamer, A. Heim, G. Jandl, R. Ji, K. Kaiser, K. Kalbitz, C. Kramer, P. Leinweber, J. Rethemeyer, A. Schaeffer, M.W.I. Schmidt, L. Schwark & G.L.B. Wiesenberg. 2008. How relevant is recalcitrance for the stabilization of organic matter in soils? *Journal of Plant Nutrition and Soil Science-Zeitschrift Fur Pflanzenernahrung Und Bodenkunde*, **171,** 91-110.

B. Marschner & K. Kalbitz. 2003. Controls of bioavailability and biodegradability of dissolved organic matter in soils. *Geoderma*, **113,** 211-235.

L.M. Mayer, L.L. Schick, K.R. Hardy, R. Wagal & J. McCarthy. 2004. Organic matter in small mesopores in sediments and soils. *Geochimica Et Cosmochimica Acta*, **68,** 3863-3872.

J.F. McCarthy, J. Ilavsky, J.D. Jastrow, L.M. Mayer, E. Perfect & J. Zhuang. 2008. Protection of organic carbon in soil microaggregates via restructuring of aggregate porosity and filling of pores with accumulating organic matter. *Geochimica Et Cosmochimica Acta*, **72,** 4725-4744.

N.P. McNamara, H.I.J. Black, N.A. Beresford & N.R. Parekh. 2003. Effects of acute gamma irradiation on chemical, physical and biological properties of soils. *Applied Soil Ecology*, **24,** 117-132.

F. Mees, R. Swennen, M. Van Geet & P. Jacobs. 2003. *Applications of X-ray computed tomography in the geosciences*. Geological Society, London, UK.

R. Mikutta, M. Kleber, M.S. Torn & R. Jahn. 2006. Stabilization of soil organic matter: Association with minerals or chemical recalcitrance? *Biogeochemistry*, **77,** 25-56.

B. Moeskops, Sukristiyonubowo, D. Buchan, S. Sleutel, L. Herawaty, E. Husen, R. Saraswati, D. Setyorini & S. De Neve. 2010. Soil microbial communities and activities under intensive organic and conventional vegetable farming in West Java, Indonesia. *Applied Soil Ecology*, **45,** 112-120.

S.J. Mooney & C. Morris. 2008. Morphological approach to understanding preferential flow using image analysis with dye tracers and X-ray computed tomography. *Catena*, **73,** 204-211.

C.P. Murphy, P. Bullock & R.H. Turner. 1977. Measurement and characterization of voids in soil thin-sections by image analysis.1.Principles and techniques. *Journal of Soil Science*, **28,** 498-&.

P. Nannipieri, E. Kandeler & P. Ruggiero. 2002. *Enzyme activities and microbiological and biochemical processes in soil*. Marcel Dekker, New York.

B.D. Nielsen. 2004. *Non-destructive soil testing using X-ray computed tomography*. Montana State University, Bozeman, Montana.

N. Nunan, T.J. Daniell, B.K. Singh, A. Papert, J.W. McNicol & J.I. Prosser. 2005. Links between plant and rhizoplane bacterial communities in grassland soils, characterized using molecular techniques. *Applied and Environmental Microbiology*, **71,** 6784-6792.

N. Nunan, K. Ritz, D. Crabb, K. Harris, K.J. Wu, J.W. Crawford & I.M. Young. 2001. Quantification of the in situ distribution of soil bacteria by large-scale imaging of thin sections of undisturbed soil. *Fems Microbiology Ecology*, **37,** 67-77.

N. Nunan, K. Ritz, M. Rivers, D.S. Feeney & I.M. Young. 2006. Investigating microbial micro-habitat structure using X-ray computed tomography. *Geoderma*, **133,** 398-407.

N. Nunan, K. Wu, I.M. Young, J.W. Crawford & K. Ritz. 2002. In situ spatial patterns of soil bacterial populations, mapped at multiple scales, in an arable soil. *Microbial Ecology*, **44,** 296-305.

N. Nunan, K.J. Wu, I.M. Young, J.W. Crawford & K. Ritz. 2003. Spatial distribution of bacterial communities and their relationships with the micro-architecture of soil. *Fems Microbiology Ecology*, **44,** 203-215.

A.G. O'Donnell, I.M. Young, S.P. Rushton, M.D. Shirley & J.W. Crawford. 2007. Visualization, modelling and prediction in soil microbiology. *Nature Reviews Microbiology*, **5,** 689-699.

W. Oh & W.B. Lindquist. 1999. Image thresholding by indicator kriging. *Ieee Transactions on Pattern Analysis and Machine Intelligence*, **21,** 590-602.

D. Or, B.F. Smets, J.M. Wraith, A. Dechesne & S.P. Friedman. 2007. Physical constraints affecting bacterial habitats and activity in unsaturated porous media - a review. *Advances in Water Resources*, **30,** 1505-1527.

N. Otsu. 1979. Threshold selection method from gray-level histograms. *Ieee Transactions on Systems Man and Cybernetics*, **9,** 62-66.

N.R. Pal & S.K. Pal. 1993. A review on image segmentation techniques. *Pattern Recognition*, **26,** 1277-1294.

J. Perret, S.O. Prasher, A. Kantzas & C. Langford. 1999. Three-dimensional quantification of macropore networks in undisturbed soil cores. *Soil Science Society of America Journal*, **63,** 1530-1543.

J. Postma & J.A. Van Veen. 1990. Habitable pore-space and survival of thrizobium-leguminosarum biovar trifolii introduced into soil. *Microbial Ecology*, **19,** 149-161.

D.S. Powlson, A.P. Whitmore & K.W.T. Goulding. 2011. Soil carbon sequestration to mitigate climate change: a critical re-examination to identify the true and the false. *European Journal of Soil Science*, **62,** 42-55.

A. Rachman, S.H. Anderson & C.J. Gantzer. 2005. Computed-tomographic measurement of soil macroporosity parameters as affected by stiff-stemmed grass hedges. *Soil Science Society of America Journal*, **69,** 1609-1616.

T. Rennert, K.U. Totsche, K. Heister, M. Kersten & J. Thieme. 2012. Advanced spectroscopic, microscopic, and tomographic characterization techniques to study biogeochemical interfaces in soil. *Journal of Soils and Sediments*, **12,** 3-23.

G.P. Robertson, K.M. Klingensmith, M.J. Klug, E.A. Paul, J.R. Crum & B.G. Ellis. 1997. Soil resources, microbial activity, and primary production across an agricultural ecosystem. *Ecological Applications*, **7,** 158-170.

H. Rogasik, I. Onasch, J. Brunotte, D. Jegou & O. Wendroth. 2003. Assessment of soil structure using X-ray computed tomography. *Geological Society, London, Special Publications*, **215,** 151-165.

C.W. Rose. 1966. *Agricultural physics*. Pergamon, Oxford, New York.

L.S. Ruamps, N. Nunan & C. Chenu. 2011. Microbial biogeography at the soil pore scale. *Soil Biology & Biochemistry*, **43,** 280-286.

P.M. Rutherford & N.G. Juma. 1992. Influence of texture on habitable pore-space and bacterial-protozoan populations in soil. *Biology and Fertility of Soils*, **12,** 221-227.

M.G. Ryan & B.E. Law. 2005. Interpreting, measuring, and modeling soil respiration. *Biogeochemistry*, **73,** 3-27.

M. Sandborg. 1995. Computed Tomography: Physical principles and biohazards. In: *Report LIU-RAD-R-081*, p. 17. Insitution for Radiology, Linköping, Sweden.

W.I. Schmidt, M.S. Torn, S. Abiven, T. Dittmar, G. Guggenberger, I.A. Janssens, M. Kleber, I. Kögel-Knabner, J. Lehmann, D.A.C. Manning, P. Nannipieri, D.P. Rasse, S. Weiner & S.E. Trumbore. 2011. Persistence of soil organic matter as an ecosystem property. *Nature*, **478**, 49-56.

N.A. Scott, C.V. Cole, E.T. Elliot & S.A. Huffman. 1996. Soil textural control on decomposition and soil organic matter dynamics. *Soil Science Society of America Journal*, **60,** 1102-1109.

A.J. Sexstone, N.P. Revsbech, T.B. Parkin & J.M. Tiedje. 1985. Direct measurement of oxygen profiles and denitrification rates in soil aggregates. *Soil Science Society of America Journal*, **49,** 645-651.

M. Sezgin & B. Sankur. 2004. Survey over image thresholding techniques and quantitative performance evaluation. *Journal of Electronic Imaging*, **13,** 146-168.

J. Six, H. Bossuyt, S. De Gryze & K. Denef. 2004. A history of research on the link between (micro)aggregates, soil biota, and soil organic matter dynamics. *Soil & Tillage Research*, **79,** 7-31.

J. Six, R.T. Conant, E.A. Paul & K. Paustian. 2002. Stabilization mechanisms of soil organic matter: Implications for C-saturation of soils. *Plant and Soil*, **241,** 155-176.

J. Six, E.T. Elliot & K. Paustian. 1999. Aggregate and soil organic matter dynamics under conventional and no-tillage systems. *Soil Science Society of America Journal*, **63,** 1350-1358.

J. Six, S.D. Frey, R.K. Thiet & K.M. Batten. 2006. Bacterial and fungal contributions to carbon sequestration in agroecosystems. *Soil Science Society of America Journal*, **70,** 555-569.

J. Six, G. Guggenberger, K. Paustian, L. Haumaier, E.T. Elliot & W. Zech. 2001. Sources and composition of soil organic matter fractions between and within soil aggregates. *European Journal of Soil Science*, **52,** 607-618.

J. Six, K. Paustian, E.T. Elliot & C. Combrink. 2000. Soil structure and organic matter: I. Distribution of aggregate-size classes and aggregate-associated carbon. *Soil Science Society of America Journal*, **64,** 681-689.

S. Sleutel, L. Bouckaert, D. Buchan, D. Van Loo, W.M. Cornelis & H.G. Sanga. 2012. Manipulation of the soil pore and microbial community structure in soil mesocosm incubation studies. *Soil Biology & Biochemistry*, **45,** 40-48.

S. Sleutel, V. Cnudde, B. Masschaele, J. Vlassenbroek, M. Dierick, L. Van Hoorebeke, P. Jacobs & S. De Neve. 2008. Comparison of different nano- and micro-focus X-ray computed tomography set-ups for the visualization of the soil microstructure and soil organic matter. *Computers & Geosciences*, **34,** 931-938.

S. Sleutel, S. De Neve, M.R.P. Roibas & G. Hofman. 2005. The influence of model type and incubation time on the estimation of stable organic carbon in organic materials. *European Journal of Soil Science*, **56,** 505-514.

A.J.M. Smucker, E.-J. Park, J. Dorner & R. Horn. 2007. Soil micropore development and contributions to soluble carbon transport within macroaggregates. *Vadose Zone Journal*, **6,** 282-290.

P. Sollins, P. Homann & B.A. Caldwell. 1996. Stabilization and destabilization of soil organic matter: Mechanisms and controls. *Geoderma*, **74,** 65-105.

L.H. Sorensen. 1974. Rate of decomposition of organic-matter in soil as influenced by repeated air-drying-rewetting and repeated additions of organic material. *Soil Biology & Biochemistry*, **6,** 287-292.

D.A. Soulides & F.E. Allison. 1961. Effect of drying and freezing of soils on carbon dioxide production, available mineral nutreints, aggregateion and bacterial population. *Soil Science*, **91,** 291-298.

G. Stoops. 2003. *Guidelines for Analysis and Description of Soil and Regolith Thin Sections*. Soil Society of America, Inc., Madison, USA.

D.T. Strong, H. De Wever, R. Merckx & S. Recous. 2004. Spatial location of carbon decomposition in the soil pore system. *European Journal of Soil Science*, **55,** 739-750.

D.T. Strong, P.W.G. Sale & K.R. Helyar. 1999. The influence of the soil matrix on nitrogen mineralisation and nitrification - V. Microporosity and manganese. *Australian Journal of Soil Research*, **37,** 345-355.

I.A. Taina, R.J. Heck & T.R. Elliot. 2008. Application of X-ray computed tomography to soil science: A literature review. *Canadian Journal of Soil Science*, **88,** 1-20.

R.K. Thiet, S.D. Frey & J. Six. 2006. Do growth yield efficiencies differ between soil microbial communities differing in fungal: bacterial ratios? Reality check and methodological issues. *Soil Biology & Biochemistry*, **38,** 837-844.

I.K. Thomsen, P. Schjonning, B. Jensen, K. Kristensen & B.T. Christensen. 1999. Turnover of organic matter in differently textured soils - II. Microbial activity as influenced by soil water regimes. *Geoderma*, **89,** 199-218.

R. Tippkötter, T. Eickhorst, H. Taubner, B. Gredner & G. Rademaker. 2009. Detection of soil water in macropores of undisturbed soil using microfocus X-ray tube computerized tomography (mu CT). *Soil & Tillage Research*, **105,** 12-20.

J.M. Tisdall & J.M. Oades. 1982. Organic-matter and water-stable aggregates in soils. *Journal of Soil Science*, **33,** 141-163.

C. Tomasi, R. Manduchi & Ieee. 1998. *Bilateral filtering for gray and color* images. Sixth International Conference on Computer Vision, 839-846.

A.M.A. van der Linden, L.J.J. Jeurissen, J.A. Van Veen & B. Schippers eds. 1989. *Turnover of the soil microbial biomass as influenced by soil compaction*. Academic Press, London.

M. Van Geet, D. Lagrou & R. Swennen. 2003. *Porosity measurements of sedimantary rocks by means of microfocus X-ray computed tomography (µCT)*. Geological Society, London, UK.

M. Van Geet, R. Swennen & M. Wevers. 2000. Quantitative analysis of reservoir rocks by microfocus X-ray computerised tomography. *Sedimentary Geology*, **132,** 25-36.

M.T. van Genuchten. 1980. A closed-form equation for predicting the hydraulic conductivity of unsaturated soils. *Soil Science Society of America Journal*, **44,** 892-898.

D. Van Loo, S. Sleutel, L. Bouckaert, O. Leroux, E. Pauwels, M. Dierick, L. Van Hoorebeke, V. Cnudde & S. De Neve. 2012. The use of contrast agents for X-ray Computed Tomography visualization of soil phases. *PLoS ONE*, submitted.

J.A. Van Veen & P.J. Kuikman. 1990. Soil structural aspects of decomposition of organic-matter by microorganisms. *Biogeochemistry*, **11,** 213-233.

E.D. Vance, P.C. Brookes & D.S. Jenkinson. 1987. An extraction method for measuring soil microbial biomass-C. *Soil Biology & Biochemistry*, **19,** 703-707.

B.W. Veen, M. Vannoordwijk, P. Dewilligen, F.R. Boone & M.J. Kooistra. 1992. Root-Soil contact of Maize, as measured by a Thin-Section Technique.3. Effects on shoot growth, nitrate and water-uptake efficiency. *Plant and Soil*, **139,** 131-138.

H. Vereecken, J. Maes, J. Feyen & P. Darius. 1989. Estimating the soil moisture retention characteristic from texture, bulk density, and carbon content. *Soil Science*, **148**, 389-403.

J. Vlassenbroeck, M. Dierick, B. Masschaele, V. Cnudde, L. Hoorebeke & P. Jacobs. 2007. Software tools for quantification of X-ray microtomography at the UGCT. *Nuclear Instruments & Methods in Physics Research Section a-Accelerators Spectrometers Detectors and Associated Equipment*, **580,** 442-445.

M. von Lützow, I. Kögel-Knabner, K. Ekschmitt, E. Matzner, G. Guggenberger, B. Marschner & H. Flessa. 2006. Stabilization of organic matter in temperate soils: mechanisms and their relevance under different soil conditions - a review. *European Journal of Soil Science*, **57,** 426-445.

W. Wang, A.N. Kravchenko, A.J.M. Smucker & M.L. Rivers. 2011. Comparison of image segmentation methods in simulated 2D and 3D microtomographic images of soil aggregates. *Geoderma*, **162,** 231-241.

W.J. Wang, R.C. Dalal, P.W. Moody & C.J. Smith. 2003. Relationships of soil respiration to microbial biomass, substrate availability and clay content. *Soil Biology & Biochemistry*, **35,** 273-284.

G.S. Warner, J.L. Nieber, I.D. Moore & R.A. Geise. 1989. Characterising macropores in soil by computed-tomography. *Soil Science Society of America Journal*, **53,** 653-660.

D. Wildenschild, J.W. Hopmans, C.M.P. Vaz, M.L. Rivers, D. Rikard & B.S.B. Christensen. 2002. Using X-ray computed tomography in hydrology: systems, resolutions, and limitations. *Journal of Hydrology*, **267,** 285-297.

V. Wolters. 2000. Invertebrate control of soil organic matter stability. *Biology and Fertility of Soils*, **31,** 1-19.

P.T.W. Wong & D.M. Griffin. 1976. Bacterial movement at high matric potentials.1. Artificial and natural soils. *Soil Biology & Biochemistry*, **8,** 215-218.

D.A. Wright, K. Killham, L.A. Glover & J.I. Prosser. 1995. role of pore-size location in determining bacterial-activity during predation by protozoa in soil. *Applied and Environmental Microbiology*, **61,** 3537-3543.

M. Yanuka, F.A.L. Dullien & D.E. Elrick. 1984. Serial sectioning and digitization of porous-media for two-dimensional and three-dimensional analysis and reconstruction. *Journal of Microscopy-Oxford*, **135,** 159-168.

I.M. Young & J.W. Crawford. 2004. Interactions and self-organization in the soil-microbe complex. *Science*, **304,** 1634-1637.

I.M. Young, J.W. Crawford, N. Nunan, W. Otten & A. Spiers. 2008. Microbial distribution in soils: physics and scaling. *Advances in Agronomy, Vol 100*, **100,** 81-121.

I.M. Young, J.W. Crawford & C. Rappoldt. 2001. New methods and models for characterising structural heterogeneity of soil. *Soil & Tillage Research*, **61,** 33-45.

I.M. Young & K. Ritz. 2000. Tillage, habitat space and function of soil microbes. *Soil & Tillage Research*, **53,** 201-213.

X.X. Zhang, L.K. Deeks, A.G. Bengough, J.W. Crawford & L.M. Young. 2005. Determination of soil hydraulic conductivity with the lattice Boltzmann method and soil thin-section technique. *Journal of Hydrology*, **306,** 59-70.

Appendices

APPENDIX I: IMAGE ARTEFACTS

Artefacts are image features that do not correspond to the soil's real internal structure. Artefacts can originate from the polychromatic beam characteristics, problems arising in the detection of the incoming X-rays on the detector, or extreme properties of the object of interest.

Beam hardening is the most frequent artefact in CT-scanning (Cnudde, 2005). In a polychromatic beam, low-energy X-rays are preferentially attenuated when passing through the sample. In the reconstructed images, this will result in attenation values which are relatively larger near the edges of the sample than in the centre (Figure I-1a). Beam hardening can best be avoided by scanning with monochromatic X-ray bundles. Otherwise, attenuation filters can be applied before or after the X-rays penetrate the object. However, these filters degrade the X-ray intensity al all energies to some degree, negatively affecting image contrast. Beam hardening can also be corrected during the reconstruction procedure.

Ring artefacts can happen when local defects in the detection device are present and rings appear in the reconstructed image. Ring artefacts can be reduced during the reconstruction process by software enhancements.

Line artefacts are the result of oversaturated detector pixels when X-rays hit the detector directly. This artefact can be reduced with a median filter, an algorithm designed for the removal of noise.

Star artefacts appear when very dense inclusions are present within the object (Figure I-1b). This artefact is the result of photon scattering, photon starvation, beam hardening and partial volume effects. Star artefacts can be reduced with an attenuating homogenous metal filter between X-ray source and detector.
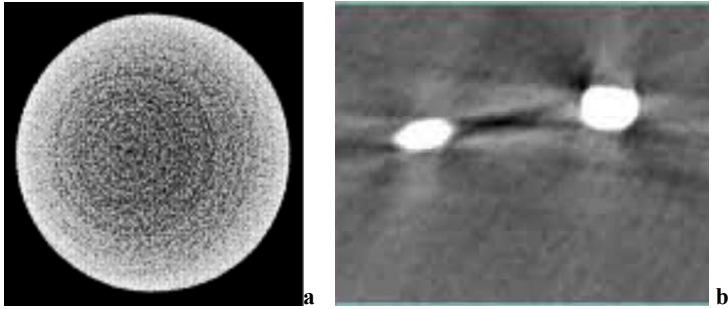
Figure I-1: Common artifacts in CT-images (a) beam hardening and (b) star artifact.

Partial volume effects appear when voxels contains more than one phase and the attenuation value is an average of the attenuation values of multiple phases (Ketcham & Carlson, 2001). Due to this effect, the minimum object size that can be detected is twice the pixel dimension (Rogasik *et al.*, 2003) (Figure I-2).

Figure I-2: Schematic presentation of the Partial Volume Effect (PVE): The attenuation value of a voxel containing two phases is an average value of both phases.

APPENDIX II: IMAGE ANALYSIS
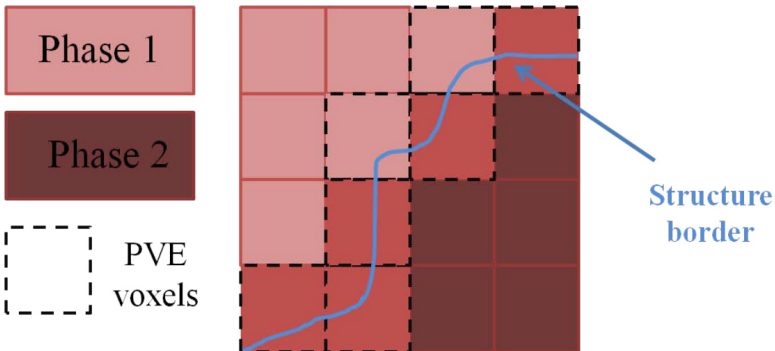
A. Image filtering

Image filtering is applied for several purposes including smoothing and sharpening of objects, for noise removal and for edge detection. A filter is defined by a kernel, which is an array applied to each pixel (or voxel) and its neighbors. This kernel passes across all the voxels in an image, applying its programmed algorithm to that voxel and its neighbors. Three image filters are implemented in Morpho+, the software package (Brabant *et al.*, 2011) used throughout the present PhD work.

The most common filter used for noise removal is a **median filter**. The median filter uses for example a kernel of 3x3x3 voxels and replaces the center voxel's grey scale value (0-256 or 0-65536) with the mean of its 26 neighbors. It is mostly used to remove random noise from CT volumes and preserves edges rather well.

The **Gaussian filter** replaces each voxel by a linear combination of voxels with a certain kernel size around the considered voxel. This filter operates faster than the median filter. The disadvantage of this filter is a blurring effect around the edges that is caused by a similar treatment of voxels representing background or another phase compared with neighboring voxels of the phase of interest. This problem is solved by the bilateral filter.

The **bilateral filter** uses multiplication factors of the kernel that are based on the actual grey values of the neighboring voxels. Both the distance to the central voxel and the difference in grey value is taken into account. Consequently, nearby voxels with a significantly deviating grey value (for example belonging to another phase) are reduced in weight, while distant voxels with a gray value close to the values of the central voxel (thus probably belonging to the same phase as the central voxel) can still have a substantial weight.

B. Image segmentation

Segmentation represents the process of image partitioning into two or more regions of interest, representing objects that can be further analyzed (Taina *et al.*, 2008). Interpretation of micro scale features is, however, only possible when these are a magnitude greater than the scan resolution (Grevers *et al.*, 1989). There therefore exists a fundamental link between

segmentation and image resolution. However, an important remark regarding image segmentation is that no method preserves pore characteristics in any case (Baveye *et al.*, 2010; Wang *et al.*, 2011).

The most common method used in X-ray CT of soil for segmentation, is **histogram thresholding**, whereby a fixed threshold grey scale value is chosen on the basis of the CT volume's grey value histogram. On the other end, **indicator kriging based thresholding** (Oh & Lindquist, 1999) uses both the spatial covariance of the image and indicator kriging to segment an image. First, two partial populations are assigned by thresholding T_0 and T_1 by histogram thresholding (Figure II-1) and secondly, kriging is applied on the remainder of the voxels (x_0) to complete population assignments.
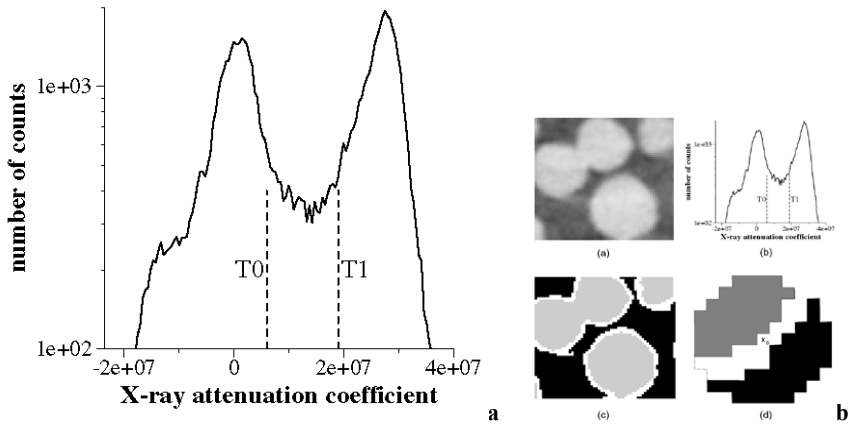

Figure II-1: X-ray attenuation coefficient histogram for an entire sample and (b) illustration of a two dimensional kriging window used in determining the population assignment for voxel x_0 (from Oh & Lindquist, 1999).

When the image histogram has clearly distinguishable peaks, Wang *et al.* (2011) concluded that indicator thresholding is the best segmentation method for microtomographic images of soil aggregates. Otherwise, the second best method in line was **Otsu's method**, an automatic histogram shape-based image thresholding. This algorithm assumes that the grey scale image contains two classes of pixels or bi-modal histogram, a foreground and background, and calculates the optimum threshold separating those two classes so that their combined spread (intra-class variance) is minimal (Otsu, 1979; Brabant *et al.*, 2011).

An important remark regarding image segmentation is that no method preserves pore characteristics in all cases (Baveye *et al.*, 2010; Wang *et al.*, 2011). For more information on

the high number of thresholding techniques that exist, the reader is referred to the reviews of Pal & Pal (1993) and Sezgin & Sankur (2004).

C. <u>Pore space separation based on pore necks</u>

Once a binary image has been built from an original grey scale CT volume with objects of interest having values of 1 and background 0, each part of the objects not connected with another part is assigned a different label. Next, a distance map calculation labels each voxel of the image with the minimum distance to the object edge (Figure II-2a). This distance map is used as input image for the watershed-based separation of the pore space. The watershed-based separation can separate objects that are not physically connected but appear to be connected because of limited resolution and/or limited contrast of the scan (Brabant *et al.*, 2011). Watershed lines are the minima of the inverse distance map and subtracting them from the binary segmented image results into a separation of all objects. The separation is based on the openings or 'necks' between those objects, which is the overlap between the segmented image and the watershed lines (Figure II-2b).
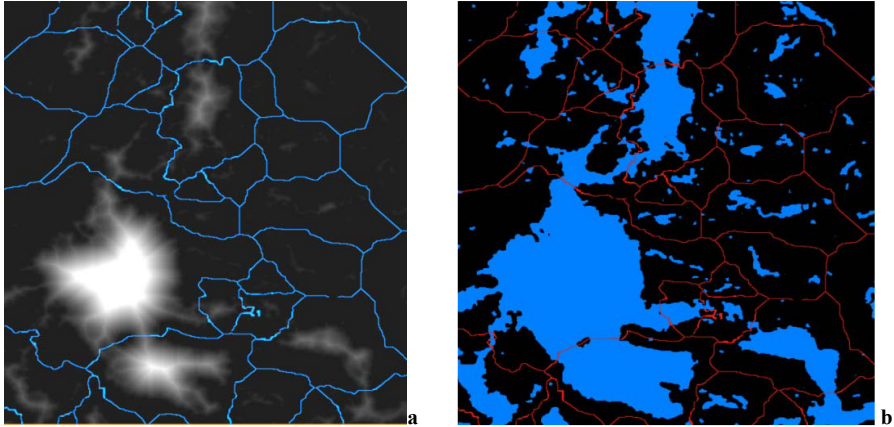
Figure II-2: (a) Watershed lines on top of distance map and (b) watershed lines on top of segmented image.

Following object separation, all sorts of pore characteristics can be calculated such as total porosity (Rachman *et al.*, 2005), pore diameter (Anderson *et al.*, 1990), perimeter and area (Adderley *et al.*, 2001), circularity (Rachman *et al.*, 2005), equivalent circular diameter (Gantzer & Anderson, 2002), tortuosity, connectivity (Perret *et al.*, 1999) and necks (Brabant

et al., 2011). The purpose of image analysis in this study was an assessment of a pore size distribution based on pore necks.

Curriculum Vitae

<div style="border:1px solid">PERSONALIA</div>

Last name	Bouckaert
First name	Liesbeth
Address	Bellestraat 22
	8908 Vlamertinge
	BELGIUM
Phone	0479/ 76 26 87
Email	lbouckae@gmail.com
Place/date of birth	Ieper, 31/07/1985
Nationality	Belgian

<div style="border:1px solid">EDUCATION</div>

2009-2012   Instituut voor Permanente Vorming, Technologiepark 913, 9052 Zwijnaarde
Environmental coordinator, type A

2003-2008   Faculty of Bioscience engineering, UGent, Coupure Links 653, 9000 Gent
Bio-engineer in Land and Forest management, option nature and forest management

     Erasmus (2007):   Swedish University of Agriculture Sciences, SLU Verkstadsgatan 13, S-904 32 Umeå

         Courses: Ecological forest landscape planning
Conservation Biology
Faunistics of forest animals

2001-2003   Sint-Amandscollege, Diksmuidekaai 6, 8500 Kortrijk
Secondary education Sciences-Mathematics

2000-2001   Sint-Vincentiuscollege, Guido Gezelleplein 11, 8900 Ieper
Secondary education Economy-mathematics

1998-2000   Technisch Instituut Immaculata, Rijselsestraat 83, 8900 Ieper
Secondary education Technical sciences

1997-1998   Sint-Vincentiuscollege, Guido Gezelleplein 11, 8900 Ieper
Secondary education Latin

PROFESSIONAL EXPERIENCE

2008-2012   Department of soil management, Ghent University Research associate at the Laboratory of Soil Fertility and Nutrient Management with Prof. dr. ir. S. De Neve and dr. ir. S. Sleutel as scientific promoters. This research was financed by FWO (Fonds Wetenschappelijk Onderzoek).

SCIENTIFIC PUBLICATIONS

Publications in international Journals with peer review (A1)

P.C. Baveye, M. Laba, W. Otten, L. Bouckaert, P. Dello Sterpaio, R.R. Goswami, D. Grinev, A. Houston, Y. Hu, J. Liu, S. Mooney, R. Pajor, S. Sleutel, A. Tarquis, W. Wang, Q. Wei & M. Sezgin. 2010. Observer-dependent variability of the thresholding step in the quantitative analysis of soil images and X-ray microtomography data. Geoderma, 157, 51-63.

F.E. Moyano, N. Vasilyeva, L. Bouckaert, F. Cook, J. Craine, J.C. Yuste, A. Don, D. Epron, P. Formanek, A. Franzluebbers, U. Ilstedt, T. Katterer, V. Orchard, M. Reichstein, A. Rey, L. Ruamps, J.A. Subke, I.K. Thomsen & C. Chenu. 2012. The moisture response of soil heterotrophic respiration: interaction with soil properties. Biogeosciences, 9, 1173-1182.

S. Sleutel, L. Bouckaert, D. Buchan, D. Van Loo, W.M. Cornelis & H.G. Sanga. 2012. Manipulation of the soil pore and microbial community structure in soil mesocosm incubation studies. Soil Biology & Biochemistry, 45, 40-48.

L. Bouckaert, D. Van Loo, N. Ameloot, D. Buchan, L. Van Hoorebeke & S. Sleutel. 2012. Compatibility of X-ray micro-Computed Tomography with soil biological experiments. Soil Biology & Biochemistry (In Press).

L. Bouckaert, D. Van Loo, L. Brabant, V. Cnudde, L. Van Hoorebeke, S. Sleutel & S. De Neve. 2012. Carbon mineralization and pore network structure in undisturbed soil cores. Soil Research (submitted).

Articles in proceedings of scientific congresses, symposia and workshops

L. Bouckaert, D. Van Loo, S. Sleutel, S. De Neve, P. Jacobs & L. Van Hoorebeke. 2009. Application of X-ray tomography for quantification of the soil pore structure and visualization of soil organic matter. Geochimica Et Cosmochimica Acta, 73, A145-A145.

L. Bouckaert, D. Van Loo, S. Sleutel, S. De Neve, P. Jacobs & L. Van Hoorebeke. 2009. Application of X-ray tomography for quantification of the soil pore structure and visualization of soil organic matter. In: Conference Program and abstracts of the International Symposium on Soil Organic Matter Dynamics: Land Use, Management and Global Change, Colorado state University, USA, p. PS2_16.

L. Bouckaert, D. Van Loo, B. Hantson, L. Van Hoorebeke, S. De Neve & S. Sleutel. 2010. Localization of organic carbon pools in the soil matrix with X-ray computed tomography. In: Program of Organic matter stabilization and ecosystem functions conference, Presqu'île de Giens, France, p. 213.

L. Bouckaert, B. Hantson, D. Van Loo, S. Sleutel, V. Cnudde, M. Dierick, P. Jacobs, L. Van Hoorebeke & S. De Neve. 2011. Organic matter decomposition in the soil pore network: a combined X-ray CT – incubation study. In: Book of abstracts of Day of young soil scientist, Brussels, Belgium, p.24.

L. Bouckaert, S. Sleutel, D. Van Loo, V. Cnudde, M. Dierick, P. Jacobs, L. Van Hoorebeke & S. De Neve. 2011. Overcoming practical constraints in the application of X-ray CT to soil science. In: Book of abstracts of the International symposium of Interactions of Soil Minerals with Organic Components and Microorganisms: Soil Interfaces in an changing world, Montpellier, France, p. 16.

POSTER AND ORAL PRESENTATIONS

L. Bouckaert, D. Van Loo, S. Sleutel, S. De Neve, P. Jacobs & L. Van Hoorebeke. Application of X-ray tomography for quantification of the soil pore structure and visualization of soil organic matter. Day of the Young soil scientists, February 29, 2009, Brussels, Belgium. *Poster presentation*

L. Bouckaert, D. Van Loo, S. Sleutel, S. De Neve, P. Jacobs & L. Van Hoorebeke. Application of X-ray tomography for quantification of the soil pore structure and visualization of soil organic matter. Goldsmith 2009: our volatile planet, June 21-25, 2009, Davos, Switzerland. *Poster presentation*

L. Bouckaert, D. Van Loo, S. Sleutel, S. De Neve, P. Jacobs & L. Van Hoorebeke. Application of X-ray tomography for quantification of the soil pore structure and visualization of soil organic matter. International Symposium on Soil Organic Matter Dynamics: Land Use, Management and Global Change, July 6-9, 2009, Colorado, USA. *Poster presentation*

L. Bouckaert, D. Van Loo, S. Sleutel, S. De Neve, P. Jacobs and L. Van Hoorebeke. X-ray Computed Tomography of Soil Aggregates: from micro to nano scale. Micro soil workshop: Integrating biological, physical and chemical techniques for the study of soil micro-habitats, September 16-17, 2009, Dundee, Scotland. *Poster presentation*

L. Bouckaert, D. Van Loo, S. Sleutel, S. De Neve, P. Jacobs and L. Van Hoorebeke. X-ray Computed Tomography of Soil Aggregates: from micro to nano scale. PhD symposium on Applied Biological Sciences, November 6, 2009, Leuven, Belgium. *Poster presentation*

L. Bouckaert, D. Van Loo, S. Sleutel, P. Van Oostveldt, S. De Neve, P. Jacobs & L. Van Hoorebeke. Visualization and quantification of organic matter coatings on sand particles with X-ray CT and CLSM. Day of the Young soil scientists, February 23, 2010, Brussels, Belgium. *Poster presentation*

L. Bouckaert, D. Van Loo, S. Sleutel, P. Van Oostveldt, S. De Neve, P. Jacobs & L. Van Hoorebeke. Comparison of CLSM, X-ray CT and light microscopy for the visualization and quantification of organic matter coatings on sand particles. Geox 2010: Third International Workshop on Applications of x-ray CT for Geomaterials, February 28-March 3, 2010, New Orleans, Louisiana, USA. *Poster presentation*

L. Bouckaert, D. Van Loo, B. Hantson, L. Van Hoorebeke, S. De Neve & S. Sleutel. Localization of organic carbon pools in the soil matrix with X-ray computed tomography. Organic matter stabilization and ecosystem functions conference, September 19-23, 2010, Presqu'île de Giens, France. *Oral presentation*

L. Bouckaert, D. Van Loo, B. Hantson, L. Van Hoorebeke, S. De Neve & S. Sleutel. Localization of organic carbon pools in the soil matrix with X-ray computed tomography. PhD symposium on Applied Biological Sciences, December 20, 2010, Gent, Belgium. *Poster presentation*

L. Bouckaert, B. Hantson, D. Van Loo, S. Sleutel, V. Cnudde, M. Dierick, P. Jacobs, L. Van Hoorebeke & S. De Neve. Organic matter decomposition in the soil pore network: a combined X-ray CT – incubation study. Day of the Young soil scientists, February 23, 2011, Brussels, Belgium. *Poster presentation*

L. Bouckaert, S. Sleutel, D. Van Loo, V. Cnudde, M. Dierick, P. Jacobs, L. Van Hoorebeke & S. De Neve. Overcoming practical constraints in the application of X-ray CT to soil science. International symposium of Interactions of Soil Minerals with Organic Components and Microorganisms: Soil Interfaces in an changing world, June 26-July 1, 2011, Montpellier, France. *Oral presentation*